INVESTIGATION OF HEME-PROTEIN INTERACTIONS IN TRUNCATED HEMOGLOBINS

by

Selena Loring Rice

A dissertation submitted to Johns Hopkins University in conformity with the requirements for the degree of Doctor of Philosophy

Baltimore, Maryland
October 2015

Abstract

Fe-protoporphyrin IX, otherwise known as heme *b*, is found in all hemoglobins. The heme iron is coordinated by four nitrogen atoms from the tetrapyrrole ring of protoporphyrin IX. In hemoglobin the heme is bound to the protein via a proximal histidine residue, resulting in a 5-coordinate heme. Many hemoglobins also have a sixth distal ligand in the form of an exogenous ligand, such as water or oxygen, or, in some cases, a protein residue. Despite having highly conserved tertiary structure and the same cofactor, hemoglobins display a variety of functions, such as oxygen transport, oxygen sensing, and nitric oxide scavenging. Hemoglobins and heme proteins in general are capable of controlling the chemistry performed by the heme, and therefore the function of the protein, via two primary methods: posttranslational modification (PTM) and axial ligation.

In two cyanobacterial truncated hemoglobins (trHbs, from *Synechococcus* sp. PCC 7002 and *Synechocystis* sp. PCC 6803, collectively named GlbN), when the heme contains a ferrous iron and is not carrying oxygen or carbon monoxide, a covalent bond forms between the heme-2 vinyl and a nearby histidine residue. The PTM in GlbN has been extensively studied and these studies show it is not dependent on the distal endogenous ligand and the local environment around the reactive histidine. To confirm that the main determinant of PTM is the relative positions of the reactants I engineered the PTM in the heme domain of *Chlamydomonas eugametos* LI637 protein (CtrHb). CtrHb is structurally similar to GlbN, sharing an average ~46% identity with them. The differences between CtrHb and GlbN are distributed throughout the structures and include some the heme pocket. Of the 21 residues that are in contact with the heme, 10 are different between the two proteins. This difference provides an altered chemical environment in which to test the reaction that generates the PTM. Enhanced chemiluminescence detection of the heme in reacted CtrHb variants shows

that it is possible to engineer the PTM in this protein. This suggests that the heme pocket of GlbN does not greatly contribute to the PTM reaction and that the PTM could be engineered in other proteins.

The nature of the distal heme ligand is variable and can affect the rate exogenous ligand binding, the electron transfer rate, and the redox potential of heme proteins. Owing to the importance of the distal ligand, special attention was placed on identifying the distal ligand during the optical and crystallographic characterization of the eukaryotic trHb from *Chlamydomonas reinhardtii*, THB1, in addition to investigating the function of this protein. In this work I expanded upon our knowledge of these two heme proteins, CtrHb and THB1, in order to gain a better understanding of how proteins control heme reactivity.

Thesis Advisor

Dr. Juliette Lecomte

Thesis Committee

Dr. Bertrand Garcia-Moreno

Dr. Vincent Hilser

Dr. Gregory Bowman

Intended to be Blank

Acknowledgments

Many people made it possible for me to produce this body of work. First and foremost I must thank my thesis advisor, Juliette Lecomte, for not only allowing me to pursue my research in her lab but also for her sharp insight, keen eye for detail, and most of all for her patience, compassion, and kindness. I know that I have become a better scientist because of her guidance. I must also thank my thesis committee members, Bertrand Garcia-Moreno, Vincent Hilser, and Greg Bowman for their input while completing my research. I am also grateful to past current administrators of both the Biology and Biophysics Departments, especially Joan Miller, Barbara Birsit, Jessica Appel, Lexi Ebert, and Nancy Foltz.

I am very fortunate to have worked with wonderful people in the lab over the years. I am especially grateful to Matthew Pond, who was my first mentor in the lab and taught me everything I know about preparing proteins and Matthew Preimesberger who has been a constant for me over the past four years and is always willing to help out with NMR. Eric Johnson has also been a wonderful co-worker and has taught me a great deal about *Chlamydomonas reinhardtii* culture and techniques. There are also the other past and present lab members who I must thank: Emily Adney, Belinda Wenke, Dillon Nye, and Miranda Russo.

During my graduate career I have also had the privilege of making wonderful friends outside of the lab. There are my basement buddies Jaime Sorenson and Aaron Robinson who were always available to talk to about anything from science to books. Other friends that I have made along the way who helped support me are Karen McMurdie, Diamond Ling, Mollie Rappé, Alex Chin, Andrew Martens, and Jessica Houtz.

Last but not least I am extremely grateful for my family. My parents Robert and Nora Rice who have always supported me throughout my life and without whom I would

not be writing this thesis. Finally, I am most grateful to my husband, Sven Cattell, who stood by me through all of the ups and downs of graduate school and who made certain that I stayed sane and fed.

Table of Contents

List of Tables

List of Figures

Intended to be Blank

Chapter 1

Introduction

Hemoglobins comprise a large and ancient protein superfamily. The first hemoglobins are hypothesized to have evolved at least 3.5 billion years ago, prior to the oxygenation of Earth's atmosphere, and were present in the last universal common ancestor. The hemoglobin ancestor was likely necessary to protect ancient organisms from pockets of oxygen, which would be toxic, produced by early photosynthetic life. Hemoglobins have a rich evolutionary history that is often overlooked owing to the common thought that nothing more can be learned from vertebrate erythrocyte hemoglobin[1] and its close relative, myoglobin. However, this could not be further from the truth; the hemoglobin superfamily consists of many more proteins than the proteins found in blood and red muscle[2,3,4].

The hemoglobin superfamily is divided into three families, flavohemoglobins, globin coupled sensors, and truncated hemoglobins (trHbs). Recent research has greatly expanded our knowledge of hemoglobins and showed that there is still much that we do not know about this complex protein family. In the last two decades alone two additional hemoglobins have been discovered in humans, and enzymatic hemoglobin functions have been characterized from proteins found in a variety of organisms. In an effort to expand upon our knowledge of these proteins I have included a brief introduction into hemoglobin chemistry and the proteins that were investigated in this work.

1.1 Heme Reactivity

All hemoglobins contain a heme *b*, which is composed of protoporphyrin IX (a cyclic tetrapyrrole) and a central iron ion (Fig. 1.1). The heme is a reactive molecule, which can cause damage when it is free within an organism. Specifically, free heme is capable of reacting with several oxygen compounds, including dioxygen, nitric oxide and hydrogen peroxide, which can lead to the formation of reactive species, such as peroxynitrite and hydroxyl radicals. These molecules, as well as the free ferric heme, can damage macromolecules, disrupting biological processes and causing inflammation in vertebrates[5]. Organisms have evolved to harness the versatile chemistry of the heme, while protecting themselves from heme related oxidative damage, by binding heme molecules to a protein fold, resulting in heme proteins.

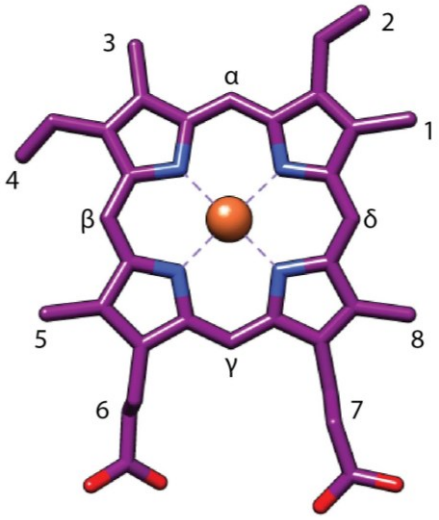

Fig. 1.1 Schematic of *b* heme. Methyl, vinyl, and propionate groups are numbered; meso carbons have Greek letter labels.

In general, heme proteins exhibit a large variety of functions, ranging from oxygen binding to nitrite reduction. Hemoglobin is a classical example of a heme protein and has long been known to bind and transport oxygen in multicellular organisms. Other examples

of heme binding proteins include cytochrome *c*, which transfers electrons and is critical for cellular respiration; nitrite reductase, which reduces nitrite to ammonium; and peroxidase, which reduces hydrogen peroxide and oxidizes halides. This diverse set of functions is possible primarily through interactions between protein side chains and the heme cofactor.

There are two primary ways, posttranslational modification and axial heme ligation, in which heme proteins control the reactivity of the heme, and therefore the function of the protein. Posttranslational modifications (PTM) occurs in the form of covalent bonds between a protein side chain and the heme. Covalent linkage between the heme and protein is seen predominantly in peroxidases and cytochromes; however, there are two Hbs that also exhibit covalent heme linkage (Fig. 1.2).

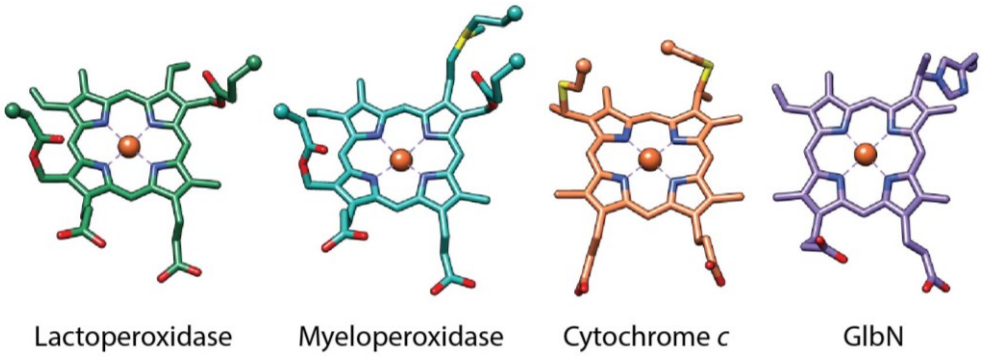

Fig. 1.2 Different forms of covalent heme linkage. All lactoperoxidases have a heme with two heme protein linkages between the heme 1-methyl and a glutamate residue and the heme 5-methyl and an aspartate (PDB ID: 2GJ1). Myeloperoxidases have the two conserved covalent bonds seen in lactoproxidases, but also have a third linkage between the heme 2-vinyl and a methionine (PDB ID: 3F9P). *c*-Type cytochromes also have two covalent linkages to the heme, but they occur between the two vinyl groups and two cysteine residues (PDB ID: 1HRC). Only two hemoglobins are known to have a covalent linkage between the heme and the protein, GlbN from *Synechocystis* sp. PCC 6803 (PDB ID: 1RTX) and *Synechococcus* sp. PCC 7002 (PDB ID: 4MAX).

1.1.1 Covalent Heme Modification

A good example of how heme PTM can affect protein function is the mammalian peroxidase family. The enzymes of this protein family have the heme covalently bound to the protein via ester linkages between the 1- and 5-heme methyl groups and the carboxyl groups of conserved glutamate and aspartate residues, respectively. Myeloperoxidase also has a third covalent linkage between the β-carbon of the 2-vinyl with the sulfur atom of a methionine. Extensive research has shown that the peroxidase PTMs regulate the redox potential of the protein by altering the thermodynamic stability of the ferric heme[3]. While most peroxidases have negative redox potentials, -180 to -300 mV, that stabilize the ferric catalytic form of the protein[6,7], myeloperoxidase has a positive redox potential, 5 mV, similar to hemoglobins. This increased redox potential is hypothesized to be due to the third covalent modification on the 2-vinyl. Structural comparisons to other peroxidases and mutagenesis studies support this hypothesis and show that the covalent bond causes larger distortions in the myeloperoxidase heme plane compared to other peroxidases, which when coupled with the electron withdrawing effect of the sulfonium ion linkage leads to destabilization of the ferric state and thus a higher redox potential[6,7,8]. Additionally, unlike in plant peroxidases, which do not have covalently bound hemes, mammalian peroxidases are resistant to heme modification by the oxidation of halides, one of their physiological functions[8,9,10].

In cytochrome *c* proteins the effect of covalent modification on the heme is less clear. *c*-Type cytochromes covalently bind the heme via two thioether linkages between the heme-vinyls and two cysteine side chains in a CXXCH protein motif. In many organisms the formation of these linkages is a complex process that requires a large cohort of cytochrome *c* maturation proteins. Much is still unclear about the cytochrome *c* maturation process, but it

is known that both of these cysteines are necessary for efficient release from the cytochrome *c* maturation protein, holocytochrome *c* synthase, and thus for successful cytochrome *c* folding[11]. Mutagenesis studies to elucidate the function of the thioether linkages have been hindered by the important role these cysteines play in cytochrome *c* folding and maturation., Despite this complication variants of a cytochrome *c* from a thermophilic bacterium have led to some insights. These studies show that removing the thioether linkages at the vinyl groups do not greatly affect the reduction potential in this protein. However, the loss of both linkages does significantly decrease the stability of the protein to both thermal and chemical denaturation[12,13].

These two examples of heme PTM show that the effect of covalent bonding between the heme and protein side chains can affect the redox potential and stability of the heme protein. In hemoglobins heme protein covalent binding is rare. As yet this form of PTM has only been identified in two cyanobacterial trHbs, collectively named GlbN[14,15]. The PTM in these globins will be discussed later in this work. Clearly, the presence of covalent bonds between the heme and the protein can greatly affect either the function and/or the stability of heme proteins and further study of a rare form of this PTM, and how it affects hemoglobin function, is necessary.

1.1.2 Axial Ligation

The second, and predominant, mechanism by which heme reactivity is tuned is through heme axial ligation. Several different protein side chains can act as axial ligands, Fig. 1.3. All hemoglobins, *c*- and *b*-type cytochromes, and peroxidases bind the heme cofactor via a proximal histidine residue, whereas catalases use a tyrosine residue and cytochrome P450's utilize a cysteine residue. The position of the axial residue on the proximal helix or loop, the presence of a hydrogen bond between the proximal histidine and a nearby residue, and the

length of the Fe-N bond between the iron atom and the proximal histidine are all ways in which the proximal ligand can affect heme reactivity[16].

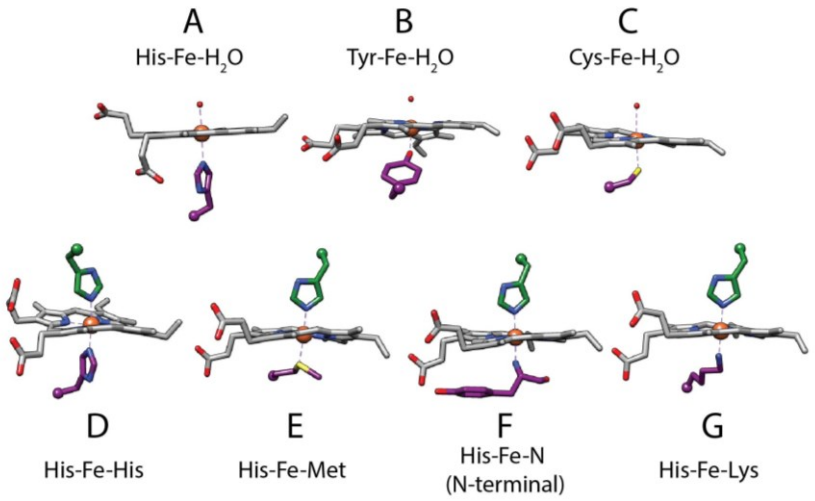

Fig. 1.3 Examples of different types of heme ligation. (A) 1JP6, aquomet sperm whale myoglobin. **(B)** 4B7G, *Corynebacterium glutamicum* catalase. **(C)** 4ICT, *Mycobacterium tuberculosis* cytochrome P450. **(D)** 4MAX, *Synechococcus* sp. PCC 7002 GlbN. **(E)** 1HRC, horse heart cytochrome *c*. **(F)** 1EWH, *Chlamydomonas reinhardtii*, cytochrome *f*. **(G)** 2BH5, *Paracoccus versutus* M100K cytrochrome *c*-550.

The environment on the distal side of the heme is crucial in determining the function of a heme protein. The distal side of the heme iron may be coordinated by either an exogenous ligand, such as a water molecule or oxygen, or by an endogenous ligand, such as a protein side chain. In some cases there is no distal ligand. There are many amino acid residues that can act as a distal heme ligand and the identity of the residue often correlates to protein family. For example, most peroxidases have a methionine as a distal ligand, whereas *b* cytochromes generally have a histidine. Some hemoglobins also have a histidine as a distal endogenous ligand, which can bind the heme in both the ferric and ferrous states. Many simply have an exogenous water bound in the ferric state, and in the ferrous state have O_2, CO, or no ligand. The presence and identity of the endogenous distal ligand can have

profound effects on exogenous ligand binding kinetics[17,18,19], electron transfer rates[20,18], and redox potential[21]. Thus, identification of the distal ligand in heme proteins is critical for understanding the function of the protein.

Unfortunately, prediction of the distal ligand in heme proteins based on protein sequence is not a simple matter, especially for hemoglobins given the range of possible side chains, as well as the possibility of no endogenous ligand binding[22,23]. The presence of an endogenous distal ligand can often be deduced from optical spectra; however, identification of the ligand requires structural data via NMR spectroscopy, X-ray crystallography, Resonance Raman spectroscopy, or other techniques. Given that hemoglobins have a highly conserved tertiary structure and yet display diverse functions, they are an ideal system in which to study how heme protein interactions affect heme reactivity.

1.2 GlbN: trHbs with a posttranslational modification

Two cyanobacterial species, *Synechocystis* sp. PCC 6803 and *Synechococcus* sp. PCC 7002, each express one truncated hemoglobin, collectively called GlbN. As members of the truncated hemoglobin family these proteins have a fold in which the heme is held in a 2-over-2 (2/2) α-helical bundle rather than the canonical 3-over-3 (3/3) α-helical fold. GlbN has been extensively studied owing to two unusual structural features: *bis*-histidine axial heme coordination[24] and covalent PTM[14] between the heme 2-vinyl and a nearby histidine residue (Fig. 1.4 A). Although GlbN has a distal endogenous ligand, His46, the protein is still capable of binding exogenous ligands, such as cyanide in the ferric state or oxygen in the ferrous state[25], indicating that the distal ligand can be displaced. Mutagenesis studies have shown that upon removal of the distal histidine the thermal stability of the holoprotein decreases[26]; GlbN's resistance to hydrogen peroxide induced damage[27] is also impaired by

the modification. Upon removal of the distal histidine another, unknown, ligand coordinates the heme[27]. Identification of this ligand "X" is still underway.

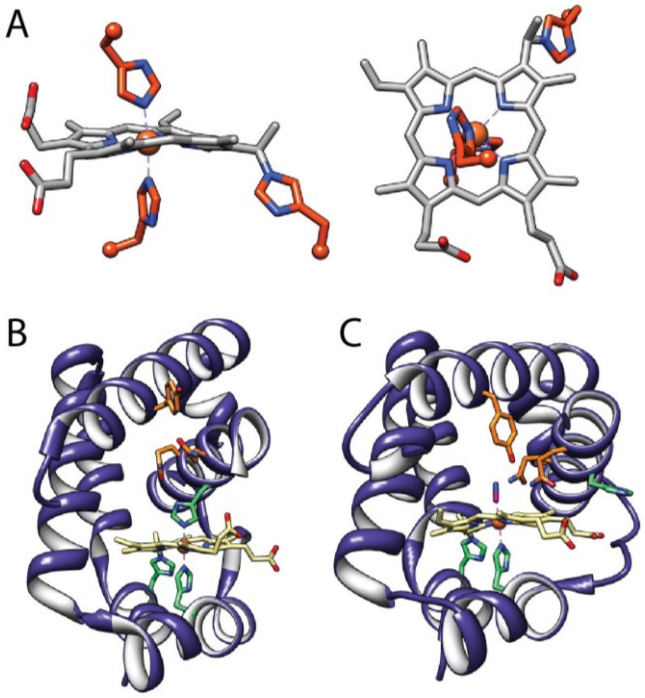

Fig. 1.4 GlbN structure. (A) Two views of GlbN heme showing axial ligands, H46 and H70, and the PTM between H117 and the heme 2-vinyl. **(B)** Crystal structure of *Synechococcus* sp. PCC 7002 bis-His GlbN (PDB ID 4MAX). **(C)** Crystal structure of *Synechococcus* sp. PCC 7002 cyanomet GlbN (PDB ID 4L2M).

In order for GlbN to bind exogenous ligands the E helix (following customary hemoglobin nomenclature) must rotate significantly, placing the dissociated distal histidine into solvent and placing two glutamine residues into the heme pocket (Fig. 1.4 B,C)[28,29]. These two glutamine residues (E7 and E11) are part of a hydrogen bonding network, which including TyrB10, stabilizes the binding of the exogenous ligand to the heme. This H-bond network is conserved among Group I trHbs, to which GlbN belongs[30,31]. Although a great deal of in vitro data has been collected on trHbs, not much is known about the function of these proteins in vivo. The Group I trHb in *Mycobacterium tuberculosis* is the only trHb with a

known function, detoxification of nitric oxide[32]. In the case of GlbN deleting the *glbN* gene in *Synechococcus* sp. PCC 7002 results in higher levels of reactive oxygen/nitrogen species (ROS/RNS) compared to WT cells. Futhermore, when *ΔglbN* cells were cultured in medium containing high levels of nitrate, the cells were unable to grow under oxic conditions and grew only slowly under microoxic conditions, whereas WT growth was unhindered. When a plasmid with the *glbN* gene was added back to the knockout cells, there was a partial recovery of growth in nitrate medium[33]. These data suggest that in *Synechococcus* sp. PCC 7002 GlbN is involved in ROS/RNS detoxification, thereby protecting the organism from redox stress.

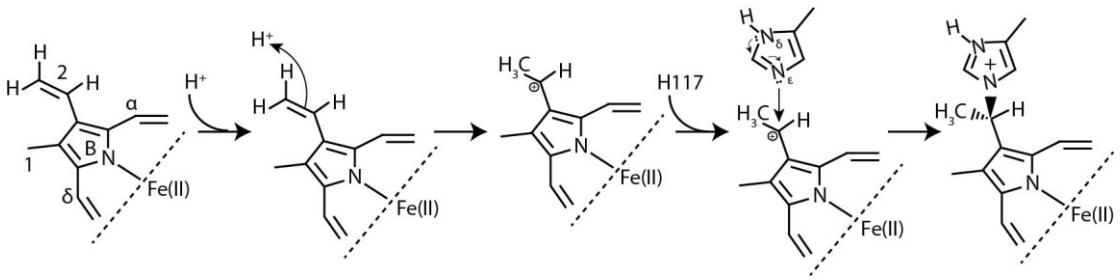

Fig. 1.5 Schematic of the PTM reaction in GlbN. Figure is modified from Nothnagel *et al.* (2011).[27]

As alluded to earlier GlbN is able to form a covalent cross-link between the heme 2-vinyl and the Nε2 atom of a nearby histidine residue. In GlbN this PTM forms spontaneously in solution and the reaction requires ferrous heme to occur[15]. In the proposed mechanism of PTM, reduction of the heme iron increases the electron density at the 2-vinyl allowing for protonation of the β-carbon generating an α-carbocation. This is followed by nucleophilic attack by the neutral histidine at position 117 to form a covalent bond between the α-carbon of the heme 2-vinyl and the histidine Nε2 (Fig. 1.5) [28]. Extensive mutagenesis studies have been performed to gain a better understanding of how the PTM affects the chemistry of GlbN and the factors involved in PTM formation. Elimination of the PTM by

replacing His117 with an alanine does not greatly affect the structure of the protein, although in the cyanomet state it does lead to a 5-10% increase in heme isomerization where the heme is in a "flipped" orientation with the 4-vinyl near H117. The H117A variant is also less stable and binds cyanide much more slowly than WT[34,35].

In order to understand the factors controlling PTM formation in GlbN several other variants were generated. The H117C variant was created to determine if a different nucleophile could bind to the vinyl. It did upon heme iron reduction, which supports the mechanism described above. The distal heme ligand is not necessary for PTM formation, as seen in successful formation of the cross-link in the H46L variant[28]. Investigations were conducted to explore if the environment around H117 plays a role in cross-link formation. To that end an L79H/H117A variant of GlbN was generated. In this variant the histidine reaching the heme (H117) in the WT protein was removed and a histidine was placed on the other side of the heme pocket, to provide an alternate site for PTM. Upon reduction of the iron to the ferrous state from the ferric state in which the protein is prepared, L79H/H117A GlbN forms the same crosslink as the WT except the bond is between the α-carbon of the heme 4-vinyl and the engineered histidine. In the L79H single variant the reactive H117 is present and crosslinks form at both the 2- and 4-vinyls[36]. These experiments highlight the robustness of the PTM and suggest that the primary factor in GlbN PTM is the location of a reactive residue near the heme vinyls.

1.3 Eukaryotic truncated hemoglobins

All of the previously discussed trHbs are found in prokaryotes; however, trHbs also exist in eukaryotic organisms, including unicellular algae and some higher plants. The first trHb to have its tertiary structure solved was CtrHb (the heme domain of the *LI637* gene product) from the unicellular photosynthetic eukaryote *Chlamydomonas eugametos*[30]. The *LI637*

gene was first identified by Couture, *et al.* in 1994 and was chosen for further study as it is expressed in response to light and the LI637 protein is localized within the chloroplast of *C. eugametos*, suggesting involvement in photosynthesis[37]. The crystal structure of CtrHb is of the cyanomet protein and gives insight into the H-bonding network that is seen in other trHbs, as well as illustrating the structural differences between trHbs (2/2) and the canonical mammalian Hb (3/3) structure.

Optical studies of CtrHb reveal that it is has a 6th endogenous ligand, but is nevertheless capable of binding standard Hb ligands, such as cyanide, oxygen, and carbon monoxide[38]. CtrHb is unusual in that it can bind cyanide in both the ferric and ferrous states. The latter complex is obtained when the cyanomet form of the protein is reduced[39]. Whether or not the distal endogenous ligand binds the heme is dependent upon pH. In the ferric protein there is a high-spin to low-spin transition as the pH is raised with an apparent pKa of 6.3. Resonance Raman experiments on CtrHb suggest that there is an $-O^-$ group bound to the heme iron. ^{18}O exchange experiments indicate that the oxygen atom does not come from water or hydroxide. Furthermore, mutagenesis studies show that upon replacement of Lys87 (E10) with an alanine the pKa of the high-spin to low-spin transition increases to above 10. Based on these data the authors hypothesize that the distal ligand of CtrHb is a tyrosine (TyrB10) and that ligation to the iron is stabilized by the lysine residue at position E10[40].

At alkaline pH the heme of ferrous CtrHb is also coordinated by a distal endogenous ligand.[41] The pH titration of ferrous CtrHb shows two transitions corresponding with pKa's of 6.4 and 8.5. The spectral changes associated with the first transition are consistent with conversion from un-ligated, 4-coordinate, heme to 5-coordinate heme, with the proximal histidine bound, as the pH increases. The spectra of the second transition indicate the binding of the distal endogenous ligand[41]. Although much has been learned about CtrHb in

vitro, determining the function of this protein in vivo is difficult given the lack of genetic tools for this organism, thus little work has been done to investigate the function of the in vivo form of this protein. This is a common problem with trHb research, since many of these proteins are found in organisms that are difficult to culture or to transform.

Chlamydomonas reinhardtii is an organism related to *C. eugametos*. However, unlike *C. eugametos*, *C. reinhardtii* has been used as a model system for decades to study photosynthesis[42,43], cilia biogenesis[44,45], and hydrogen production[46]. Furthermore, the nuclear genome of *C. reinhardtii* has been sequenced and recently a system to produce interfering RNAs was developed to knockdown specific genes[47,48]. *C. reinhardtii* also has at least 10 genes that contain trHb domains[49] (Fig. 1.6). This, coupled with the powerful genetic tools available for *C. reinhardtii*, makes this organism a rare system in which we can study trHbs both in vitro and in vivo. To date three trHb genes are known to be expressed in *C. reinhardtii* and have been preliminarily characterized: THB1, THB8, and THB2.

THB8 transcription is known to occur under hypoxic conditions and experiments on cells in which the *THB8* gene was knocked down suggest that THB8 is involved in anaerobic cell growth[50]. *THB2* is another trHb gene known to be expressed in *C. reinhardtii*. *THB2* is expressed when *C. reinhardtii* cells are grown in nitrate containing medium, but *THB2* expression is downregulated in the presence of NO. This suggests that THB2 may play a role in the nitrate assimilation pathway in *C. reinhardtii*[51]. The third trHb gene is known to be expressed in *C. reinhardtii* is *THB1*. The protein product of this gene is also expressed in the organism and was initially discovered in the flagella of mutant *C. reinhardtii* cells[52]. Native THB1 has been purified from cell lysate of *C. reinhardtii* cells and is shown to bind heme. Additionally, mass spectrometry analysis of native THB1 indicates that the protein undergoes N-terminal acetylation, the purpose of which is unknown[53].

In the following work I further explore the factors involved in cross-link formation by engineering the PTM found in GlbN into a chemically different, but structurally related trHb, CtrHb. I also provide an initial in vitro characterization of THB1 and identify a rare heme ligation scheme in this protein, the functional implications of which are yet to be determined.

1.4 References

(1) Vinogradov, N. S., Hoojewis, D., Bailly, X., Mizuguchi, K., Dewilde, S., Moens, L., and Vanfleteren, J. R. (2007) A model of globin evolution. *Gene 398*, 132-142.

(2) Burmester, T. and Hankeln,, T. (2014) Function and evolution of vertebrate globins. *Acta Physiologica, 221*, 501-514.

(3) Vinogradov, S. N., Bailly, X., Smith, D. R., Tinajero-Trejo, M., Poole, R. K., and Hoogewijs. (2013) Microbial eukaryote globins. *Advances in Microbial Physiology, 63*, 391-446.

(4) Johnson, E. A. and Lecomte, J. T. J. (2013) The globins of cyanobacteria and algae. *Advances in Microbial Physiology, 63*, 195-272.

(5) Schaer, D. J., Buehler, P. W., Alayash, A. I., Belcher, J. D., Vercellotti, G. M. (2013) Hemolysis and free hemoglobin revisited: exploring hemoglobin and hemin scavengers as a novel class of therapeutic proteins. *Blood 121*, 1276-1284.

(6) Battistuzzi, G., Stampler, J., Belli, M., Vlastis, J., Soudi, M., Furtmüller, P. G., and Obinger, C. (2011) Influence of covalent heme-protein bonds on the redox thermodynamics of human myeloperoxidase. *Biochemistry 50*, 7987-7994.

(7) Brogioni, S., Stampler, J., Furtmüller, P. G., Feis, A., Obinger, C., and Smulevich, G. (2008) The role of the sulfonium linkage in the stabilization of the ferrous form of myeloperoxidase: A comparison with lactoperoxidase. *Biochimica et Biophysica Acta-Proteins and Proteomics, 1784*, 843-849.

(8) Zederbauer, M., Furtmüller, P. G., Brogioni, S., Jakopitsch, C., Smulevich, G., and Obinger, C. (2007) Heme to protein linkages in mammalian peroxidases: impact on spectroscopic, redox and catalytic properties. *Natural Products Reports, 24*, 571-584.

(9) Huang, L., Wojciechowski, G., and Ortiz de Montellano, P.R. (2006) Role of heme-protein covalent bonds in mammalian peroxidases: Protection of the heme by a single engineered heme-protein link in horseradish peroxidase. *Journal of Biological Chemistry, 281*, 18983-18988.

(10) Huang, L. and Ortiz de Montellano, P.R. (2006) Heme-protein covalent bonds in peroxidases and resistance to heme modification during halide oxidation. *Archives of Biochemistry and Biophysics, 446*, 77-83.

(11) Babbitt, S. E., San Fransico, B., Mendez, D. L., Lukat-Rodgers, G. S., Rodgers, K. R., Bretsnyder, E. C., and Kranz, R. G. (2014) Mechanisms of mitochondrial holocytochrome c synthase and the key roles played by cysteins and histidine of the heme attachement site, Cys-*XX*-Cys-His. *Journal of Biological Chemistry, 289*, 28795-28807.

(12) Tomlinson, E. J. and Ferguson, S. J. (2000) Conversion of a *c* type cytochrome to a *b* type that spontaneously forms *in vitro* from apo protein and heme: Implications for *c* type cytochrome biogenesis and folding. *Proceedings of the National Academy of Sciences, 97*, 5156-5160.

(13) Tomlinson, E. J. and Ferguson, S. J. (2000) Loss of either of the two heme-binding cysteines from a class I c-type cytochrome has a surprisingly small effect on physicochemical properties. *Journal of Biological Chemistry, 275*, 32530-32534.

(14) Vu, B. C., Jones, A. D., and Lecomte, J. T. J. (2002) Novel histidine-heme covalent linkage in a hemoglobin. *Journal of the American Chemical Society, 124*, 8544-8545.

(15) Vu, B. C., Vuletich, D. A., Kuriakose, S. A., Falzone, C. J., and Lecomte, J. T. J. (2004) Characterization of the heme-histidine cross-link in cyanobacterial hemoglobins from *Synechocystis* sp. PCC 6803 and *Synechococcus* sp. PCC 7002. *Journal of Biological Inorganic Chemistry, 9*, 183-194.

(16) Poulos, T. L. (1996) The role of the proximal ligand in heme enzymes. *Journal of Biological Inorganic Chemistry, 1*, 356-359.

(17) Hvitved, A. N., Trent III, J. T., Premer, S. A., and Hargrove, M. S. (2001) Ligand binding and hexacoordination in *Synechocystis* hemoglobin. *J Biol Chem, 276*, 34714-34721.

(18) Kiger, L., Tilleman, L., Geuens, E., Hoogewijs, D., Lechauve, C., Moens, L., Dewilde, S., and Marden, M. C. (2011) Electron transfer function versus oxygen delivery: A

comparative study for several hexacoordinated globins across the animal kingdom. *PLoS ONE, 6*, e20478

(19) Kakar, S., Hoffman, F. G., Storz, J. F., Fabian, M., and Hargrove, M. S. (2010) Structure and reactivity of hexacoordinate hemoglobins. *Biophysical Chemistry, 152*, 1-14.

(20) Nagai, M., Yubisui, T., and Yoneyama, Y. (1980) Enzymatic reduction of hemoglobins M Milwaukee-1 and M Saskatoon by NADH-Cytochrome b_5 reductase and NADPH-flavin reductase purified from human erythrocytes. *Journal of Biological Chemistry, 255*, 4599-4602.

(21) Battistuzzi, G., Borsari, M., Cowan, J. A., Ranieri, A., and Sola, M. (2002) Control of cytochrome c redox potential: Axial ligation and protein environment effects. *Journal of the American Chemical Society, 124*, 5315-5324.

(22) Geuens, E., Hoogewijs, D., Nardini, M., Vinck, E., Pesce, A., Kiger, L., Fago, A., Tilleman, L., De Henau, S., Marden, M. C., Weber, R. E., Van Doorslaer, S., Vanfleteren, J., Moens, L., Bolognesi, M., and Dewilde, S. (2010) Globin-like proteins in *Caenorhabditis elegans*: *in vivo* localization, ligand binding and structural properties. *BMC Biochemistry, 11*.

(23) Sturms, R., Kakar, S., Trent III, J. T., and Hargrove, M. S. (2010) *Trema* and *Parasponia* hemoglobins reveal convergent evolution of oxygen transport in plants. *Biochemistry, 49*, 4085-4093.

(24) Falzone, C. J., Vu, C. B., Scott, N. L., and Lecomte, J. T. J. (2002) The solution structure of the recombinant hemoglobin from the cyanobacterium *Synechocystis* sp. PCC 6803 in its hemichrome state. *Journal of Molecular Biology, 324*, 1015-1029.

(25) Scott, N. L. and Lecomte, J. T. J. (2000) Cloning, expression, purification, and preliminary characterization of a putative hemoglobin from the cyanobacterium *Synechocystis* sp. PCC 6803. *Protein Science, 9*, 587-597.

(26) Nothnagel, H. J., Love, N., and Lecomte, J. T. J. (2009) The role of the heme distal ligand in the post-translational modification of *Synechocystis* hemoglobin. *Journal of Inorganic Biochemistry, 103*, 107-116.

(27) Nothnagel, H. J., Preimesberger, M. R., Pond. M. P., Winer, B. Y., Adney, E. M., and Lecomte, J. T. J. (2011) Chemical reactivity of *Synechococcus* sp. PCC 7002 and *Synechocystis* sp. PCC 6803 hemoglobins: covalent heme attachment and bishistidine coordination. *Journal of Biological Inorganic Chemistry, 16*, 539-552.

(28) Trent III, J. T., Kundu, S., Hoy, J. A., and Hargrove, M. S. (2004) Crystallographic analysis of *Synechocystis* cyanoglobin reveals the structural changes accompanying ligand binding in a hexacoordinate hemoglobin. *Journal of Molecular Biology, 341*, 1097-1108.

(29) Wenke, B. B., Lecomte, J. T. J., Héroux, A., and Schlessman, J., L. (2014) The 2/2 hemoglobin from the cyanobacterium *Synechococcus* sp. PCC 7002. *Proteins, 82*, 528-534.

(30) Pesce, A., Couture, M., Dewilde, S., Guertin, M., Yamauchi, K., Ascenzi, P., Moens, L., and Bolognesi, M. (2000) A novel two-over-two α-helical sandwich fold is characteristic 2of the truncated hemoglobin family. *EMBO Journal, 19*, 2424-2434.

(31) Vuletich, D. A. and Lecomte, J. T. J. (2006) A phylogenetic and structural analysis of truncated hemoglobins. *Journal of Molecular Evolution, 62*, 196-210.

(32) Ouellet, H., Ouellet, Y., Richard, C., Labarre, M., Wittenberg, B., Wittenberg, J., Guertin, M. (2002) Truncated hemoglobin HbN protects *Mycobacterium bovis* from nitric oxide. *Proceedings of the National Academy of Sciences, 99*, 5902-5907.

(33) Scott, N. L., Xu, Y., Shen, G., Vuletich, D. A., Falzone, C. J., Li, Z., Ludwig, M., Pond, M. P., Preimesberger, M. R., Bryant, D. A., and Lecomte, J. T. J. (2010) Functional characterization of the 2/2 hemoglobin from *Synechococcus* sp. PCC 7002. *Biochemistry, 49*, 7000-7011.

(34) Vu, C. B., Nothnagel, H. J., Vuletich, D. A., Falzone, C. J., and Lecomte, J. T. J. (2004) Cyanide binding to hexacoordinate cyanobacterial hemoglobins: Hydrogen-bonding network and heme pocket rearrangement in ferric H117A *Synechocystis* hemoglobin. *Biochemistry, 43*, 12622-12633.

(35) Hoy, J. A., Smagghe, B. J., Halder, P., and Hargrove, M. S. (2007) Covalent heme attachment in *Synechocystis* hemoglobin is required to prevent ferrous heme dissociation. *Protein Science, 16*, 250-260.

(36) Preimesberger, M. R., Wenke, B. B., Gilevicius, L., M., Pond, and Lecomte, J. T. J. (2013) Facile heme vinyl posttranslational modification in a hemoglobin. *Biochemistry, 52*, 3478-3488.

(37) Couture, M., Chamberland, H., St-Pierre, B., Lafontaine, J., and Guertin, M. (1994) Nuclear genes encoding chloroplast hemoglobins in the unicellular green alga *Chlamydomomans eugametos*. *Molecular and General Genetics, 243*, 185-197.

(38) Couture, M. and Guertin, M. (1996) Purification and spectroscopic characterization of a recombinant chloroplastic hemoglobin from the unicellular green alga *Chlamydomomans eugametos*. *European Journal of Biochemistry, 242*, 779-787.

(39) Milani, M., Oullete, Y., Oullete, H., Guertin, M., Boffi, A., Antonini, G., Bocedi, A., Mattu, M.,Bolognesi, M., and Ascenzi, P. (2004) Cyanide binding to truncated hemoglobins: A crystallographic and kinetic study. *Biochemistry, 43*, 5213-5221.

(40) Das, T. P., Couture, M., Lee, H. C., Peisach, J., Rousseau, D. L., Wittenberg, B. A., Wittenberg, J. B., and Guertin, M. (1999) Identification of the ligands to the ferric heme of *Chlamydomonas* chloroplast hemoglobin: Evidence for ligation of Tyrosine-63 (B10) to the heme. *Biochemistry, 38*, 15360-15368.

(41) Couture, M., Das, T. P., Lee, H. C., Peisach, J., Rousseau, D. L., Wittenberg, B. A., Wittenberg, J. B., and Guertin, M. (1999) *Chlamydomonas* chloroplast ferrous hemoglobin: Heme pocket structure and reactions with ligands. *Journal of Biological Chemistry, 274*, 6898-6910.

(42) Dent, R. M., Haglund, C. M., Chin, B. L., Kobayashi, M. C., and Niyogi, K. K. (2005) Functional genomics of eukaryotic photosynthesis using insertional mutagenesis of *Chlamydomonas reinhardtii*. *Plant Physiology, 137*, 545-556.

(43) Grovenstein, P. B., Wilson, D. A., Lennox, C. G., Smith, K. P., Contractor, A. A., Mincey, J. L., Lankford, K. D., Smith, J. M., Haye, T. C., and Mitra, M. (2013) Identification and molecular characterization of a novel *Chlamydomonas reinhardtii* mutant defective in chlorophyll biosynthesis. *F1000Research, 2*.

(44) Pazour, G. J., Wilkerson, C. G., and Witman, G. B. (1998) A dynein light chain is essential for the retrograde particle movement of intraflagellar transport (IFT). *Journal of Cell Biology, 141*, 979-992.

(45) Blacque, O. E., Cevik, S., and Kaplan, O. I. (2008) Intraflagellar transport: From molecular characterisation to mechanism. *Frontiers in Bioscience, 13*, 2633-2562.

(46) Tolleter, D., Ghysels, B., Alric, J., Petroutsos, D., Tolstygina, I., Krawietz, D., Happe, T., Auroy, P., Adriano, J-M., Beyly, A., Cuiné, S., Plet, J., Reiter, I. M., Genty, B., Cournac, L., Hippler, M., and Peltier, G. (2011) Control of hydrogen photoproduction by the proton gradient generated by cyclic electron flow in *Chlamydomonas reinhardtii*. *Plant Cell, 23*, 2619-2630.

(47) Merchant, S. S., Prochnik, S. E., Vallon, O., Harris, E. H., Karpowicz, S. J., Witman, G. B., Terry, A., Salamov, A., Fritz-Laylin, L. K., Marechal-Drouard, L., Marshall, W. F., Qu, L. H., Nelson, D. R., Sanderfoot, A. A., Spalding, M. H., Kapitonov, V. V., Ren, Q., Ferris, P., Lindquist, E., Shapiro, H., Lucas, S. M., Grimwood, J., Schmutz, J., Cardol, P., Cerutti, H., Chanfreau, G., Chen, C. L., Cognat, V., Croft, M. T., Dent, R., Dutcher, S., Fernandez, E., Fukuzawa, H., Gonzalez-Ballester, D., Gonzalez-Halphen, D., Hallmann, A., Hanikenne, M., Hippler, M., Inwood, W., Jabbari, K., Kalanon, M., Kuras, R., Lefebvre, P. A., Lemaire, S. D., Lobanov, A. V., Lohr, M., Manuell, A., Meier, I., Mets, L., Mittag, M., Mittelmeier, T., Moroney, J. V., Moseley, J., Napoli, C., Nedelcu, A. M., Niyogi, K., Novoselov, S. V., Paulsen, I. T., Pazour, G., Purton, S., Ral, J. P., Riano-Pachon, D. M., Riekhof, W., Rymarquis, L., Schroda, M., Stern, D., Umen, J., Willows, R., Wilson, N., Zimmer, S. L., Allmer, J., Balk, J., Bisova, K., Chen, C. J., Elias, M., Gendler, K., Hauser, C., Lamb, M. R., Ledford, H., Long, J. C., Minagawa, J., Page, M. D., Pan, J., Pootakham, W., Roje, S., Rose,

A., Stahlberg, E., Terauchi, A. M., Yang, P., Ball, S., Bowler, C., Dieckmann, C. L., Gladyshev, V. N., Green, P., Jorgensen, R., Mayfield, S., Mueller-Roeber, B., Rajamani, S., Sayre, R. T., Brokstein, P., Dubchak, I., Goodstein, D., Hornick, L., Huang, Y. W., Jhaveri, J., Luo, Y., Martinez, D., Ngau, W. C., Otillar, B., Poliakov, A., Porter, A., Szajkowski, L., Werner, G., Zhou, K., Grigoriev, I. V., Rokhsar, D. S., and Grossman, A. R. (2007) The *Chlamydomonas* genome reveals the evolution of key animal and plant functions. *Science, 318*, 245-250.

(48) Molnar, A., Bassett, A., Thuenemann, E., Schwach, F., Karkare, S., Ossowski, S., Weigel, D., and Baulcombe, D. (2009) Highly specific gene silencing by artificial microRNAs in the unicellular alga *Chlamydomonas reinhardtii*. *Plant Journal, 58*, 165-174.

(49) Vinogradov, S. N., Fernández, I., Hoogewijs, D., and Arredondo-Peter, Raúl. (2011) Phylogenetic relationships of 3/3 and 2/2 hemoglobins in Archaeplastida genomes to bacterial and other eukaryotic hemoglobins. *Molecular Plant, 4*, 42-58.

(50) Hemschemeier, A., Duner, M., Casero, D., Merchant, S. S., Winkler, M., and Happe, T. (2013) Hypoxic survival requires a 2-on-2 hemoglobin in a process involving nitric oxide. *Proceedings of the National Academy of Sciences, 110*, 10854-10859.

(51) Sanz-Luque, E., Ocaña-Calahorro, F., de Montaigu, A., Chamizo-Ampudia, A., Llamas, Á., Galván, A., and Fernández, E. (2015) THB1, a truncated hemoglobin, modulates nitric oxide levels and nitrate reductase activity. *Plant Journal, 81*, 467-479.

(52) Lechtrek, K-F., Johnson, E. C., Sakai, T., Cochran, D., Ballif, B. A., Rush, J., Pazour, G. J., Ikebe, M., and Witman G. B. (2009) The *Chlamydomonas reinhardtii* BBSome is an IFT cargo required for export of specific signaling proteins from flagella. *Journal of Cell Biology, 187*, 1117-1132.

(53) Johnson, E. A. and Lecomte, J. T. J. (2014) Characterization of the truncated hemoglobin THB1 from protein extracts of *Chlamydomonas reinhardtii*. *F1000Research, 3*.

Chapter 2

Introduction of a covalent histidine–heme linkage in a hemoglobin: A promising tool for heme protein engineering

*This chapter was previously published in the *Journal of Inorganic Biochemistry* (**Rice S.L.**, *et al.*, 2014). Figures 2.1-2.3, 2.7 and 2.8 were contributed by coauthors, all other results in this chapter represent original work. For this dissertation, modifications were made to the text and additional figures were added (Fig. 2.5, 2.7, 2.9, and 2.10).

Author Contributions

Selena L. Rice: designed research, constructed pET3c-H19 expression plasmid, performed mutagenesis, purified proteins, performed optical and ECL experiments, performed NMR sample preparation and assisted in NMR data collection, wrote the paper

Matthew R. Preimesberger: designed research, collected and analyzed NMR data, performed structural analysis, wrote the paper

Juliette T.J. Lecomte: designed research, analyzed data, and wrote the paper

2.1 Abstract

The hemoglobins of the cyanobacteria *Synechococcus* and *Synechocystis* (GlbNs) are capable of spontaneous and irreversible attachment of the *b* heme to the protein matrix. The reaction, which saturates the heme 2-vinyl by addition of a histidine residue, is reproduced in vitro by preparing the recombinant apoprotein, adding ferric heme, and reducing the iron to the ferrous state. Spontaneous covalent attachment of the heme is potentially useful for protein engineering purposes. Thus, to explore whether the histidine–heme linkage can serve in such applications, we attempted to introduce it in a test protein. We selected as our target the heme domain of *Chlamydomonas eugametos* LI637 (CtrHb), a eukaryotic globin that exhibits less than 50% sequence identity with the cyanobacterial GlbNs. We chose two positions, 75 in the FG corner and 111 in the H helix, to situate a histidine near a vinyl group. We characterized the proteins with gel electrophoresis, absorbance spectroscopy, and NMR analysis. Both T111H and L75H CtrHbs reacted upon reduction of the ferric starting material containing cyanide as the distal ligand to the iron. With L75H CtrHb, nearly complete (> 90%) crosslinking was observed to the 4-vinyl as expected from the X-ray structure of wild-type CtrHb. Reaction of T111H CtrHb also occurred at the 4-vinyl in a 60% yield, indicating a preference for the flipped heme orientation in the starting material. The work suggests that the His–heme modification will be applicable to the design of proteins with a non-dissociable heme group.

2.2 Introduction

Proteins requiring a *b* heme at their active site hold this essential molecule with multiple interactions. Protein–heme contacts, heme exposure to solvent, coordination of protein residues to the heme iron[1] and apoprotein structure[2] all contribute to the energetics of heme binding. As a consequence, the heme affinity of a given protein depends on solution conditions and properties such as the redox state of the iron[3] and the nature of its exogenous ligands[4,5]. These last two features can dominate heme affinity. For example, soluble guanylate cyclase, which has an axial histidine ligand, loses heme upon oxidation from the ferrous to the ferric state[6], whereas Dap1p, which has an axial tyrosine ligand, exhibits enhanced heme loss upon reduction from the ferric state to the ferrous state[7]. Various enzymes experience heme loss upon exposure to nitric oxide ($NO^{\bullet}$)[8].

In part because of the toxicity of free heme, enzymes, gas sensors, and gas or small molecule carriers that use a *b* heme have evolved to maintain sufficient affinity as they visit the various ligation and redox states required by their physiological role. Uncontrolled heme loss occurs rarely. However, the structural features dictating heme affinity and reactivity are intimately intertwined. Thus, heme retention can be problematic when modifying native heme proteins[9,10] or designing artificial ones[11]. In those instances, optimization for the desired chemical properties may compromise heme binding and vice versa.

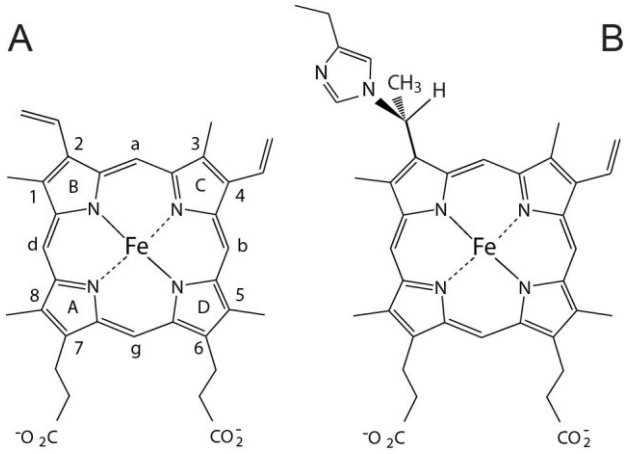

Fig. 2.1 Structure of heme b and the PTM (A) The structure and nomenclature of the *b* heme (iron-protoporphyrin IX). Heme orientational isomerism involves a 180° rotation about the α–γ axis. **(B)** The heme PTM present in GlbN. His117, in the H helix, adds to the 2-vinyl group. Addition can also occur to the 4-vinyl group when the heme is in the flipped orientation[21,22].

Covalent attachment of the heme to the protein matrix offers a versatile solution to heme loss. Such post-translational modification (PTM) grants several advantages aside from heme retention, notably correct heme positioning and increased thermodynamic stability[12]. In addition, the PTM allows for a departure from the typical composition of a *b* heme cavity, i.e., the introduction of polar residues and weak axial ligands. The heme group, shown in Fig. 2.1A offers several possible points for crosslinking to the protein, the most common of which are the vinyl substituents. In *c* cytochromes, reductive reaction with cysteines produces thioether bridges[13]. The formation of these linkages in the cell is controlled by dedicated enzymatic machineries that ensure the correct localization of the apoprotein prior to heme binding and modification[14,15]. This complicated process can be harnessed to prepare artificial cytochromes[16,17], and thus far the molecular biology procedure to producing the thioether linkages surpasses non-enzymatic methods[18,19]. For purposes of creating new proteins with non-dissociable heme and studying the effects of heme crosslinking, a

chemical approach avoiding the use of cysteines would be advantageous. We have shown previously that the globins from two cyanobacteria (GlbNs from *Synechocystis* sp. PCC 6803 and *Synechococcus* sp. PCC 7002) can undergo enzyme-free heme attachment to a histidine, and we now explore the suitability of this reaction for protein engineering applications.

The heme modification in GlbN is the alkylation of histidine Nε by a heme vinyl Cα as shown in Fig. 2.1B. Several studies have defined the conditions under which the reaction occurs and have amounted to a plausible mechanism[20,21]. Following reduction to the ferrous state, the key steps are the protonation of the heme vinyl Cβ followed by (or in concert with) a nucleophilic attack by a neutral histidine. In wild-type (WT) ferrous GlbNs, the modification reaches completion in a few seconds at neutral pH and is accelerated by decreasing pH as long as acid denaturation is avoided. We have monitored the reaction in variants of GlbN and proposed that the main determinant of linkage formation is sterics, i.e., whether a productive orientation of the vinyl and histidine ring can be adopted. This is evident in the preparation of a protein containing the WT crosslink (H117 to heme 2-vinyl) and an engineered crosslink (L79H to heme 4-vinyl)[22]. Additionally, we have noted that certain ligands to the ferrous state such as the π-acids CO[21], NO$^{\bullet}$ and O_2 (unpublished observations) inhibit the reaction, presumably because of their propensity for a redistribution of electron density of the ferrous heme (e.g., formation of Fe(III)–O_2^- from Fe(II)–O_2,[23]) disfavoring vinyl protonation.

The consequences of the linkage for the reactivity of the heme group have been under investigation as well. A variant of GlbN unable to form the PTM loses the ferrous heme more readily than the ferric heme, which has led to the proposition that the linkage is a physiological necessity[24]. In WT GlbNs, the PTM enhances substantially the thermal stability of the holoprotein[25]. On the other hand, the PTM appears to have only moderate

effects on the structure of GlbN and its chemical properties such as electron self-exchange rate, redox potential[26], susceptibility to H_2O_2-mediated degradation[21], backbone dynamics[25,27], and response to pressure[28]. In view of these observations, the histidine–heme linkage appears as a mostly benign modification, well suited for protein engineering purposes. However, the general utility of the linkage must be demonstrated by introduction into a protein different from the two original cyanobacterial globins.

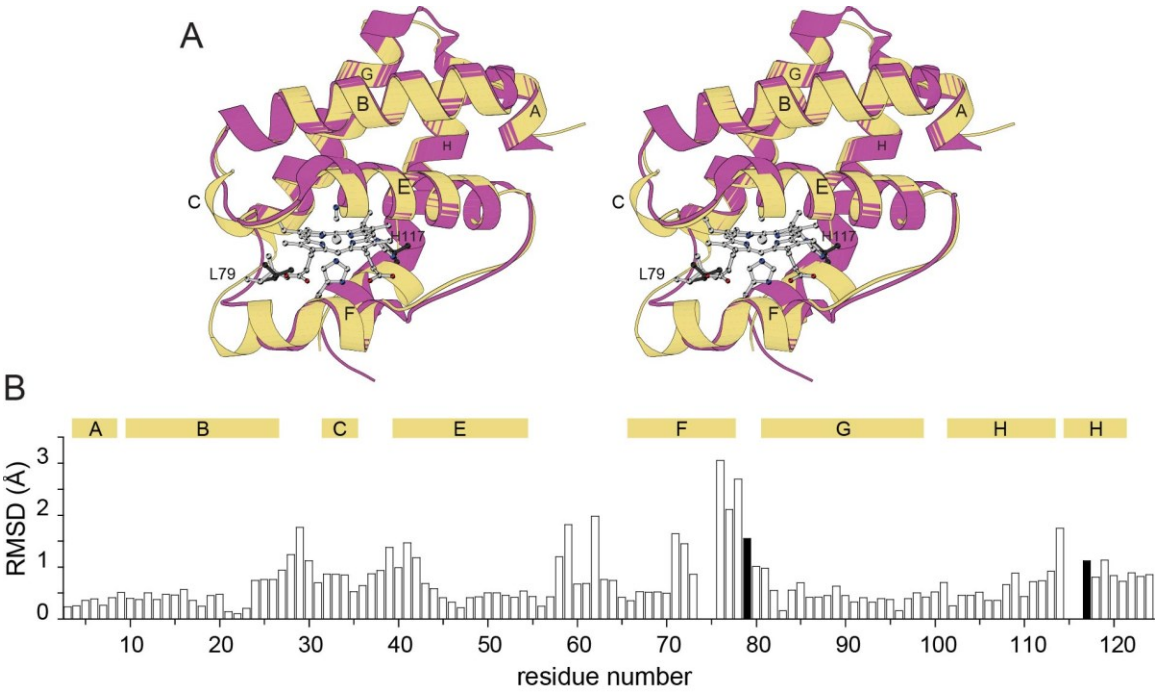

Fig. 2.2 Structural comparison of cyanomet *C. eugametos* L1637 CtrHb (PDB ID: 1DLY) **with cyanomet *Synechocystis* sp. PCC 6803 GlbN-A** (PDB ID: 1S69)**. (A)** Stereo view of the superimposition of the two structures. *Synechocystis* GlbN-A is in yellow with L79 and H117 shown in light gray sticks. Dark gray sticks mark L75 and T111 in CtrHb. **(B)** Cα rmsd for the superimposition shown in (A). The numbering is that of GlbN. The black vertical bars indicate the position of L79 and H117. The secondary structure of GlbN is indicated with horizontal bars above the rmsd values.

The heme domain of *Chlamydomonas eugametos* LI637, CtrHb, was chosen as a validation protein for several reasons. (1) CtrHb has been the focus of spectroscopic[23,29,30]

and structural[31] studies. The WT protein is therefore already well characterized. (2) Sequence identity with *Synechococcus* and *Synechocystis* GlbNs (Fig. 2.2) is a modest ~46% with differences distributed throughout the structure, including the heme cavity. (3) In GlbN, the WT reactive histidine is in the H helix (His117, at helical position "H16") and the engineered reactive histidine is in the FG corner (His79). A superimposition of the three-dimensional structures of cyanomet (ferric state with cyanide bound) CtrHb and post-translationally modified cyanomet *Synechocystis* GlbN (hereafter GlbN-A) (Fig. 2.2) reveals that CtrHb has two-residue deletions near the 79 and 117 sites of GlbN. (4) Unlike both GlbNs, CtrHb does not have a histidine that can reversibly coordinate the iron on the distal side. At neutral pH and in the ferrous state, CtrHb is primarily a 5-coordinate species[29]. Thus, CtrHb has distinct heme pocket composition, local backbone geometry, and iron coordination that render it a rigorous test case for the histidine–heme modification of the type depicted in Fig. 2.1B.

In this report, we inspected the reactivity of CtrHb variants with a histidine facing either the heme 2- or 4-vinyl group on the proximal side of the heme. We demonstrate that the histidine–heme modification can be successfully implanted in CtrHb. Although spontaneous crosslinking does not occur upon reduction to the ferrous state, the addition of cyanide prior to reduction promotes the reaction. The results support that histidine alkylation may be a generalizable reaction for the production of proteins containing a non-dissociable heme.

2.3 Materials and Methods

2.3.1 Plasmid construction and protein production

The gene coding for WT CtrHb (UNIPROTKB Q08753, residues 44–164, "H19" in reference[32]) was synthesized with 5'-*Nde*I and 3'-*Bam*HI restriction sites and inserted in a pJexpress 404 vector by DNA 2.0 (Menlo Park, CA). Because expression levels were low with this plasmid, WT and mutated CtrHb genes were subsequently cloned into a pET3c vector (Novagen, Inc., Madison, WI). Site directed mutagenesis was performed to introduce the T111H or L75H replacement using the QuikChange (Qiagen, Valencia, CA) protocol provided by the manufacturer and primers purchased from Integrated DNA Technologies (Coralville, IA). Restriction enzymes and ligase were from New England Biolabs (Ipswich, MA), and sequencing was performed by GENEWIZ, Inc. (South Plainfield, NJ).

E. coli BL21(DE3) cells (New England Biolabs) were used for overexpression of CtrHb. Cells were grown on M9 medium supplemented with ampicillin (Sigma-Aldrich, St. Louis, MO or Research Products International, Corp., Mount Prospect, IL). Induction was achieved by addition of 1 mM dioxane-free isopropyl β-D-1-thiogalactopyranoside (Santa Cruz Biotechnologies, Santa Cruz, CA). For uniformly labeled ^{15}N protein, $^{15}NH_4Cl$ (Sigma-Aldrich) was used as the sole nitrogen source.

2.3.2 CtrHb purification

WT and T111H CtrHbs were purified from inclusion bodies as described previously for *Synechocystis* GlbN[33]. The protocol calls for treatment of the harvested and washed inclusion bodies with 8 M urea, followed with apoprotein refolding by passage over a gel filtration column (Sephadex G-50 Fine, Sigma-Aldrich) equilibrated with 50 mM Tris, 50 □ M EDTA pH 8.0 at 4 °C. Further purification was performed by passage through an

anion exchange column (DEAE Sephacel, Sigma) either before or after addition of bovine hemin chloride (Fe(III)-protoporphyrin IX, Sigma/Alfa Aesar) to generate the ferric holoprotein. Elution was achieved with a 0–0.4 M NaCl gradient. Although WT and T111H CtrHbs could be lyophilized and resuspended without loss or damage, such was not the case for L75H CtrHb, and solutions of this protein were used immediately upon purification. The yields were ~15 mg/L for L75H CtrHb, ~39 mg/L for T111H CtrHb, and ~50 mg/L for WT CtrHb when the cells were grown in minimal medium.

Apoprotein concentrations were estimated using a calculated extinction coefficient of 10 mM^{-1} cm^{-1} at 280 nm. The optical spectra of the WT CtrHb in the ferric, ferrous, cyanomet, and ferrous cyanide states were comparable to those reported in the original work of Guertin and colleagues[29,32,34] (Table 2.2). The T111H and L75H replacements affected the spectral properties to varying degrees, with minimal effect on the cyanomet state (Fig. 2.5). Ferric holoprotein concentrations were determined on a per-heme basis with an extinction coefficient of 117 mM^{-1} cm^{-1} at 410 nm at neutral pH, back-calculated from the published WT cyanomet coefficient[34].

2.3.3. NMR sample preparation

Lyophilized protein was resuspended in either 100 or 250 mM phosphate buffer in H_2O or 100 mM phosphate in D_2O. 10% v:v D_2O was added to the H_2O samples. Protein concentration varied from ~0.6 mM to ~3 mM (final volume of ~300 μL). Sample pH ranged between 7.1 and 7.5. Iron reduction was performed by adding 3- to 13-fold excess sodium dithionite (DT, Sigma-Aldrich). Alternatively, freshly purified protein was concentrated, exchanged in the appropriate buffer, and used without lyophilization. Cyanomet CtrHb was generated by adding a 5-fold excess of potassium cyanide to ferric holoprotein solutions.

2.3.4 Heme modification

Stocks of ferric WT (as a negative control), T111H, and L75H CtrHbs were prepared either from lyophilized protein, or, in the case of L75H CtrHb, from freshly purified protein. A 5-fold excess of cyanide was added to each sample, followed by 20–30 min incubation at room temperature to ensure saturation of the heme site. An excess of DT (200- to 500-fold for optical samples or 3- to 13-fold for NMR samples) was then added to the solutions. Cyanomet CtrHb samples were incubated for ~3–8 h (WT and T111H) or ~0.5–2 h (L75H) and then oxidized by exposure to air or potassium ferricyanide. Aliquots of the total samples were saved at different stages of the process for optical characterization.

2.2.5 Hemochromogen and enhanced chemiluminescence assays

Reacted CtrHb samples were analyzed by the hemochromogen assay[35,36] for rapid assessment of *b* heme modification. Aliquots were taken from samples used for NMR analysis, diluted to reach an absorbance between 0.3 and 0.6 in the α/β region (500–600 nm), and treated as previously described[20] with basic pyridine followed by DT reduction. Absorbance measurements were performed on an AVIV Spectrophotometer 14DS UV-Vis (AVIV Biomedical Inc., Lakewood, NJ) as described previously[22].

Covalent heme attachment was detected by enhanced chemiluminescence (ECL)[37,38]. Samples of CtrHb were prepared for DT reduction in pair, one with cyanide present (referred to as "KCN+") and the other without cyanide (referred to as "KCN−"). CtrHb samples were also prepared with 10-fold excess imidazole (Sigma) or 10 mM azide (Sigma) as alternatives to cyanide as the distal iron ligand. *Synechocystis* GlbN treated with excess DT to generate GlbN-A[39] was used as a covalently-linked positive control. The ECL assay relies on the peroxidase activity of the heme group. This activity is inhibited by cyanide and high concentrations of either imidazole or azide. Prior to ECL detection, reduced samples

containing these ligands were treated by passage over a ~1.3 mL DEAE column. This procedure did not eliminate all exogenous ligand, and the ECL results for these samples are therefore only qualitative.

Electrophoresis was performed with Mini-PROTEAN® 16.5% Tris-Tricine Precast Gel (BIO-RAD, Hercules, CA). The protein samples (5 μM) were denatured by boiling for 10 min with SDS but in the absence of β-mercaptoethanol. After separation, the gels were thoroughly rinsed and exposed to the ECL reagent (Immobilon Western Chemiluminescent HRP (horseradish peroxidase) Substrate, Millipore, Billerica, MA) prepared per manufacturer's instructions. The ECL reaction was allowed to proceed for 7 min before applying the film (Carestream® Kodak® BioMax® light film, Sigma-Aldrich, St. Louis, MO). Exposure times were 30 s for samples containing no exogenous ligand and 10 s, 30 s, or 7 min for samples partially stripped of exogenous ligand. After the ECL procedure, gels were stained with Coomassie Blue for protein detection.

2.3.6 Reaction kinetics monitored by absorbance spectroscopy

Samples of WT, T111H, and L75H CtrHb containing ~4 μM protein were prepared in 100 mM phosphate buffer pH 7.0 from concentrated stocks (lyophilized WT and T111H) or freshly prepared protein (L75H). Five-fold excess KCN was added to the samples, and CN^- binding was monitored via electronic absorption spectroscopy. Approximately 500-fold excess DT was added to cyanide-saturated samples and reduction was monitored with spectra taken every 30 s for the first 10 min, every 2 min for the following 20 min, and every 5 min for the remaining 1.5 h. Time course experiments were performed on a Varian Cary 50 Bio UV-Vis spectrophotometer with acquisition parameters similar to those reported previously[22].

2.3.7 NMR spectroscopy

NMR data were acquired on Bruker AVANCE or AVANCE-II spectrometers operating at a ^{1}H Larmor frequency of 600.13 or 600.53 MHz, respectively, and each equipped with a cryoprobe. Reduction and reaction progress of cyanomet CtrHbs were monitored by ^{1}H 1D NMR spectroscopy with water presaturation. Reactants and products were additionally studied using ^{1}H-^{1}H NOESY (nuclear Overhauser effect spectroscopy), DQF-COSY (double-quantum filtered correlation spectroscopy), TOCSY (total correlation spectroscopy) with TOWNY (total correlation spectroscopy without NOESY) sequence, and natural abundance ^{1}H-^{13}C HMQC (heteronuclear multiple quantum correlation) spectra[40-42]. These data were sufficient to assign most heme resonances and locate many conserved heme pocket residues of each cyanomet CtrHb. Labile protons were identified by acquisition of the same data in 99.9% D_2O. ^{1}H-^{15}N HSQC (heteronuclear single quantum correlation) and long-range (lr) histidine selective ^{1}H-^{15}N HMQC spectra[43] were used to confirm the assignments of the engineered and native histidines within WT, T111H and L75H cyanomet CtrHbs[21,22]. ^{1}H chemical shifts were referenced to DSS (4,4-dimethyl-4-silapentane-1-sulfonic acid) indirectly through the water resonance (4.76 ppm at 298 K); ^{13}C and ^{15}N chemical shifts were referenced as described in[44]. NMR data were processed with TopSpin 2.1 or NMRPipe[45]. Spectral analysis was conducted with Sparky 3[46].

2.4 Results

2.4.1 Choice and preparation of CtrHbs

The selection of sites for histidine introduction was guided by inspection of the CtrHb and GlbN structures (Fig. 2.2). A significant proportion of CtrHb molecules contain the heme group in a "flipped" orientation that interchanges pyrroles A and B with pyrroles

D and C, respectively[31]. These two forms of the protein are referred to as "major" and "minor" heme rotational isomers according to their relative population at equilibrium. The X-ray structure (PDB ID: 1DLY[31]) is that of the major isomer. The two heme conformations effectively double the number of vinyl geometries available for histidine addition. Minimal modeling (amino acid replacement in 1DLY and optimization with UCSF Chimera[47]) suggests that a histidine at position 111, the closest equivalent to H117, can reach the heme 2-vinyl group as positioned in the major heme rotational isomer. The favored rotameric state of H111 points the ring away from the heme toward solvent and generates few clashes. Another potentially reactive site, facing the 4-vinyl group of the major heme rotational isomer, was identified at position 75 as the equivalent of H79 in L79H GlbN. At this position, clashes are predicted regardless of histidine rotameric state. Sites 75 and 111 were chosen despite their suboptimal geometric properties for lack of better candidates.

The apoproteins of WT CtrHb and its L75H and T111H variants aggregated into inclusion bodies during *E. coli* cell growth. Purification included unfolding in urea, refolding over a size-exclusion column, and reconstitution with ferric heme. For WT and T111H CtrHb, stoichiometric amounts of heme were added prior to a final purification step by anion exchange chromatography. L75H CtrHb had low ferric heme affinity, and passage through this last column resulted in substantial heme loss. To minimize this problem, heme was titrated to a slightly sub-stoichiometric level as the last step of holoprotein preparation, after apoprotein purification by anion exchange chromatography. It is likely that the presence of H75 disrupts the hydrophobic packing near the heme and interferes with heme binding. This was also the proposed explanation for the low heme affinity of the L79H variants of *Synechocystis* GlbN[22].

2.4.2 NMR characterization of cyanomet CtrHbs

Ferric CtrHbs to which KCN was added to generate the cyanomet state ($S = 1/2$) yielded high quality NMR spectra. Fig. 2.3A, B, and C show the ^{1}H 1D spectrum of cyanomet WT CtrHb and the T111H and L75H variants. In all cases, two sets of resonances are detected per protein. These arise from the heme rotational isomers, which typically exchange slowly on the chemical shift time scale[48,49]. Assignments of most heme resonances of both isomers in WT CtrHb and the T111H and L75H variants were obtained by established procedures[50]. Portions of spectra with representative through-bond and through-space connectivities are shown in Appendix Fig. A1–A8. Heme and protein assignments confirm that in WT, T111H, and L75H cyanomet CtrHbs, the major isomer corresponds to approximately 60–70% of the sample and has the heme positioned as in the crystallographic WT structure (1DLY[31], Appendix Fig. A9A–F). Heme ^{1}H chemical shifts of WT and variant cyanomet CtrHbs are listed in Table 2.1.

Inspection of Fig. 2.3 shows that at neutral pH the histidine replacement at position 111 perturbs the spectrum more profoundly than at position 75. In the major heme isomer of T111H CtrHb, the substituents of the B pyrrole undergo a relatively large chemical shift perturbation, apparently related to the reorientation of the 2-vinyl group from a "*cis*"-like conformation in WT CtrHb (i.e., with Cβ out of the heme plane and pointing toward the 3-CH_3, Appendix Fig. A1) to a "*trans*"-like conformation (i.e., Cβ pointing toward the 1-CH_3, Appendix Fig. A4). NOEs are detected between H111 Hδ2 and the heme 1-CH_3, whereas H111 Hε1 makes dipolar contact with F48 Hζ. The geometry is consistent with an outward position of the histidine Nε (g^- rotameric state) and forecasts a low probability for reaction with the 2-vinyl Cα. In the minor isomer, H111 Hδ2 contacts the 4-vinyl $H\beta_{cis}$ and exhibits the same NOE to F48, in support of a similar conformation for H111 in both major and

minor isomers. ^{1}H-^{15}N lr-HMQC data collected at neutral pH do not reveal the H111 spin system (Appendix Fig. A10), presumably because of broadening due to exchange between neutral and protonated states.

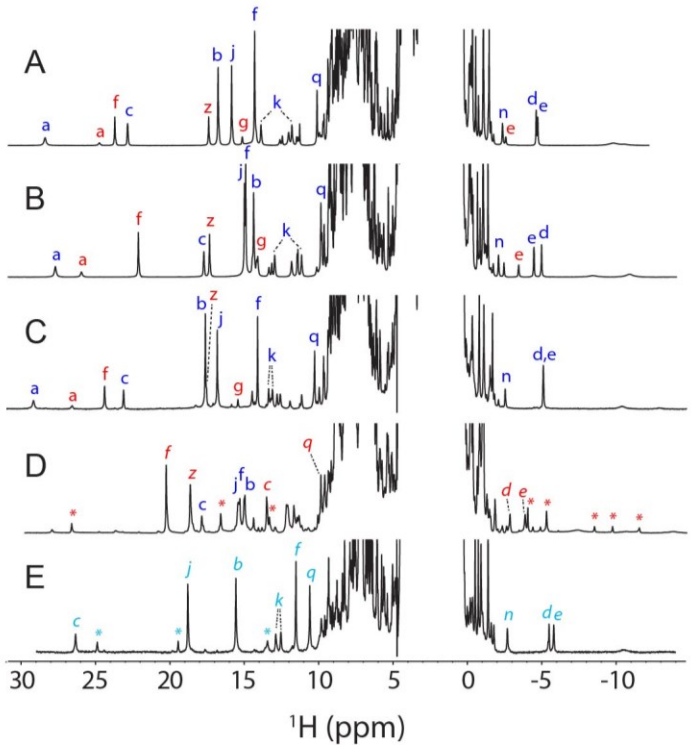

Fig. 2.3 Comparison of WT, T111H, and L75H cyanomet CtrHb ^{1}H NMR spectra. (A–C). Spectra collected prior to DT treatment. The major and minor heme orientational isomers are indicated with blue and red letters, respectively. **(A)** Wild-type cyanomet CtrHb (72% major, 28% minor). **(B)** T111H cyanomet CtrHb (67% major, 33% minor). **(C)** L75H cyanomet CtrHb (62% major, 38% minor). (d–e). Spectra collected after DT treatment and reoxidation. **(D)** T111H cyanomet CtrHb-A[4] product mixture. The predominant form (~60%, H111 reaction with the 4-vinyl group) is marked with red italics. The spectrum also contains 25% of the unreacted major isomer (starting material, b, blue letters), and a small amount of a third species (marked with red *). **(E)** L75H cyanomet CtrHb-B product (~90%, H75 reaction with the 4-vinyl group). A second product species (10%, likely H75 reaction with the 2-vinyl group) is marked with cyan *. Peak labeling: a, Tyr20 OηH; b, heme 1-CH_3; c, heme 2-vinyl Hα; d, e, heme 2-vinyl $H\beta_{cis}$, $H\beta_{trans}$; f, heme 3-CH_3; g, heme 4-vinyl Hα; j, heme 5-CH_3; k, heme 6-propionate Hα, Hα'; n, heme 7-propionate Hβ; q,Tyr20 CεHs; z, heme 8-CH_3.

Table 2.1 Heme and engineered histidine chemical shifts of WT, T111H, and L75H cyanomet CtrHbs[a].

	WT	WT*	T111H	T111H*[b]	L75H	L75H*
1-CH_3	16.77	3.2	14.38	3.13?	17.64	
2-v α	22.87	12.46	17.75	13.20	23.14	12.85
2-v β_c, β_t	−4.55, −4.65	−1.69, −2.49	−4.84, −4.34	−2.34, −3.32	−5.10, −5.11	−1.11, −1.42
3-CH_3	14.35	23.71	14.97	22.08	14.17	24.42
4-v α	6.68	15.17	7.04	14.23	6.59	15.46
4-v β_c, β	0.29, 0.58	−1.53, −0.12	0.38, 0.72	−1.13, −0.05	0.33, 1.12	−1.81, −0.47
5-CH_3	15.87	5.65	15.02	6.02?	16.83	6.17?
6-p α, α'	13.88, 11.76	9.35, 2.75	12.96, 11.16	9.28, 2.77	13.35, 13.08	8.69, 3.60
6-p β, β'	0.32, −0.98	−0.84, −1.53	0.30, −0.99	−1.63, −0.89	0.09, −1.06	−1.27, −2.08
7-p α, α'	7.84, 3.68	14.21, 11.38	7.97, 4.57	14.46, 11.44	7.06, 3.66	12.79, 11.90
7-p β, β'	−1.34, −2.31	1.00, −0.22	−1.99, −1.08	0.59, −0.68	−1.56, −2.53	0.62, −0.42
8-CH_3	6.17	17.42	7.49	17.36	5.91	17.64
H111 Hε1, Hδ2	n/a	n/a	7.86, 7.28	7.91, 7.32	n/a	n/a
H75 Hε1, Hδ2	n/a	n/a	n/a	n/a	9.43, 6.29	
H75 Nδ1, Nε2	n/a	n/a	n/a	n/a	252.1, 163.0	

[a] pH 7.2, 298 K.

[b] A * refers to the minor heme orientational isomer. A ? indicates a tentative assignment.

The heme chemical shifts of cyanomet L75H CtrHb form a pattern similar to that of WT CtrHb. The side chain of H75 in the major isomer was identified by comparison with WT spectra; the unusual Hε1 and Hδ2 chemical shifts (9.30 ppm and 6.15 ppm, respectively) reflect paramagnetic and heme ring current contributions. NOEs to the heme and proximal histidine further define the position of the imidazole ring (not shown). Observed contacts

are between H75 Hε1 and H68 (proximal histidine) Hβs, and between H75 Hδ2 and the heme 3-CH_3 and 4-vinyl. The 4-vinyl has a *trans*-like orientation (i.e., Cβ pointing toward the 3-CH_3, Appendix Fig. A7, and analogous to the WT and T111H variant, Appendix Fig. A1and A4, respectively). The data are consistent with a g^- rotameric state, which orients the imidazole ring toward the heme and may favor reaction. Comparison of WT and L75H ^{1}H-^{15}N lr-HMQC spectra confirms the histidine assignments and further indicates that, at neutral pH, the engineered H75 side chain is in the Nε H tautomeric state (Appendix Fig. A10).

2.4.3 Heme modification in T111H and L75H CtrHb

The first attempt at producing CtrHbs with covalently attached heme was based on results obtained with *Synechococcus* and *Synechocystis* GlbNs. For these proteins to undergo the reaction, it suffices to reduce the heme iron[39]. Ferric T111H and L75H CtrHb were incubated with excess DT for variable periods of time, up to ~2 h, oxidized with potassium ferricyanide, and then exposed to an excess of KCN for NMR comparison with their respective untreated form. Absence of reaction is hinted at by unchanged optical spectra and made apparent by ECL assay of denaturing gels, which detects heme only in the dye front of DT-treated CtrHbs (Fig. 2.4a, lanes 1–3). In this assay *Synechocystis* GlbN-A shows a strong signal at the protein's molecular weight (Fig. 2.4a, lane 4), as expected. The NMR spectra of the treated CtrHbs are not presented as they are identical to those of the non-reduced starting material.

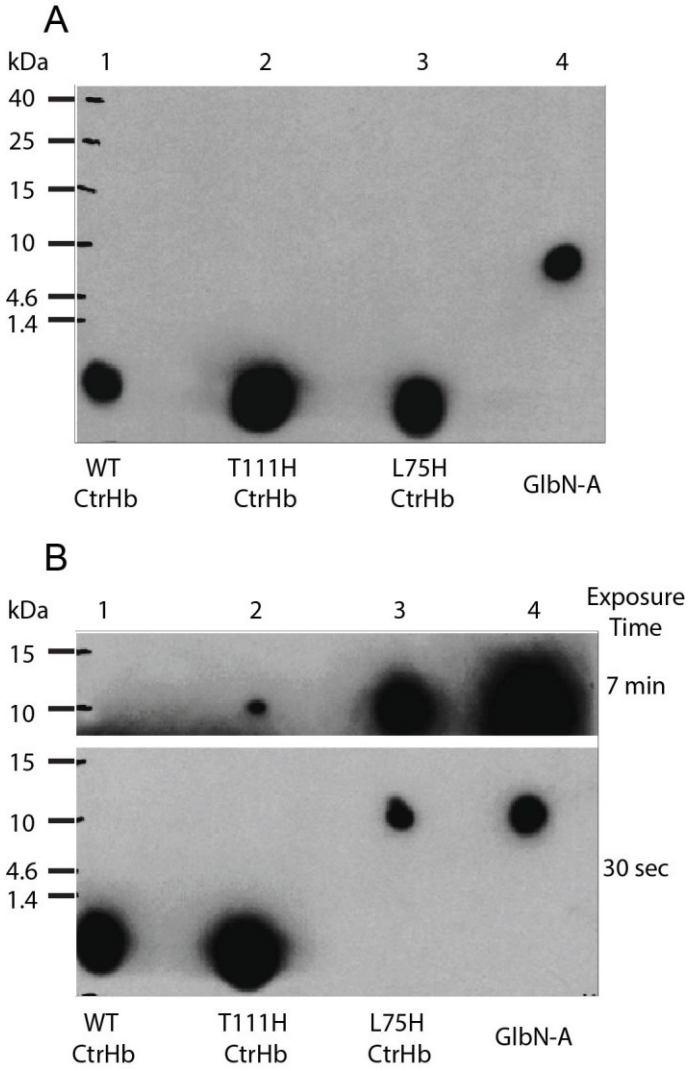

Fig. 2.4 ECL SDS-PAGE detection of covalently bound heme in CtrHbs. (A) Ferric samples were reduced with 2 mM DT for ~30 min then re-oxidized with air before being subjected to electrophoresis. The image was obtained with a 30-s exposure. The heme of WT CtrHb and the T111H and L75H variants (lane 1-3) migrates at the dye front. WT GlbN-A (lane 4) is included as a positive control for covalent linkage. **(B)** Ferric WT and variant CtrHbs were first saturated with cyanide and then reduced for ~30 min. The figure shows images of film that was exposed for either 30 s or 7 min. The heme from WT CtrHb (lane 1) migrates with the dye front. The T111H CtrHb lane (lane 2) shows incomplete heme attachment. The longer exposure time was necessary to observe the faint crosslinked T111H CtrHb band. The L75H CtrHb lane (lane 3) shows complete crosslinking as in the GlbN-A control (lane 4).

Failure to react can be due to various factors, including heme dissociation, incorrect histidine–vinyl geometry or unfavorable electron distribution of the porphyrin ring[22]. Binding of a suitable (permissive) ligand on the distal side may alleviate some of these problems. We therefore chose to initiate reduction from the stable and well-folded cyanomet state. The resulting ferrous–cyanide complex has a distinctive optical spectrum[34] (Fig. 2.5A-D), and although it is not expected to be as stable as its ferric counterpart[51], it may persist long enough to assist in the reaction.

Reduction of cyanomet WT CtrHb with 500-fold excess DT at pH 7.0 was monitored optically (Fig. 2.6A). Over a period of 40 min, the Soret maximum shifts from 416 nm to 431 nm and sharpens considerably. The end spectrum displays resolved α and β bands and corresponds to that of the cyanide adduct of ferrous CtrHb reported by Milani and coworkers[34] (Table 2.2). The transition displays isosbestic points, which is an indication of an apparent two-state process. At longer incubation times, a slow but nearly uniform decay in absorbance is observed and attributed to DT-mediated heme bleaching. Reduction of the WT protein without exogenous ligand but under otherwise identical conditions is considerably faster (complete within 2 min) and leads to a broad Soret band at neutral pH (Fig. 2.5B). The WT CtrHb behavior was used to gauge the reaction of the variants.

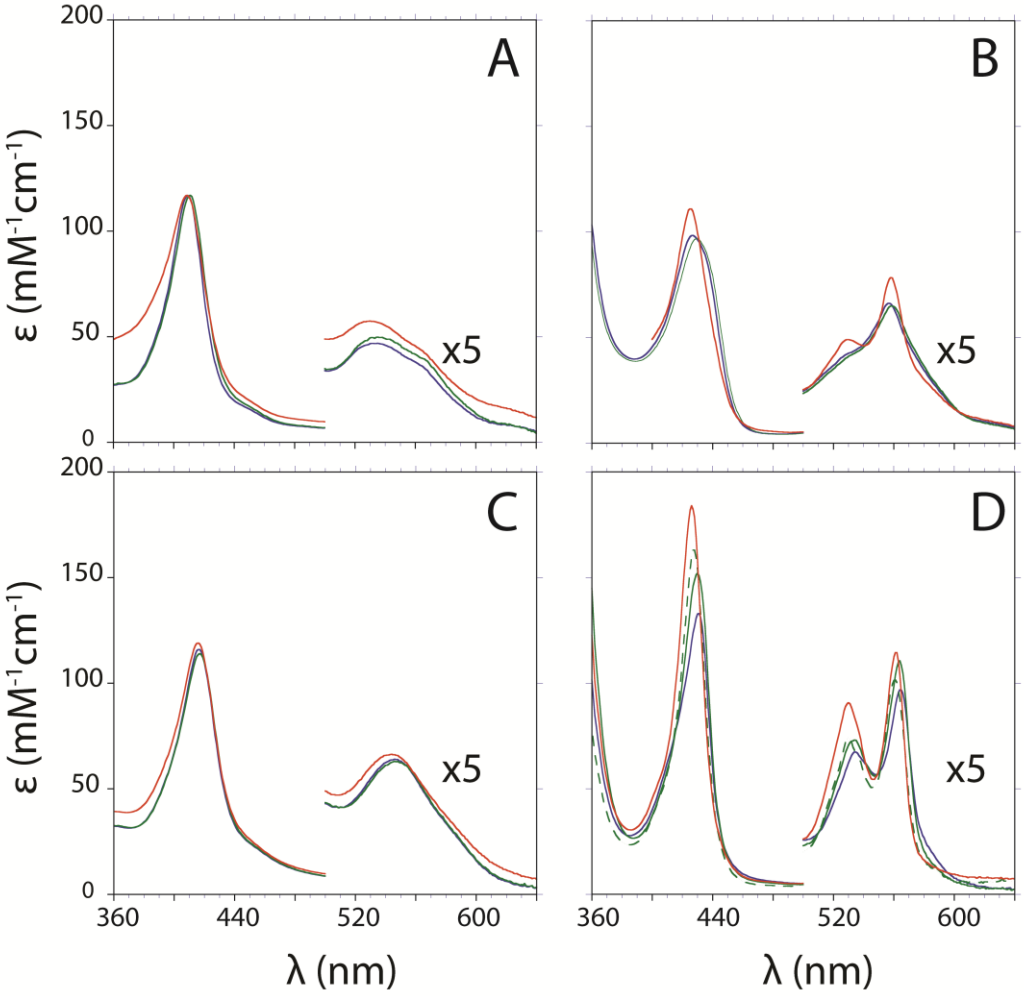

Fig. 2.5 Reference optical spectra of WT (blue), T111H (green), and L75H (red) CtrHbs. All protein samples (4–10 μM) were prepared in 100 mM phosphate, pH ~7.1, and spectra were collected at room temperature. **(A)** Ferric state. The L75H variant exhibits some light scattering caused by aggregation. **(B)** Ferrous state. **(C)** Cyanomet state, prepared by addition of a 5-fold excess of KCN. (D) Ferrous cyanide-bound state prepared by DT reduction (~2 mM) of the cyanomet starting material. For T111H CtrHb, the solid line corresponds to the spectrum obtained initially after reduction; the dashed green line corresponds to the final product. Note the blue shift of the T111H and L75H variants relative to WT CtrHb.

Cyanomet T111H CtrHb shows a response similar to that of cyanomet WT CtrHb, albeit on a slightly faster time scale for reduction (complete within 25 min under the same conditions as WT CtrHb). In addition, after 2 h of incubation with excess DT, the Soret maximum has moved from 430 nm to 428 nm (Fig. 2.6B, red to orange traces). Similar

changes are observed for the α and β bands. These blue shifts suggest a decreased degree of conjugation of the macrocycle as caused by crosslink formation.

Table 2.2 Optical properties of WT, T111H, and L75H CtrHbs[a]

State/Protein[b]	WT CtrHb	T111H CtrHb	L75H CtrHb
ferric (this work)	409 (117)[c]	411 (117)	409 (117)
	535 (8.7)	531 (9.6)	530 (12)
ferric[d]	410 (110)		
	535 (8.5)		
cyanomet (this work)	416 (97.6)[e]	417 (114)	416 (119)
	546 (11)	545 (13)	544 (13)
cyanomet[e]	416 (97.6)		
	547 (11)		
ferrous (this work)	427 (98.3)	429 (96.8)	425 (111)
	529 (sh), 557 (13)	530 (sh), 559 (13)	529 (10), 558 (17)
ferrous[d]	426 (108)		
	529 (sh), 557 (15)		
ferrous cyanide (this work)[f]	431 (142)	430 (152)	n/a
	534 (14), 564 (21)	534 (15), 564 (22)	
ferrous cyanide[e]	434 (149)		
ferrous cyanide	n/a	428 (163)	426 (184)
(X-linked, this work)		530 (15), 561 (20)	530 (18), 561 (23)

[a] Data at pH 7.1, room temperature. Wavelength maxima are given in nm (extinction coefficients are in mM^{-1} cm^{-1}).

[b] For all three proteins, mass spectrometry data (Acquity / Xevo-G2 UPLC-MS, Waters) were consistent with the coded sequences from which the initial methionine had been cleaved. The experimental molecular masses were: WT CtrHb, 13297.7 Da (expected 13298.2 Da); L75H CtrHb, 13321.1 Da (expected 13322.2 Da); and T111H CtrHb (^{15}N labeled), 13491.7 Da (expected 13493.2 Da for 98% ^{15}N abundance). The WT CtrHb mass was unaffected by aerobic reduction with 2mM dithionite.

[c] Extinction coefficient calculated from the cyanomet value of 97.6 mM^{-1} cm^{-1} provided in[34]. The 117 mM^{-1} cm^{-1} value was applied to all three ferric CtrHbs. All other values calculated from the ferric state reference spectra.

[d] From(32), pH 7.5.

[e] From(34), pH 7.0, 20° C.

[f] The same spectrum with a Soret at 431 nm is obtained upon DT reduction of a cyanomet sample or addition of cyanide to a DT-reduced sample. This is in contrast to the observations published in[34].

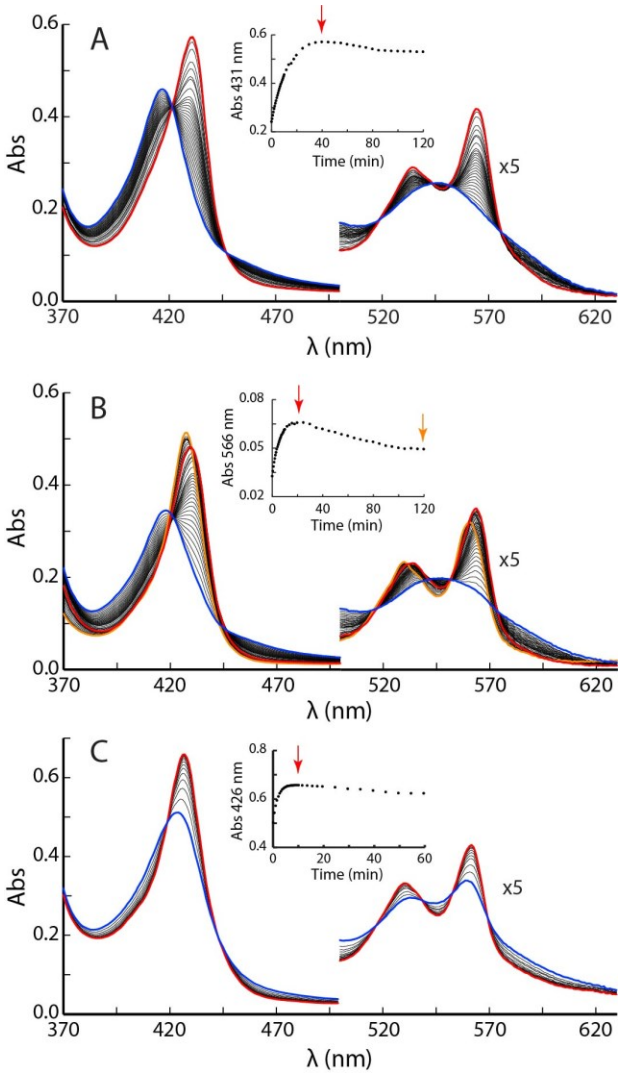

Fig. 2.6 DT-mediated reduction of cyanomet CtrHbs monitored by UV-vis spectrophotometry. (A) Reduction of cyanomet WT CtrHb. The reduction progresses over 40 min from the blue spectrum to the red spectrum. Inset: kinetic trace at 431 nm; the decrease in signal after 40 min (red vertical arrow) is attributed to damage by DT. **(B)** Reduction of cyanomet T111H CtrHb. The initial response occurs within 25 min. An additional blue shift of the spectrum is distinguished after this first phase (red to orange spectrum). Inset: kinetic trace at 566 nm to show the biphasic nature of the spectral evolution. The red and orange arrows mark the time of the red and orange spectra. **(C)** Reduction of cyanomet L75H CtrHb. The Soret band shifts to ~426 nm within the ~10-s manual mixing dead time. The reduction progresses over 10 min from the blue spectrum to the red spectrum, which is distinct from ferrous L75H CtrHb and corresponds to crosslinked L75H. Inset: kinetic trace at 426 nm, the decrease in signal after 10 min (red vertical arrow) is attributed to damage by DT. Note that only the first 60 min are shown.

Reduction of cyanomet L75H CtrHb gives distinct results (Fig. 2.6C). Addition of DT leads to a rapid (< 2 min) sharpening of the Soret maximum with a shift to 426 nm. The intensity is at first lower than expected based on the WT extinction coefficient and increases over time while remaining at 426 nm. The final spectrum (Fig. 2.5D) differs from that of the ferrous protein (Fig. 2.5B) and is inconsistent with a simple loss of cyanide from the reduced state.

The hemochromogen assay was performed to judge heme integrity. Both T111H and L75H CtrHbs treated with DT in the cyanomet state exhibit a blue shift of the hemochrome α and β maxima compared to WT CtrHb (data not shown) in support of a modified heme. Furthermore, Fig. 2.4B illustrates that ECL staining of treated cyanomet L75H CtrHb detects heme only where the protein has migrated, similar to WT GlbN-A and in support of covalent attachment. ECL staining of treated cyanomet T111H CtrHb showed the presence of heme associated with the protein as well as free heme migrating with the dye front.

The changes observed in the optical spectra upon reduction of cyanomet T111H and L75H CtrHbs, along with the ECL results, indicated the presence of a covalent bond between the heme and protein in treated samples, but did not reveal the nature of the bond. Thus, these data warranted a detailed examination of the products by NMR spectroscopy. For both variants, the ferric cyanomet form was first generated by incubation with excess potassium cyanide and upon saturation, reacted with excess DT and monitored kinetically by ^{1}H NMR spectroscopy for at least 2 h (Appendix Fig. A11–13). At the end of this period, the samples were exposed to potassium ferricyanide or air and completely reoxidized to generate the $S = 1/2$ cyanomet state. WT cyanomet CtrHb, when subjected to this treatment shows signs of modification. Reaction extent is small but reproducible, clearly

detectable by NMR spectroscopy (Appendix Fig. A11C), but does not yield a covalently attached heme (Fig. 2.4B, lane 1). This illustrates the potential for protein damage, likely due to the production of O_2^- or H_2O_2, when using DT to generate the crosslink. Comparison of the cyanomet ^{1}H-1D NMR spectra of T111H and L75H CtrHbs before and after treatment shows significant differences (Fig. 2.3B–E).

2.4.4 NMR Identification of the heme modification in T111H CtrHb

The T111H CtrHb spectrum resulting from the treatment (Fig. 2.3D) contains a multitude of hyperfine shifted lines with intensities suggesting a mixture of at least three species. The new predominant set of resonances corresponds to a major product accounting for ~60% of the sample. The inability for DT to reduce cyanomet T111H CtrHb completely under these NMR conditions can be seen from Appendix Fig. A12 and explains the second set of peaks, which corresponds to the cyanomet major heme orientational isomer of the starting material (~25%). Finally, a third set corresponds to a minor product that may be due to a different modification of the heme or DT-damaged protein. Notably, after treatment, peaks corresponding to the minor cyanomet isomer of the T111H starting material have vanished. We therefore hypothesize that the primary product contains a covalent linkage between H111 and the heme 4-substituent in an orientation analogous to the minor isomer starting material. We refer to this product as T111H CtrHb-A^4 (Fig. 2.7A).

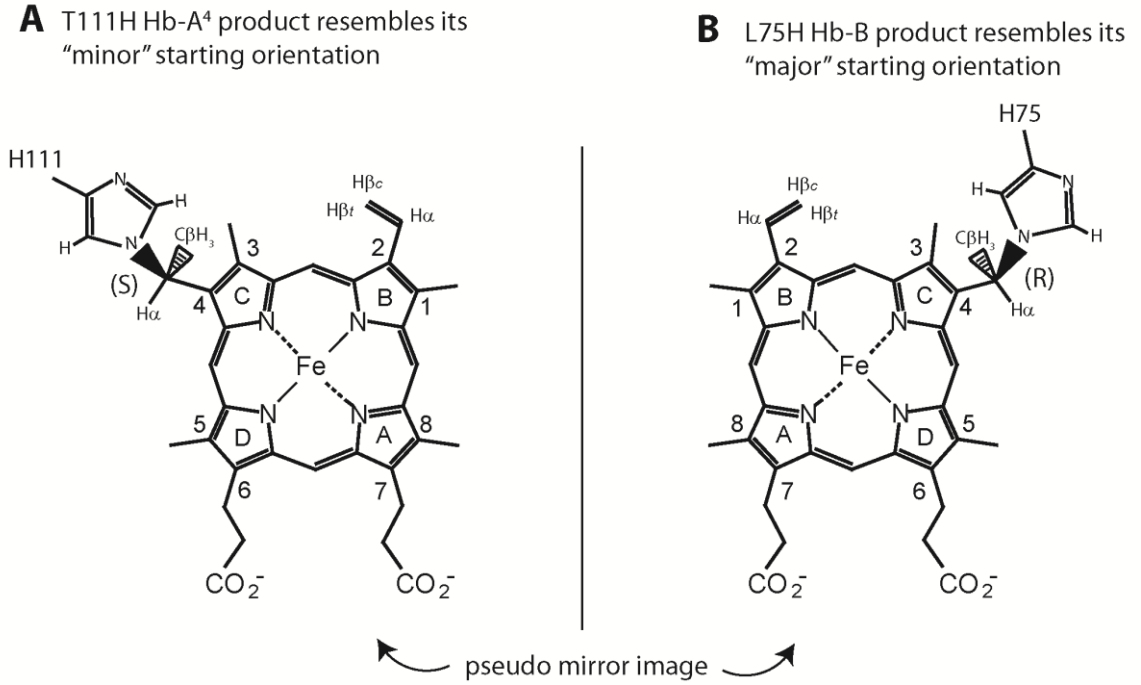

Fig. 2.7 Proposed structures of the histidine-heme modifications in (A) T111H CtrHb-A[4] and (B) L75H CtrHb-B. The T111H product is tentative as no long-range coupling was observed between the modified His111 Nε and the heme. However, NOEs between the His111 Hδ2 and Hε1 are consistent with the orientation depicted. With regards to the L75H product, the long-range ^{15}Nε2-CβH$_3$ *J*-correlation establishes that modification occurred at His75 Nε2. Since a methyl group was detected at the 4-substituent, a Nε2-Cα3 CβH$_3$ His-heme linkage can be inferred. As shown, the model is consistent with NOEs observed between the modified H75 side chain and covalently bound heme.

Signals corresponding to heme methyl groups of T111H CtrHb-A[4] are assigned on the basis of their high intensity and characteristic paramagnetic downfield ^{1}H and upfield ^{13}C shifts. DQF-COSY spectra reveal one vinyl and both propionate spin systems. Intra-heme NOEs between the 1-CH$_3$ and 8-CH$_3$, along with contacts between the heme 1- and 2-substituents indicate that the heme 2-vinyl group has remained intact (Appendix Fig. A14). Cyanomet T111H CtrHb ^{1}H-^{15}N lr-HMQC data collected before and after DT treatment and compared with WT data indicate the presence of a peculiar imidazole system[52] in the T111H CtrHb-A[4] product, exhibiting two downfield shifted ^{15}N signals *J*-coupled to a

proton at 8.36 ppm, itself coupled to a proton at 6.48 ppm. These resonances are attributed to H111 (Table 2.2). Restraints defining the position of the side chain include: H111 Hε1 to heme 3-CH_3 and F48 Hζ and Hε protons, and H111 Hδ2 to the heme 3-CH_3 and V115 side chain methyls. Both H111 Hε1 and Hδ2 protons have shared NOEs (strong and weak, respectively) to a methyl group at 3.39 ppm, which is assigned to the modified heme 4-CβH_3 group. Accordingly, a scalar connectivity is observed between the 4-CβH_3 and a single proton at 6.15 ppm (Appendix Fig. A14) corresponding to the modified heme 4-CαH. This proton, like the 4-CβH_3, is in dipolar contact with H111 Hε1. Although J_{HN}-coupling between H111 ^{15}Nε2 and the newly produced 4-CβH_3 or 4-CαH was not detected in the long-range data, the observed NOEs, heme methyl ^{1}H chemical shift dispersion pattern[53], propionate shifts, and unusual H111 ^{15}N shifts are all consistent with modification occurring at H111 and the heme 4-substituent (Fig. 2.7A).

2.4.5 NMR Identification of the heme modification in L75H CtrHb

Unlike WT and T111H cyanomet CtrHbs, which are reduced slowly and with different efficiencies between the major and minor forms (Appendix Fig. A11–12), DT reduction of L75H cyanomet CtrHb leads to complete and rapid disappearance of all cyanomet resonances (Appendix Fig. A13). Reoxidation results in a spectrum (Fig. 2.3E) distinct from the starting material (Fig. 2.3C) and consistent with high yield of one major product (> 90 %, henceforth L75H CtrHb-B). Only one heme vinyl group can be identified in DQF-COSY data of the product (Appendix Fig. A15). The intact vinyl Hα exhibits an NOE to a heme methyl, itself having a weak intraheme connectivity to a second heme methyl. The vinyl and methyl chemical shifts (Table 2.2) and NOE pattern are analogous to the WT 2-vinyl ↔ 1-CH_3 ↔ 8-CH_3 sequence and suggest that the reaction occurs on pyrrole

C. Also similar to the WT, characteristic 1-CH_3 ↔ F48 and 2-vinyl H□ ↔ F80 contacts are observed. Of the 2-vinyl β_{cis} and β_{trans} protons, the latter is oriented toward a third heme methyl, assigned as the heme 3-CH_3 (Appendix Fig. A15C). This methyl shows distinctive dipolar contacts, including strong NOEs to the side chain methyls of V83 and the ring of F80. In addition, the heme 3-CH_3 displays an NOE to a methyl group, the latter (–0.49 ppm, Appendix Fig. A15D) *J*-coupled to a proton resonating at 0.54 ppm. The relative intensity of the 0.54 ppm and –0.49 resonances is consistent with a 4-CαH-CβH_3 heme moiety. The 3:1:1:3 splitting pattern observed in the ^{13}C dimension of the ^{1}H-coupled natural abundance ^{13}C spectrum confirms that the signal at –0.49 ppm corresponds to a methyl group (Appendix Fig. A16). The 4-CαH is oriented towards the heme 5-CH_3 and the 4-CβH_3 is proximal to the heme 3-CH_3, as in the starting material L75H major isomer.

Because WT CtrHb does not form a crosslink, H75 is the logical candidate for modification. ^{1}H-^{15}N lr-HMQC spectra collected on cyanomet WT and L75H CtrHbs before and after treatment demonstrate that, in L75H CtrHb-B, signals corresponding to intact H75 are missing and a new set of shifted cross peaks are detected. Both H75 imidazole nitrogens exhibit *J*-coupling to a proton at 7.12 ppm (Hε1). The ring ^{15}Nε2 is also *J*-coupled to a proton at 5.42 ppm (Hδ2) and to the heme 4-CβH_3 (–0.49 ppm, Fig. 2.8). NOE connectivities define the position of the modified histidine: H75 Hδ2 has strong dipolar interactions with both the heme 3- and 4-CβH_3 groups, whereas H75 Hε1 is oriented towards the 5-CH_3 group (data not shown). Together, these data support that the H75 ring undergoes a rotation from its original position and forms the anticipated crosslink, with R stereochemistry at the heme 4-Cα, as depicted in Fig. 2.7B. Interestingly, for both T111H and L75H CtrHbs, the engineered histidine reorients in order to react with the heme.

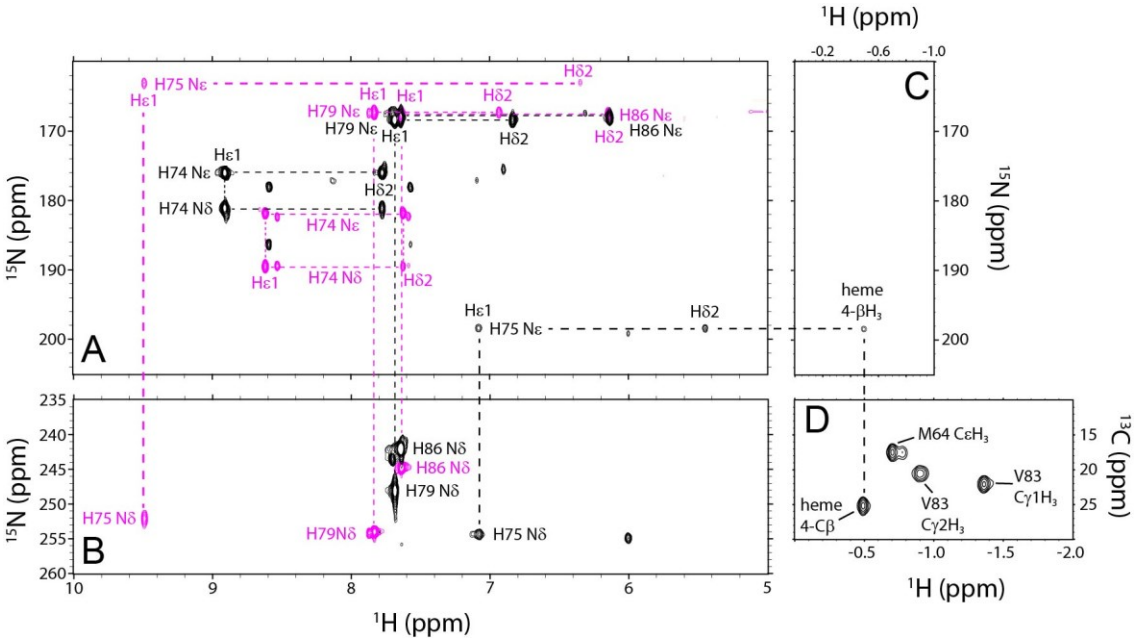

Fig. 2.8 Histidine assignment in cyanomet L75H CtrHb and product CtrHb-B by NMR spectroscopy (pH 7.1–7.2, 298 K). **(A)** Overlay of ^{1}H-^{15}N lr-HMQC data (^{15}N upfield region). Signals from all histidine residues (except proximal H68) were detected. Reactant (magenta) and product (black) L75H histidine spin systems are connected with dashed lines. **(B)** Overlay of ^{1}H-^{15}N lr-HMQC data (^{15}N downfield region). Colors are as in (A). Note that the similarity of the H86, H74, and H79 imidazole signals (A, B) in CtrHb and CtrHb-B. Conversely, H75 Nε2, along with Hε1 and Hδ2, undergoes significant changes. **(C)** ^{1}H-^{15}N lr-HMQC data (^{1}H far-upfield region). In L75H cyanomet CtrHb-B, H75 Nε2 has a cross peak at −0.49 ppm, indicative of histidine N-alkylation. **(D)** Portion of a natural abundance ^{1}H-^{13}C HMQC spectrum collected on L75H cyanomet CtrHb-B. The coupled ^{1}H-^{13}C HSQC spectrum (Appendix Fig. A16) confirms that the resolved peak at a proton shift of −0.49 ppm is a methyl group

2.4.6 Mechanistic considerations

The data accumulated with GlbN[20-22,26] has provided a set of criteria for the addition of histidine to the ferrous heme. The first is proximity. The histidine must be within reach of a heme vinyl, and sp^3 geometry at the vinylic Cα atom must be sterically possible; however, the histidine need not be optimally oriented in the starting material as long as the barrier to adopt the productive state can be overcome thermally. The second is the ionization state of the histidine. In GlbN, data are consistent with the histidine providing

the proton to the vinyl Cβ. Protonation is the rate determining step and the reaction should be carried out at a sufficiently low pH. A third criterion is the nature of the iron distal ligand. These are either permissive (histidine, cyanide, water/5-coordinate)[20] or inhibiting (O_2 and NO, data not shown; CO)[21,26]. The inhibiting ligands have a slow dissociation rate constant, and their electron-withdrawing property is presumably responsible for the inhibition. In GlbN, the permissive ligands are not tightly bound and may or may not be released prior to protonation and nucleophilic attack.

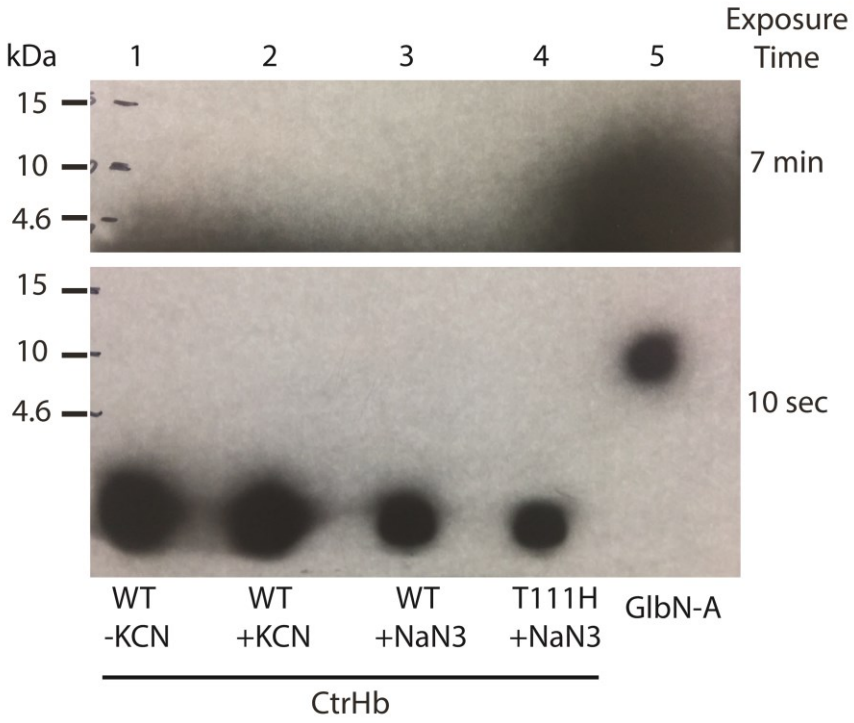

Fig. 2.9 ECL SDS-PAGE showing no heme attachment in T111H CtrHb when azide is used in place of cyanide. Five-fold excess KCN (+KCN) or 10 mM NaN_3 (+NaN_3) was added to the ferric form of the designated protein and incubated for 20 min. Subsequently, 2 mM DT was added to each sample and incubated for 3 h at RT, followed by passage over a ~1.3 cm^3 DEAE column. The figure shows film that was exposed for either 10 s or 7 min. Crosslinked GlbN (GlbN-A, lane 5) was used as a control.

The behavior of the CtrHb variants brings new insights into the mechanism and limitations of the histidine addition. Ferrous WT CtrHb at neutral pH is reported to be a

mixture of 4-, 5-, and 6-coordinate species, with equilibrium favoring the 5-coordinate high-spin complex[29]. In preliminary experiments, this protein was found to lose heme rapidly to apomyoglobin (half-life of ~8 min at pH 7.7, data not shown). Optical spectra suggest the same mixture of species in reduced T111H CtrHb and a slight increase in the population of a 6-coordinate species in L75H CtrHb (Fig. 2.5B). The failure of ferrous T111H and L75H CtrHbs to react therefore appears related to absent or fleeting heme–protein contacts.

The modification occurs when reducing the well-folded cyanomet state. *A priori*, steric (i.e., correct seating of the heme), electrostatic, or heme electronic factors can all contribute to the reactivity. Attempts to crosslink in the presence of azide as an alternative anionic ligand were not successful (Fig. 2.9). No crosslinked heme was detected in the T111H sample even after exposing the film for 7 min. To account for possible inhibition of peroxidase activity by azide, a sample of the more reactive L75H CtrHb was treated with azide/DT and then purified by DEAE chromatography. The protein lost heme on the column. This demonstrates that, unlike cyanide, azide does not facilitate crosslink formation in T111H or L75H CtrHb. Imidazole coordination led only to partial crosslinking (Fig. 2.10). The L75H CtrHb +Im/-DEAE sample in lane 2 does not show heme migrating with the protein. However, this sample was not passed over a DEAE column to strip some of the imidazole from the heme. Thus, when compared to the L75H CtrHb +Im/+DEAE sample (Fig. 2.2.10, lane 3) that was cleaned by passage through a short DEAE column, imidazole is shown to inhibit the ECL reaction. In contrast to L75H CtrHb that was bound with cyanide prior to reduction (Fig. 2.2.10, lane 4), the imidazole sample that was cleaned by passage through DEAE (L75H +Im/+DEAE, Fig. 2.2.10, lane 3) only shows partial crosslinking. The possibility that cyanide promotes the covalent modification by stabilizing the protonated vinyl seems unlikely given that binding of this anionic ligand is not expected to perturb

significantly the electron distribution of the ferrous heme[54]. Thus, the data point to steric effects as the major determinants of reactivity in the absence of inhibiting ligands.

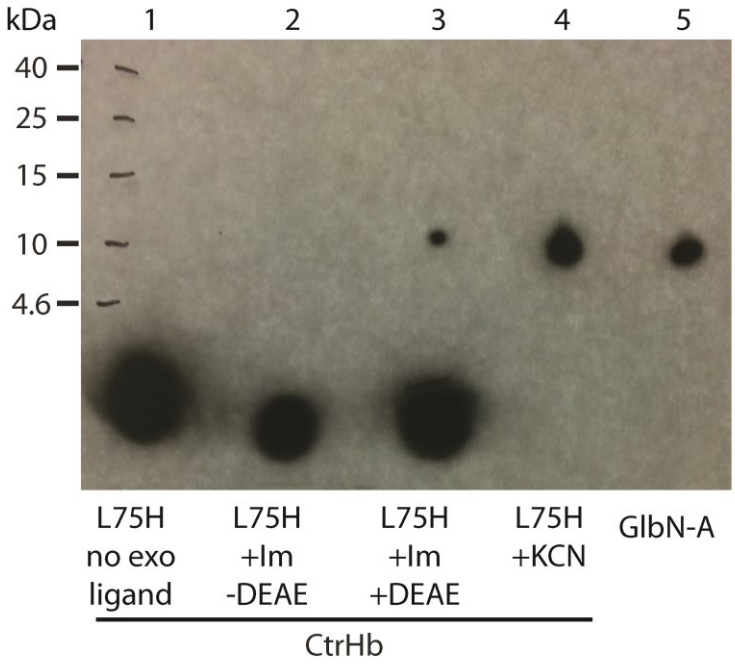

Fig. 2.10 ECL SDS-PAGE demonstrating partial modification of L75H CtrHb when imidazole is used instead of cyanide. Ten-fold excess imidazole (+Im) or 5-fold excess KCN (+KCN) was added to L75H and incubated for at least 4 h or 20 min with imidazole or cyanide, respectively. The L75H +Im samples were either passed over a DEAE column (+DEAE) to strip the Im off the heme, or were not were not passed over a DEAE (-DEAE) column. All L75H CtrHb samples, except the L75H CtrHb sample to which no exogenous ligand was added (lane 1), were subsequently reduced with 2 mM DT for 3 h. *Synechocystis* 6803 GlbN-A (lane 5) and L75H CtrHb with no exogenous ligand added were used as positive and negative controls, respectively. The film was exposed for 7 min.

The protein conformation adopted when cyanide is bound may influence the reaction via subtle effects on the vinyl groups. We showed above that in the cyanomet complex, the major heme orientational isomer of WT CtrHb has the 2-vinyl group out of the heme plane and in a *cis*-like orientation, whereas T111H CtrHb undergoes a rearrangement to a *trans*-like orientation (Appendix Fig. A8). The stereochemistry of the products indicates that the reactive vinyl is in a *trans*-like conformation. This conformation has a higher degree

of conjugation with the porphyrin ring than *cis*-like conformations[55] and may undergo protonation more readily. Whether a *trans* vinyl configuration is in general a necessary condition for reaction is not clear. Regardless, the lack of reaction between H111 and the 2-vinyl (major isomer) in T111H CtrHb shows that a *trans* vinyl near a histidine is an insufficient feature for reaction. Facile heme reorientation associated with low heme and exogenous ligand affinity in the ferrous state presents H111 with the 4-vinyl group as a competitive alternative to the 2-vinyl group. Thus, the yield of T111H CtrHb-A^4 exceeds the minor isomer content in the cyanomet starting material. Likewise, the yield of L75H CtrHb-B exceeds the initial major isomer content. As anticipated, heme reorientation on a relatively rapid time scale emerges as a significant advantage for reaction.

In natural heme proteins, the vinyl groups are often surrounded by hydrophobic side chains. In prior work, we surveyed over 300 structures for the presence of leucines with Cα atom within 7 Å of a vinyl Cα atom and Cβ atom within 6 Å of the same vinyl Cα atom[15]. These criteria identified L79 in GlbN and L75 in CtrHb as candidates for histidine replacement and heme modification. Many other leucines were found. Examples include L106 in nitrophorin 2 (1PEE), L211 in chlorite dismutase (2VXH), L37 in ascorbate peroxidase (1APX), and L71 in cytochrome b_5 (3NER), chosen to highlight proteins that have architectures different from that of globins. Many isoleucines, filtered by the same distance criteria, also occupy positions where a histidine may react. For in vitro applications, screening of pH conditions and permissive exogenous ligands that seat the heme properly can be systematically explored. Thus, it is reasonable to expect that many natural heme proteins can be modified to undergo the reaction, or artificial proteins can be designed to present a histidine with appropriate geometry to the heme.

2.5 Conclusion

The present work has several implications for the chemistry of heme proteins. (1) The existence of the PTM in GlbN[40] and its engineered presence in GlbN[22] and CtrHb cautions that the PTM may occur in additional heme proteins, not only wild-type but also unwittingly in His-tagged versions, (histidine) variants, or designed proteins. (2) In preparing the histidine Nε2–heme vinyl Cα crosslink, care must be exercised in the choice of a reducing agent to avoid heme and protein damage, as occasionally caused by the oxidative by-products of aerobic DT reduction. Anaerobic DT treatment or reduction with alternative agents such as a ferredoxin system[56] if sufficiently powerful may be preferable. (3) It is possible to engineer the crosslink in a *b* heme protein using relatively mild reaction conditions. Although detailed kinetic analysis was not performed on CtrHb variants, the products are consistent with the mechanism described previously[21], in which case the pK_a of the reactive histidine, in addition to its ability to adopt the geometry of the product, is an important factor. (4) The necessity of using the cyanomet adduct as the species to be reduced rather than the ligand free protein (as in GlbNs) is likely related to the conformation of the starting material. In view of the CtrHb results, we expect that successful application to other proteins will depend principally on the position of the engineered histidine, the local flexibility of the supporting structure, the absence of inhibiting distal ligands, and possibly the orientation of the heme vinyl group.

The ability to prepare non-natively crosslinked versions of heme proteins extends the range of heme chemistry questions that can be addressed by biophysical methods. For example, to what extent does protonation of the alkylated histidine influence the heme reduction potential? How do the histidine-heme linkages differ from the cysteine–heme thioether linkages of *c*-type cytochromes? What is the electronic influence of the distal

ligand? Practical usage of the crosslinking reaction includes the formulation of artificial enzymes or oxygen transporters with non-dissociable heme; such systems are expected to have an elongated lifetime, have increased resistance to proteolytic cleavage, and may be capable of functioning over a wide range of conditions (e.g. high temperature, low pH) for industrial or biomedical applications.

Acknowledgement

This study was supported by National Science Foundation grant MCB-1330488. Data were collected at the Johns Hopkins Biomolecular NMR Center with assistance from Dr. Ananya Majumdar.

2.6 References

(1) Hargrove, M. S., Barrick, D., and Olson, J. S. (1996) The association rate constant for heme binding to globin is independent of protein structure. *Biochemistry, 35*, 11293-11299.

(2) Landfried, D. A., Vuletich, D. A., Pond, M. P., and Lecomte, J. T. J. (2007) Structural and thermodynamic consequences of *b* heme binding for monomeric apoglobins and other apoporteins. *Gene, 398*, 12-28.

(3) Cowley, A. B., Kennedy, M. L., Silchenko, S., Lukat-Rodgers, G. S., Rodgers, K. R., and Benson, D. R. (2006) Insight into heme protein redox potential control and functional aspects of six-coordinate ligand-sensing heme proteins from studies of synthetic heme peptides. *Inorganic Chemistry, 45*, 9985-10001.

(4) Traylor, T. G. and Sharma, V. S. (1992) Why nitric oxide?. *Biochemistry, 31*, 2847-2849.

(5) Gullotti, M., Santagostini, L., Monzani, E., and Casella, L. (2007) Effect of strain in the proximal ligand on the binding of nitric oxide and carbon monoxide to chelated protoheme complexes. *Inorganic Chemistry, 46*, 8971-8975.

(6) Fritz, B. G., Hu, X., Brailey, J. L., Berry, R. E., Walker, F. A., and Montfort, W. R. (2011) Oxidation and loss of heme in soluble guanylate cyclase from *Manduca sexta*. *Biochemistry, 50*, 5813-5815.

(7) Thompson, A. M., Reddi, A. R., Shi, X., Goldbeck, R. A., Moënne-Loccoz, P., Gibney, B. R., and Holman, T. R. (2007) Measurement of the heme affinity for yeast Dap1p, and its importance in cellular function. *Biochemistry, 46*, 14629-14637.

(8) Kim, Y. M., Bergonia, H. A., Muller, C., Pitt, B. R., Watkins, W. D., and Lancaster Jr., J. R. (1995) Loss and degradation of enzyme-bound heme induced by cellular nitric oxide synthesis. *Journal of Biological Chemistry, 270*, 5710-5713.

(9) Kundu, S., and Hargrove, M. S. (2003) Distal heme pocket regulation of the ligand binding and stability in soybean leghemoglobin. *Proteins, 50*, 239-248.

(10) Alayash, A. I. (2014) Blood substitutes: Why haven't we been more successful? *Trends in Biotechnology, 32*, 177-185.

(11) Gibney, B. R., Rabanal, F., Reddy, K. S., and Dutton, P. L. (1998) Effect of four helix bundle topology on heme binding and redox properties. *Biochemistry, 37*, 4635-4643.

(12) Liu, J., Chakraborty, S., Hosseinzadeh, P., Yu, Y., Tian, S., Petrik, I., Bhagi, A., and Lu, Y. (2014) Metalloproteins containing cytochrome, iron-sulfur, or copper redox centers. *Chemical Reviews, 114*, 4366-4469.

(13) Kranz, R. G., Richard-Fogal, C., Taylor, J. S., and Frawley, E. R. (2009) Cytochrome *c* biogenesis: mechanisms for covalent modifications and trafficking of heme and for hem-iron redox control. *Microbiology and Moleuclar Biology Reviews, 73,* 510-528.

(14) Bowman, S. E. and Bren, K. L. (2008) The chemistry and biochemistry of heme *c*: Functional basis for covalent attachment. *Natural Product Reports, 25*, 1118-1130.

(15) Mavridou, D. A., Ferguson, S. J., and Stevens, J. M. (2013) Cytochrome *c* assembly. *IUBMB Life, 65*, 209-216.

(16) Braun. M., Rubio, I.G., and Thöny-Meyer, L. (2005) A heme tag for in vivo synthesis of artificial cytochromes. *Applied Microbiology Biotechnology, 67*, 234-239.

(17) Braun, M. and Thöny-Meyer, L. (2004) Biosynthesis of artificial microperoxidases by exploiting the secretion and cytochomre *c* maturation aapparatuses of *Escherichia coli. Proceedings of the National Academy of Sciences, 101*, 12830-12835.

(18) Barker, P. D., Ferrer, J. C., Mylrajan, M., Loehr, T. M., Feng, R., Konishi, Y., Funk, W. D., MacGillivray, R. T., and Mauk, A. G. (1993) Transmutation of a heme protein. *Proceedings of the National Academy of Sciences, 90*, 6542-6546.

(19) Daltrop, O., Allen, J. W., Willis, A. C., and Ferguson, S. J. (2002) In vitro formation of a *c*-type cytochrome. *Proceedings of the National Academy of Sciences, 99*, 7872-7876.

(20) Nothnagel, H. J., Love, N., and Lecomte, J. T. J. (2009) The role of the heme distal ligand in the post-translational modification of *Synechocystis* hemoglobin. *Journal of Inorganic Biochemistry, 103*, 107-116.

(21) Nothnagel, H. J., Preimesberger, M. R., Pond. M. P., Winer, B. Y., Adney, E. M., and Lecomte, J. T. J. (2011) Chemical reactivity of *Synechococcus* sp. PCC 7002 and *Synechocystis* sp. PCC 6803 hemoglobins: covalent heme attachement and bishistidine coordination. *Journal of Inorganic Biochemistry, 16*, 539-552.

(22) Preimesberger, M. R., Wenke, B. B., Gilevicius, L., M., Pond, and Lecomte, J. T. J. (2013) Facile heme vinyl posttranslational modification in a hemoglobin. *Biochemistry, 52*, 3478-3488.

(23) T.K. Das, M. Couture, Y. Ouellet, M. Guertin, D.L. Rousseau (2001) Simultaneous observation of the O-O and Fe-O_2 stretching modes in oxyhemoglobins. *Proceedings of the National Academy of Sciences, 98*, 479-484.

(24) Hoy, J. A., Smagghe, B. J., Halder, P., and Hargrove, M. S. (2007) Covalent heme attachment in *Synechocystis* hemoglobin is required to prevent ferrous heme dissociation. *Protein Science, 16*, 250-260.

(25) Vuletich, D. A. and Lecomte, J. T. J. (2006) A phylogenetic and strucutral analysis of truncated hemoglobins. *Journal of Molecular Evolution, 62*, 196-210.

(26) Preimesberger, M. R., Pond, M. P., Majumdar, A., and Lecomte, J. T. J. (2012) Electron self-exchange and self-amplified posttranslational modification in the hemoglobins from *Synechocystis* sp. PCC 6803 and *Synechococcus* sp. PCC 7002. *Journal of Biological Inorganic Chemistry, 17*, 599-609.

(27) Pond, M. P., Majumdar, A. and Lecomte, J. T. J. (2012) Influence of heme post-translational modification and distal ligation on the backbone dynamics of a monomeric hemoglobin. *Biochemistry, 51*, 5733-5747.

(28) Dellarole, M., Roumestand, C., Royer, C. and Lecomte, J. T. J. (2013) Volumetric properties underlying ligand binding in a monomeric hemoglobin: A high-pressure NMR study. *Biochimica et Biophysica Acta-Proteins and Proteomics, 1834*, 1910-1922.

(29) Couture, M., Das, T. P., Lee, H. C., Peisach, J., Rousseau, D. L., Wittenberg, B. A., Wittenberg, J. B., and Guertin, M. (1999) *Chlamydomonas* chloroplast ferrous hemoglobin:

Heme pocket structure and reactions with ligands. *Journal of Biological Chemistry, 274*, 6898-6910.

(30) Das, T. K., Couture, M., Lee, H. C., Peisach, J., Rousseau, D. L., Wittenberg, B. A., Wittenberg, J. B., and Guertin, M. (1999) Identification of the ligands to the ferric heme of *Chlamydomonas* chloroplast hemoglobin: Evidence for ligation of tyrosine-63 (B10) to the heme. *Biochemistry 38*, 15360-15368.

(31) Pesce, A., Couture, M., Dewilde, S., Guertin, M., Yamauchi, K., Ascenzi, P., Moens, L., and Bolognesi, M. (2000) A novel two-over-two α-helical sandwich fold is characteristic of the truncated hemoglobin family. *EMBO Journal, 19*, 2424-2434.

(32) Couture, M. and Guertin, M. (1996) Purification and spectroscopic characterization of a recombinant chloroplastic hemoglobin from the unicellular green alga *Chlamydomomans eugametos*. *European Journal of Biochemistry, 242*, 779-787.

(33) Lecomte, J. T. J., Scott, N. L., Vu, B. C., and Falzone, C. J. (2001) Binding of ferric heme by the recombinant globin from the cyanobacterium *Synechocystis* sp. PCC 6803. *Biochemistry, 40*, 6541-6552.

(34) Milani, M., Oullete, Y., Oullete, H., Guertin, M., Boffi, A., Antonini, G., Bocedi, A., Mattu, M.,Bolognesi, M., and Ascenzi, P. (2004) Cyanide binding to truncated hemoglobins: A crystallographic and kinetic study. *Biochemistry, 43*, 5213-5221.

(35) de Duve, C. (1948) A spectrophotometric method for the simultaneous determination of of myoglobin and hemoglobin in extracts of human muscle. *Acta Chemica Scandinavica, 2*, 264-289.

(36) Berry, E. A., and Trumpower, B. L. (1987) Simultaneous determination of hemes *a*, *b*, and *c* from pyridine hemochrome spectra. *Anal Biochem, 161*, 1-15.

(37) Dorward, D. W. (1993) Detection and quantitation of heme-containing proteins by chemiluminescence. *Analytical Biochemistry, 209*, 219-223.

(38) Vargas, C., McEwan, A. G., and Downie, J. A. (1993) Detection of *c*-type cytochromes using enhanced chemiluminescence. *Analytical Biochemistry, 209*, 323-326.

(39) Vu, B. C., Vuletich, D. A., Kuriakose, S. A., Falzone, C. J., and Lecomte, J. T. J. (2004) Characterization of the heme-histidine cross-link in cyanobacterial hemoglobins from *Synechocystis* sp. PCC 6803 and *Synechococcus* sp. PCC 7002. *Journal of Biological Inorganic Chemistry, 9*, 183-194.

(40) Vu, B. C., Jones, A. D., and Lecomte, J. T. J. (2002) Novel histidine-heme covalent linkage in a hemoglobin. *Journal of the American Chemical Society, 124*, 8544-8545.

(41) Falzone, C. J., and Lecomte, J. T. J. (2002) Assignment of the ^{1}H, ^{13}C, and ^{15}N signals of *Synechocystis* sp. PCC 6803 methemoglobin. *Journal of Biomolecular NMR*, *23*, 71-72.

(42) Pond, M. P., Vuletich, D. A., Falzone, C. J., Majumdar, A. and Lecomte, J. T. J. (2009) ^{1}H, ^{15}N, and ^{13}C resonance assignments of the 2/2 hemoglobin from the cyanobacterium *Synechococcus* sp. PCC 7002 in the ferric bis-histidine state. *Biomolecular NMR Assignments, 3*, 211-214.

(43) Pelton, J. G., Torchia, D. A., Meadow, N. D. and Roseman, S. (1993) Tautomeric states of the active-site histidines of the phosphorylated and unphosphorylated III^{Glc}, a signal-transducing protein from *Escherichia coli*, using two-dimensional heteronuclear NMR techniques. *Protein Science, 2*, 543-558.

(44) Wishart, D. S., Bigam, C. G., Yao, J., Abildgaard, F., Dyson, H. J., Oldfield, E., Markley, J. L., and Sykes, B. D. (1995) ^{1}H, ^{13}C, and ^{15}N chemical shift referencing in biomolecular NMR. *Journal of Biomolecular NMR, 6*, 135-140.

(45) Delaglio, F., Grzesiek, S., Vuister, G. W., Zhu, G., Pfeifer, J., and Bax, A. (1995) NMRPipe: A multidimensional spectral processing system based on UNIX pipes. *Journal of Biomolecular NMR, 6*, 277-293.

(46) Goddard, T. D., and Kneller, D. G. (2006) SPARKY 3, University of California, San Francisco.

(47) Pettersen, E. F., Goddard, T. D., Huang, C. C., Couch, G. S., Greenblatt, D. M., Meng, E. C., and Ferrin, T. E. (2004) UCSF Chimera--A vizualization system for exploratory research and analysis. *Journal of Computational Chemistry, 25*, 1605-1612.

(48) La Mar, G. N., Davis, N. L., Parish, D. W., and Smith, K. M. (1983) Heme orientational disorder in reconstituted and native sperm whale myoglobin: Proton nuclear magnetic resonance characterizations by heme methyl deuterium labeling in the met-cyano protein. *Journal of Molecular Biology, 168*, 887-896.

(49) Lee, K.B., G.N. La Mar, L.A. Kehres, E.M. Fujinari, K.M. Smith, T.C. Pochapsky, S.G. Sligar (1990) Proton NMR study of the influence of hydrophobic contacts on protein prosthetic group recognition in rat ferricytochrome b5. *Biochemistry, 29*, 9623-9631.

(50) La Mar, G. N., Satterlee, J. D., de Ropp, and J. S. in: Smith, K. M., Kadish, K. and Guilard, R. (Eds.) (2005) The Porphyrin Handbook, vol. 5, Academic Press, Burlington, MA, 185-298.

(51) A. Bolli, C. Ciaccio, M. Coletta, M. Nardini, M. Bolognesi, A. Pesce, M. Guertin, P. Visca, P. Ascenzi (2008) Ferrous Campylobacter jejuni truncated hemoglobin P displays an extremely high reactivity for cyanide - a comparative study. *FEBS Journal, 275*, 633-645.

(52) Vila, J. A. (2012) Limiting values of the 15N chemical shift of the imidazole ring of histidine at high pH. *Journal of Physical Chemistry B, 116*, 6665-6669.

(53) Bertini, I., Luchinat, C., Parigi, G., and Walker, F. A. (1999) Heme methyl ^{1}H chemical shifts as structural parameters in some low-spin ferriheme proteins. *Journal of Biological Inorganic Chemistry, 4*, 515-519.

(54) Boffi, A., Chiancone, E., Takahashi, S., and Rousseau, D. L. (1997) Stereochemistry of the Fe(II)- and Fe(III)-cyanide complexes of the homodimeric *Scapharca inaequivalvis* hemoglobin. A resonance raman and FTIR study. *Biochemistry, 36*, 4505-4509.

(55) Marzocchi, M. P. and Smulevich, G. (2003) Relationship between heme vinyl conformation and the protein matrix in peroxidases. *Journal of Raman Spectroscopy, 34*, 725-736.

(56) Hayashi, A., Suzuki, T., and Shin, M. (1973) An enzymic reduction system for metmyoglobin and methemoglobin, and its application to functional studies of oxygen carriers. *Biochimica et Biophysica Acta-Protein Structure, 310*, 309-316.

Chapter 3

THB1, a truncated hemoglobin with lysine as a distal heme ligand, is linked to nitrogen metabolism in *Chlamydomonas reinhardtii*

*This chapter was previously published in *Biochemistry* (Johnson E.A., **Rice S.L.,** *et al.*, 2014). Figures 3.1, 3.7-3.9, and 3.14 were contributed by coauthors, all other results in this chapter represent original work. For this dissertation, modifications were made to the text and additional figures were added (Fig. 3.4-3.6, and 3.11-3.13)

Author Contributions

Selena L. Rice: designed research, purified WT protein, performed optical experiments (ligand binding, pH titration, H_2O_2 addition), performed NOD assays, wrote the paper

Eric A. Johnson: designed research, performed in vivo experiments, and wrote the paper

Matthew R. Preimesberger: designed research, performed, and analyzed NMR experiments, wrote the paper

Dillon B. Nye: made and purified Y29F and K53A variants, collected Y29F and K53A pH titration data

Juliette T.J. Lecomte: designed research, analyzed data, and wrote the paper

3.1 Abstract

The nuclear genome of the model organism *Chlamydomonas reinhardtii* contains genes for a dozen hemoglobins of the truncated lineage. Of those, *THB1* is known to be expressed but the product and its function have not yet been characterized. We present mutagenesis, optical, and NMR data on the recombinant protein and show that at pH near neutral in the absence of added ligand, THB1 coordinates the heme iron with the canonical proximal histidine and a distal lysine. In the cyanomet state, THB1 has close structural similarity to other known truncated hemoglobins, particularly the heme domain of *C. eugametos* LI637, a light-induced chloroplastic hemoglobin. Recombinant THB1 is capable of binding cyanide and nitric oxide ($NO^{\bullet}$) in either the ferric or ferrous state and has efficient $NO^{\bullet}$ dioxygenase activity. By using different *C. reinhardtii* strains and growth conditions, we demonstrate that the expression of *THB1* is under the control of the nitrate assimilation-specific regulatory gene *NIT2* and that the hemoglobin is linked to the nitrogen assimilation pathway.

3.2 Introduction

In 1992, Potts and coworkers[1] discovered in the cyanobacterium *Nostoc commune* a gene coding for a product resembling protozoan and mammalian myoglobins. It was remarkable that a protein commonly associated with dioxygen transport was found in cyanobacteria and intriguing that the gene was positioned between *nif*U and *nif*H, two essential components of a nitrogen fixation operon. Subsequent investigations have uncovered that *N. commune* "cyanoglobin" belongs to a distinct and well-represented lineage of the hemoglobin (Hb) superfamily,[2] which has been given the general name of truncated hemoglobins (TrHbs) in reference to their primary structures containing ~30 fewer amino acids than myoglobin (Mb). *N. commune* cyanoglobin is thought to be involved in dioxygen scavenging, presumably to protect the nitrogenase from oxidative damage.[3]

Shortly after the discovery of cyanoglobin, two light-induced TrHb genes, *LI410* and *LI637*, were found in the unicellular photosynthetic eukaryotic alga *Chlamydomonas eugametos (moewusii)*.[4] Crystallization and subsequent structure determination of the globin domain of the *LI637* gene product (hereafter CtrHb) provided the first glimpse of a TrHb fold.[5] The heme group is buried in the protein, which adopts a two-on-two helical topology resulting from the shortened sequence. LI637, a protein targeted to the chloroplast, was one of the first TrHbs to be studied in vivo. Protection against oxidative damage was also proposed as a function for this Hb.[6]

Genes coding for proteins containing one or more Hb domains are present in virtually all forms of life and occur in three distinct lineages including the TrHb family.[7] Recent genome analyses show a preponderance of TrHbs in cyanobacteria and green algae.[8] The phylogenetic data support the rise of TrHbs soon after the appearance of life on this planet, emerging perhaps as early as three billion years ago.[7,9] During this early phase of life

on Earth, atmospheric dioxygen levels were low (10^{-6} atm). Elevation of dioxygen level resulted from subsequent geological upheaval and the evolution of photosynthesis roughly 2 billion years ago.[10,11] Given that the TrHb scaffold was formed long before the development of our current aerobic environment, an attractive original role for these proteins is dioxygen detoxification, as put forth for the modern *N. commune* and *C. eugametos* proteins.

The search for globin physiological functions in unicellular photosynthetic organisms is further guided by the observation that many Hbs (including members of the TrHb family) are capable of reacting with nitrogen-oxygen compounds such as nitric oxide ($NO^{\bullet}$),[12,13] nitrite, and peroxynitrite.[14] The reactions include oxidation, e.g., generation of nitrate from nitric oxide by oxy Hb; reduction, e.g., formation of nitric oxide from nitrite by deoxy Hb; and isomerization, e.g., conversion of peroxynitrite into nitrate by ferric (met) Hb, each process depending on the redox and ligation state of the protein. Such chemical versatility can be attained by alterations of the heme environment without disruption of the fold. Reactive nitrogen species (RNS) are present in and around photosynthetic algae and cyanobacteria as products of enzymes involved in nitrite or nitrate reduction; they also are produced in the diffusion-limited reaction of $NO^{\bullet}$ and superoxide. Thus, deoxygenation and RNS regulation are conceivable functions for TrHbs in these organisms.

Among RNS, $NO^{\bullet}$ is a focus of Hb research as these proteins are generally capable of $NO^{\bullet}$ dioxygenation.[13,15] The overall $NO^{\bullet}$ dioxygenase (NOD) reaction can be summarized as

$$\text{Hb-Fe(II)} + O_2 \leftrightarrows \text{Hb-Fe(III)}{-}O_2^- \quad (1)$$

$$\text{Hb-Fe(III)}{-}O_2^- + NO^{\bullet} \rightarrow [\text{Hb-Fe(III)}{-}OONO^-] \quad (2)$$

$$[\text{Hb-Fe(III)}{-}OONO^-] \rightarrow \text{Hb-Fe(III)} + NO_3^- \quad (3)$$

$$\text{Hb-Fe(III)} + e^- \rightarrow \text{Hb-Fe(II)} \quad (4)$$

To undergo multiple turnovers, the protein must be re-reduced to the O_2-binding competent ferrous state (step 4). Unlike the flavohemoglobins, which contain a flavin adenine dinucleotide (FAD) binding domain that allows for efficient heme redox cycling,[16] proteins such as THB1 would require intermolecular electron transfer to accomplish this last step.

$NO^{\bullet}$ plays a role as a signaling molecule in a variety of cellular processes, including several in the model organism *C. reinhardtii,* a close relative of *C. eugametos*. Specifically in the former, $NO^{\bullet}$ inhibits the import of ammonium, nitrite, and nitrate, and also nitrate reductase activity. These observations support that $NO^{\bullet}$ can regulate the assimilation of nitrogen[17] and direct attention to the possible involvement of globins in processes related to $NO^{\bullet}$.

Several TrHb genes have been identified within the nuclear genome of *C. reinhardtii*. Following the current UniProtKB annotations these are designated *THB1* through *THB4*, but as many as ten to twelve putative genes may contain TrHb domains.[8] Most of *C. reinhardtii* TrHbs are hypothetical proteins. Exceptions are the products of "*THB8*," the expression of which is increased over a thousand-fold under anoxic conditions, and "*THB7"* and "*THB12*," which display mild up-regulation under hypoxic conditions.[18] These proteins have not been characterized fully and the chemistry associated with them is unclear. Recently, the gene product of *THB1* has been identified in in-vivo work focused on intraflagellar transport (IFT) and the BBSome, an IFT cargo adaptor.[19] In this case as well, functional information is missing.

Knowledge of amino acid sequences and in-vitro properties far exceeds physiologic data for the TrHbs of cyanobacteria and unicellular photosynthetic algae.[20] There are numerous reasons for this lack of information, including the relatively low levels of globins in the cell and the likelihood that these proteins are not essential under most growth conditions. THB1 offers a rare opportunity to explore the properties of a TrHb and

connect in-vitro and in-vivo information in a model organism. Toward this goal and the testing of specific functional hypotheses, we report on the structure and reactivity of the purified recombinant protein and we demonstrate a possible involvement of the protein in nitrogen metabolism.

3.3 Materials and Methods

3.3.1 *Chlamydomonas* cell culture

Strains CC-125, CC-1086, CC-1690 and CC-2453 were obtained through the Chlamydomonas Resource Center (University of Minnesota). Strains g1 and *bbs4-1* were from the Witman lab. Cells were maintained on tris acetate phosphate (TAP) medium agar plates until use. Liquid cell cultures were grown in Sager-Granick M medium,[21,22] unless noted otherwise, at 20 °C under constant agitation and illuminated with cool white fluorescent light on a 14/10 (on/off) cycle to synchronize cell growth. For flagella isolation experiments, cells were aerated by bubbling with 5% CO_2 and 95% air.

3.2.2 Antibody production, protein analysis, and gene expression.

Polyclonal antibodies were prepared using the synthetic peptide AADTAPADSLYSRC, which corresponds to the first 13 amino acids of THB1 (excluding the initial Met) followed by a single cysteine for covalent attachment to the keyhole limpet hemocyanin carrier protein. Antibodies were raised in rabbit (Covance, Princeton, NJ), affinity purified using the same synthetic peptide, and stored frozen at a protein concentration of approximately 1.5 mg/mL in phosphate-buffered saline (PBS) until use.

Whole cell protein was extracted from actively growing cultures of *C. reinhardtii* by resuspending approximately 1×10^7 cells per mL in 60 mM Tris-HCl pH 7.0, 10% glycerol, 2% sodium dodecylsulfate (SDS) and 50 mM tris(2-carboxyethyl)phosphine (TCEP,

BondBreaker, Thermo Scientific), followed by boiling for 10 min and separating the protein on a 16.5% tris-tricine SDS polyacrylamide gel (Bio-Rad Laboratories, Hercules, CA). For silver staining, gels were fixed and stained according to manufacturer's protocol (Silver Stain Plus Kit, Bio-Rad). Flagellar isolation was performed using the dibucaine method as previously described.[23] In these experiments, whole cell samples were collected immediately prior to dibucaine treatment. After flagellar abscission, cell bodies were separated from flagella by centrifugation (3 min; 1,150 × *g*). Concentrated whole flagella and corresponding whole cell and cell body proteins were separated on 4-15% Mini-PROTEAN TGX precast gels (Bio-Rad, Hercules, CA). For western blots, the proteins were transferred to nitrocellulose (Whatman), blocked with dry milk, probed with appropriate antibodies, and detected using chemiluminescence. Rabbit polyclonal antisera (and dilutions) were anti-PLD (1:5,000),[23] anti-BBS4 (1:2,000),[19] and anti-βF_1-ATPase (1:80,000).[24] Mouse monoclonal antibodies used were anti-IC2 (1:400)[25] and anti-IFT139 (1:20).[26]

For gene expression analysis, total cell RNA was extracted from actively growing cells using the RNeasy Plant RNA extraction kit with optional on-column DNA digest (Qiagen, USA), and the quantity and purity of RNA was determined using a NanoDrop Spectrophotometer (Thermo Scientific). cDNA was synthesized from purified RNA using iScript cDNA Synthesis kit (Bio-Rad) and analyzed using PrimeTime qPCR probes (Appendix Table A1) and 1 × SsoFast Probes Supermix (Bio-Rad) on a Bio-Rad CFX Real Time Detection system using 40 cycles with 10-s 95-°C melt and 20-s 60-°C elongation steps per cycle. Normalized gene expression was calculated from biological duplicates performed in triplicate wells and normalized relative to the expression of the *CBLP* control gene[27] using the CFX Manager software.

3.3.3 Recombinant protein production

The coding sequence for the *THB1* gene was obtained from GenBank (EU095254.1) and used to create a synthetic gene that was inserted in the pJExpress414 plasmid after codon-optimization for expression in a bacterial host system (DNA 2.0, Menlo Park, CA). Recombinant THB1 (referred to below as rTHB1) was obtained as described previously for *Synechocystis* sp. PCC 6803 GlbN.[28] As in this case, overexpression results in the production of apoprotein, which fractionates into inclusion bodies. Following urea solubilization and gel filtration chromatography, the holoprotein was prepared by addition of excess hemin (Sigma) to refolded apoprotein, further purified by anion exchange chromatography, and lyophilized for storage at −20 °C as necessary.

Mass spectroscopy was performed on an Acquity / Xevo-G2 UPLC-MS (Waters) and returned a molecular mass of 14564 Da for purified rTHB1, in excellent agreement with the 14564.4 Da expected for the polypeptide lacking the initial methionine. Protein concentration was determined on a per-heme basis with an extinction coefficient at 409 nm of 125 mM^{-1} cm^{-1} (ferric state, pH 7.0) obtained by the hemochromogen assay[29] as reported elsewhere.[30] Apoprotein extinction coefficient was estimated to be 5.96 mM^{-1} cm^{-1} on the basis of the amino acid composition.[31]

Plasmids for Y29F and K53A rTHB1 production were obtained via QuikChange (Qiagen) mutagenesis of the pJexpress414 plasmid containing the codon-optimized *THB1* gene as per manufacturer's instructions. Primers were from Integrated DNA Technologies (Coralville, IA). Sequencing was performed by GENEWIZ, Inc. (South Plainfield, NJ). Overexpression and purification of the Y29F and K53A variants were performed in the same manner as for wild-type rTHB1.

3.3.4 O_2 scavenging and reduction systems

When solutions needed to be scrubbed of dissolved O_2, the protein was incubated and data were collected in the presence of coupled glucose oxidase/catalase oxygen scavenging system (GODCAT).[32] Final concentrations of the various components were 16.7 mM D(+) glucose (Amresco, Solon, OH); 0.02 mg/mL bovine catalase (Sigma); and 0.04 mg/mL *Aspergillus niger* glucose oxidase (Sigma).

When dithionite (DT, Alfa Aesar, Ward Hill, MA) was not appropriate for reduction of the ferric protein, a ferredoxin (Fd) /$NADP^+$ reductase system[33] was used. Final concentrations of the various components (all from Sigma) were 0.04 mg/mL bovine catalase; 2.8–3.0 mM glucose-6-phosphate; 10 μM NADPH; catalytic amounts of *Leuconostoc mesenteroides* glucose-6-phosphate dehydrogenase; catalytic amounts of spinach Fd/$NADP^+$ reductase; and 30 μg/mL spinach Fd.

3.3.5 pH titration of ferric and ferrous rTHB1 by absorption spectroscopy

The pH titration of ferric wild-type rTHB1 was obtained with a sample (15 μM) in 5 mM phosphate pH 11.0. Spectra were obtained from 700 nm to 260 nm in ~0.2 pH unit decrements achieved by adding 0.1 M or 1 M HCl until a pH of 4.0 was reached. Complementary data were obtained from two separate titrations (acid range from pH 7.2 to 3.0 and base range from pH 7.2 to 13.0). The pH titration of ferric Y29F rTHB1 was obtained in a similar fashion in the pH ranges 7.4–10.2, 7.4–3.3, and 9.0–14). A coarse pH titration of ferric K53A rTHB1 was performed between pH 4.8 and 10.2 in ~1 pH unit increments. Data from the ferric wild-type and Y29F rTHB1 between pH 5 and 10 over the 430 nm and 700 nm range were subjected to singular value decomposition[34] using SciLab. Global fitting of significant vectors was performed with Savuka.[35]

The pH titration of ferrous wild-type rTHB1 was obtained from separate samples for each pH value from pH 4 to pH 10.8. Each sample contained ~7 μM ferric rTHB1 in 100 mM buffer; different buffers were used depending on the desired pH (pH 4.0 to 6.3: acetate/phosphate; pH 6.5 to 8: phosphate; pH 8.3 to 9.0: borax; pH 9.5 to 10.5: glycine). Spectra for each sample in the ferric state were collected prior to reduction in order to determine the concentration of the protein using the pH-dependent extinction coefficient determined in the above titration. Ferrous rTHB1 was then obtained by adding 2 mM DT to the sample, and the reduction was monitored as a function of time. Data points to form the titration curve were collected when the Soret band displayed maximum absorbance. The change in absorbance with time suggested protein damage by DT and the titration was therefore less accurate than in the ferric state.

3.3.6 Ligand binding studies

Lyophilized ferric rTHB1 was dissolved in 100 mM phosphate buffer, pH 7.1, to generate a concentrated stock of the protein (~2 mM). From this stock, samples containing ~8 μM rTHB1 were prepared for absorbance spectra collection. The cyanomet complex (i.e., the ferric protein with cyanide bound as the distal ligand) was obtained by addition of a 5-fold excess KCN. The ferric-$NO^{\bullet}$ adduct (Fe(II)-NO^{+}) was prepared by addition of 130-fold excess $NO^{\bullet}$ as released by 6-(2-hydroxy-1-methyl-2-nitrosohydrazino)-N-methyl-1-hexanamine (MAHMA-NONOate, Cayman Chemical, Ann Arbor, MI). In both cases, spectra were collected until saturation was observed. No autoreduction to the ferrous nitrosyl complex was observed over the timescale of the experiment (~4 min); slow return to the ferric state indicated an unstable complex. The ferrous state was generated by incubation of the rTHB1 sample with GODCAT prior to DT addition. The Fd/$NADP^{+}$ reduction

system was used when the O_2 bound state (Fe(III)-O_2^-) was sought. The ferrous cyano complex was obtained by reduction of the cyanomet complex with excess DT. Likewise, the ferrous NO• adduct (Fe(II)-NO) was obtained by DT reduction of the ferric NO• adduct. O_2 and CO bound rTHB1 samples were generated in buffer sparged with either O_2 (Air Gas, research grade, 99.999% pure) or CO gas (Air Gas, chemically pure grade, 99.5% pure) and reduced with either the Fd/$NADP^+$ reduction system or DT in the presence of GODCAT, respectively.

3.3.7 Nitric oxide dioxygenase and Griess assays

The procedure used MAHMA-NONOate as the NO• donor and the Fd/$NADP^+$ reductase system for rTHB1 reduction. Specifically, 10 μM rTHB1 samples were prepared from a concentrated rTHB1 stock in 100 mM phosphate buffer, pH 7.1, equilibrated with air (~21% O_2, 230 □ M). The components of the Fd/$NADP^+$ reduction system were added except for Fd, and a reference UV/Vis spectrum of ferric rTHB1 was collected. Approximately 30 μg of Fd was added (2.5 μM Fd, final concentration) to the sample, which resulted in observable Fd-mediated rTHB1 reduction. Absorbance data were collected from 600 nm to 300 nm every minute, with a scan rate of 600 nm/min.

Once rTHB1 was saturated with O_2, MAHMA-NONOate, quantitated by absorption spectroscopy at high pH (ε(250 nm) = 7.25 $mM^{-1}\,cm^{-1}$)[36] was added to the sample to generate 2 or 3 eq of NO•. The deadtime for manual mixing was 15 s, after which the reaction of NO• with oxy rTHB1 was followed. Once the sample recovered to the oxy state, a new addition of MAHMA-NONOate was made, and this protocol was repeated for a total of 5–8 times. As a control, a second sample containing buffer and the Fd/$NADP^+$ reductase system was prepared with no rTHB1 present (referred to as "–THB1"), and was

treated in the same manner as the sample containing rTHB1 ("+THB1"). Horse skeletal muscle Mb (Sigma) was subjected to an analogous procedure for comparison purposes.

Nitrite was quantitated at the end of each experiment using the Griess assay.[37] The NOD reaction mixtures were split into two fractions to which 4 μM FAD (final concentration) was added. To one of these samples, *Aspergillus* nitrate reductase (NR, Sigma) was added to a final concentration of 0.075 units/mL along with an NADPH regeneration system[38] to convert nitrate into nitrite stoichiometrically. After ~20 min, both samples were treated with the Griess reagents (GR) as per manufacturer's instructions (Life Technologies, Grand Island, NY). Absorbance spectra were collected from 600 nm to 300 nm every minute until complete conversion was reached by the sample containing the largest amount of nitrite (~20 min). Nitrite concentrations were obtained from a calibration curve produced under the same conditions as used for the NOD reaction and yielding ε(520 nm) = 26.9 $\mu M^{-1}cm^{-1}$ for the diazonium product. The same protocol was used to determine the amount of nitrate produced in NOD reactions in the presence of horse skeletal muscle Mb. Kinetic simulations were performed with KinTek Explorer.[39]

3.3.8 UV-Visible spectrophotometry

Absorbance spectra were collected either on Varian Cary-50 or AVIV 14DS instruments. For extinction coefficient measurement, pyridine hemochrome spectra were acquired in triplicate, from 600 to 500 nm in 1-nm steps, using a 1-s averaging time per step. Ligand binding, NOD, and Griess assays were monitored using the Cary50 scanning kinetics mode. Optical spectra were collected using a 0.1-s or 0.2-s averaging time, from 700 to 300 nm, every 30 s for 10 min, until sample equilibration was achieved. The same parameters were used for the H_2O_2 addition experiments, in which 5-fold excess H_2O_2 was added to 10 μM WT THB1, in 100 mM borate buffer, pH 9.30.

3.3.9 NMR spectroscopy

NMR data were acquired at 14.1 T with a Bruker Avance or Avance II spectrometer equipped with a cryoprobe. ^{1}H chemical shifts were referenced to 2,2- dimethylsilapentane-5-sulfonic acid through the temperature corrected $^{1}H_2O$ line (4.76 ppm at 298 K). ^{13}C and ^{15}N chemical shifts were referenced indirectly in accordance with their respective Ξ ratios.[40] NMR data were processed using the programs NMR Pipe 3.0[41] or TopSpin 2.1 (Bruker BioSpin, Rheinstetten, Germany). Analysis of NMR spectra was completed using Sparky 3.[42]

Unlabeled or uniformly ^{15}N-labeled rTHB1 samples were exchanged from 50 mM Tris purification buffer into 300 μM phosphate or 20 mM phosphate, pH 7.5–8.0, 10 % $^{2}H_2O$/90% $^{1}H_2O$, and first examined in the ferric state in the absence of exogenous ligand. Ferric wild-type, Y29F, and K53A rTHB1 samples ranged from 500 μM to 3 mM heme in 270–600 μL, pH 7.0-7.6. Initial ^{1}H spectra were collected at either 298 or 308 K over a large spectral width to detect high-spin species. Increased population of the high spin form of ferric rTHB1 was achieved by lowering the sample pH to 5.4 at 298 K.

To generate the ferrous state of wild-type, Y29F, and K53A rTHB1, a ~2 mM protein solution (25 mM borate, pH 9.5–9.1) was placed in a glovebox under continuous Ar (AirGas purity 4.8) stream. After approximately 10 min the protein was reduced with 2.5 molar eq DT. The solution was transferred to an NMR Shigemi tube, and the tube sealed with Parafilm. Samples produced in this manner remained completely reduced over the timescale of NMR data acquisition (days to weeks). Ferrous ^{15}N WT, and unlabeled Y29F, and K53A rTHB1s were investigated by collecting one-dimensional (1D) ^{1}H spectra with water presaturation. ^{1}H-^{15}N HSQC, ^{1}H-^{15}N histidine selective long-range HMQC data were collected on the wild-type protein, and homonuclear two-dimensional (2D) NOESY and DQF-COSY data were acquired on the Y29F variant as described previously.[43]

For electron self-exchange (ESE) measurements, a 1.8 mM sample of ferric wild-type ^{15}N rTHB1 in 250 mM borate, pH 9.2, 10 % $^{2}H_2O$/90% $^{1}H_2O$ was incubated with GODCAT and purged with Ar as described above. A substoichiometric amount of DT was added, resulting in a mixture containing ferric and ferrous protein in a ~2.2:1 ratio. As estimated by the relative integrated intensities of resolved amide signals in relaxed ^{1}H-^{15}N HSQC spectra, the ferrous and ferric populations remained stable over the course of 24 h (final ratio ~2.6:1 ferric:ferrous).

The kinetics of ESE were estimated on a mixture of ferric and ferrous rTHB1 using a ^{1}H-(N_Z)-^{1}H ZZ exchange experiment. The sample was initially screened by comparing standard ^{15}N-^{1}H HSQC data with an ^{15}N-(N_Z)-^{1}H 2D ZZ exchange spectrum (ZZ mixing time = 452 ms) collected as detailed previously.[44] The small difference in ^{15}N shifts between ferrous and ferric forms necessitated the use of ^{1}H-(N_Z)-^{1}H 2D ZZ exchange data.[44,45] N_Z ZZ mixing times were of 452, 271, 701, 158, 565, 362, 1018, and 452 ms. $^{1}H_Z$-$^{15}N_Z$ heteronuclear cross-relaxation was minimized with 1.3-ms G3 ^{1}H inversion pulses every 10 ms during the N_Z mixing time; these pulses were applied 2800 Hz downfield of the $^{1}H_2O$ line so as to limit the saturation of water magnetization, which was maintained at equilibrium during the ZZ period. Because of the low cross-peak intensity and sample variation with time, the data provide a lower limit estimate of the kinetics of ESE.

3.4 Results and Discussion

Figure 3.1A presents the primary structure of THB1, which has the features of a "Group I" TrHb (TrHb1 for short), one of three branches of the TrHb family.[2] Of the few TrHb1s that have been studied, the closest relatives are also shown: *C. eugametos* LI637[4] (CtrHb, 48% identity), and the cyanobacterial globins from *Synechocystis* sp. PCC 6803 (49% identity) and *Synechococcus* sp. PCC 7002 (46% identity). The three-dimensional structures of

these proteins are available in the cyanomet form (PDB ID: 1DLY, 1S69, and 4L2M, respectively). The Cα traces of the three structures superimpose with root mean square deviations under 0.8 Å over 90% of the chain. This close similarity raises the expectation that the TrHb1 fold is robust and representative of THB1. The structure of cyanomet CtrHb with appropriate amino acid replacements (Fig. 3.1B) was used to guide the analysis of the NMR data.

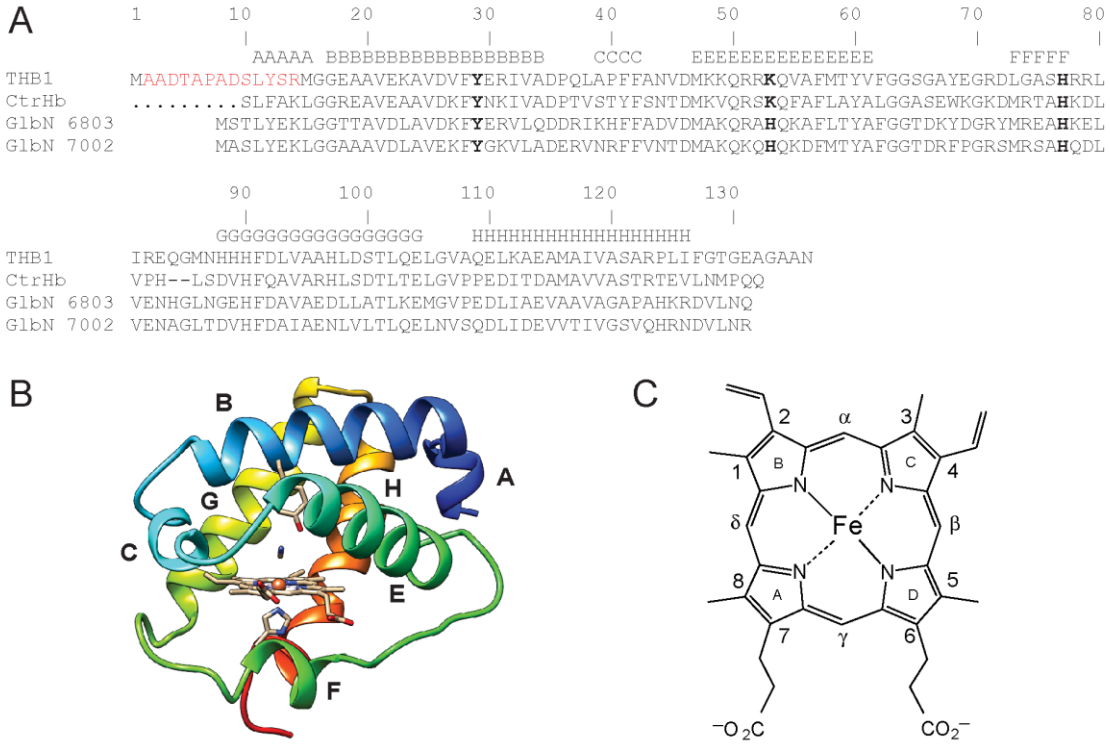

Fig. 3.1 THB1 sequence and structural model. (A) Sequence alignment of THB1 and related TrHb1s. CtrHb: heme domain of *C. eugametos* LI637; GlbN 6803: GlbN from *Synechocystis* sp. PCC 6803; GlbN 7002, GlbN from *Synechococcus* sp. PCC 7002. Sequence numbering is for THB1. Helices are denoted A–H according to the secondary structure of CtrHb (PDB ID: 1DLY) and Perutz notation. Residues of interest are His77 (the proximal histidine), Tyr29 (referred to as "B10" by analogy to the three-dimensional structure of mammalian Hbs), and Lys53 ("E10"). These positions are highlighted with boldface font. **(B)** Structural model of THB1 prepared with SWISS-MODEL.[79] The program selected CtrHb with bound cyanide (PDB ID: 1DLY) as the best template for homology modeling.[79] **(C)** The heme structure and numbering.

3.4.1 rTHB1 binds diatomic ligands

Figure 3.2A–D shows the absorption spectra of rTHB1 with and without the usual complement of diatomic ligands at neutral pH: O_2, CO, and $NO^{\bullet}$ in the ferrous state and CN^- and $NO^{\bullet}$ in the ferric state. Of note is the formation of the cyanide adduct of the ferrous state (Fig. 3.2C) by DT reduction of cyanomet rTHB1. Ferrous cyano rTHB1, however, could not be obtained by addition of cyanide to reduced rTHB1. Absorbance maxima and extinction coefficients are listed in Table 3.1. Each spectrum is distinctive and can be used for the purpose of identifying species occurring in mixtures and enzymatic assays.

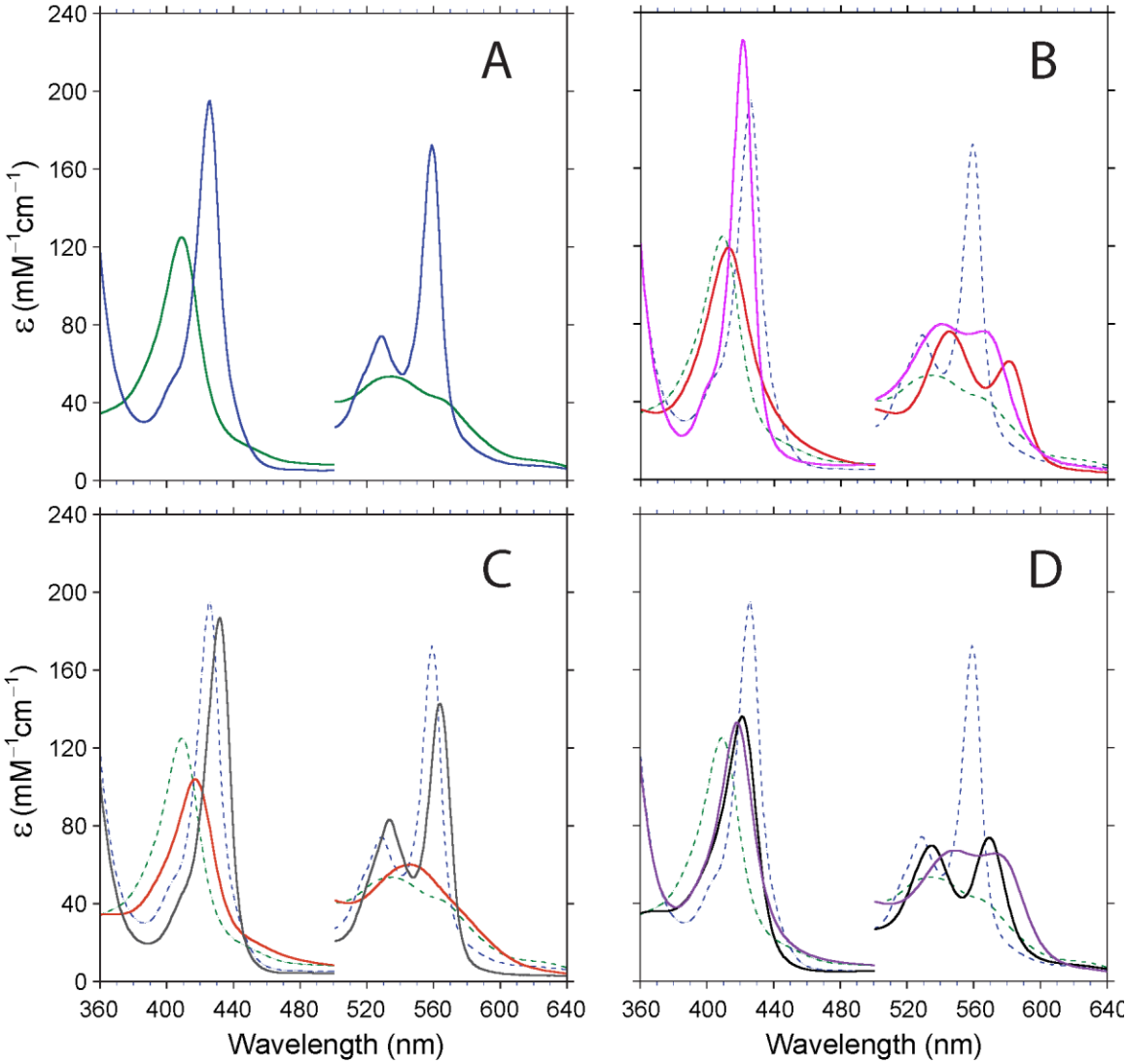

Fig. 3.2 Absorption spectra of various forms of rTHB1 (~10 μM, 100 mM phosphate buffer, pH 7.1). The vertical scale was adjusted to provide the extinction coefficient, ε in $mM^{-1}cm^{-1}$. The intensity of the α–β band region was magnified by a factor of 5. **(A)** Ferric (green) and ferrous (blue) proteins at pH 7.1. These two spectra are reproduced with dashed lines in panels B, C and D. **(B)** The oxy (red) and carbonmonoxy (magenta) states. **(C)** The cyanide complexes of the ferrous (gray) and ferric (orange) states. **(D)** The $NO^{\bullet}$ adducts of the ferrous (purple) and ferric (black) states.

Table 3.1 Optical properties of various rTHB1 complexes at pH 7.1

Protein State	Soret max (nm)	α (nm)	β (nm)	CT[a] (nm)	ε at Soret max (mM^{-1} cm^{-1})
Fe(III) (pH 4.8)	408	503, 542 (sh)		630	144
Fe(III) (pH 7.1)	410	536, 568 (sh)		630 (sh)	125
Fe(III) (pH 10.8)	412	538, 570 (sh)			118
Fe(II)	426	529	559		195
Fe(III)-CN^-	417	546			104
Fe(II)-CN^-	432	534	564		187
Fe(III)-NO	421	535	570		136
Fe(II)-NO	418	548	573		133
Fe(II)-O_2	412	545	581		119
Fe(II)-CO	421	541	564		226

[a] Charge transfer band.

3.4.2 pH dependence of heme axial coordination in ferric rTHB1

Figure's 3.3 and 3.4 illustrate the pH response of rTHB1 monitored with absorbance measurements in the absence of added ligand. Below pH 4.8, the Soret band experiences a sharp decrease in intensity (apparent pK_a = 3.72 ± 0.01, Hill coefficient = 3.45 ± 0.15); a shallower drop occurs at pH higher than 10.8 (apparent pK_a = 12.49 ± 0.01, Hill coefficient = 1.25 ± 0.03). Both acid and alkaline transitions (Fig. 3.4) are accompanied with spectral alterations between 400 and 700 nm characteristic of a change in heme coordination. The acid transition is likely coupled with protonation of the proximal histidine, heme loss from the protein cavity, and protein unfolding, whereas the nature of the alkaline transition is

unclear as the spectral features at very high pH (broad absorption band at 588 nm, Soret maximum at 398 nm, and shoulder at 350 nm) do not match those of free hemin under the same conditions.

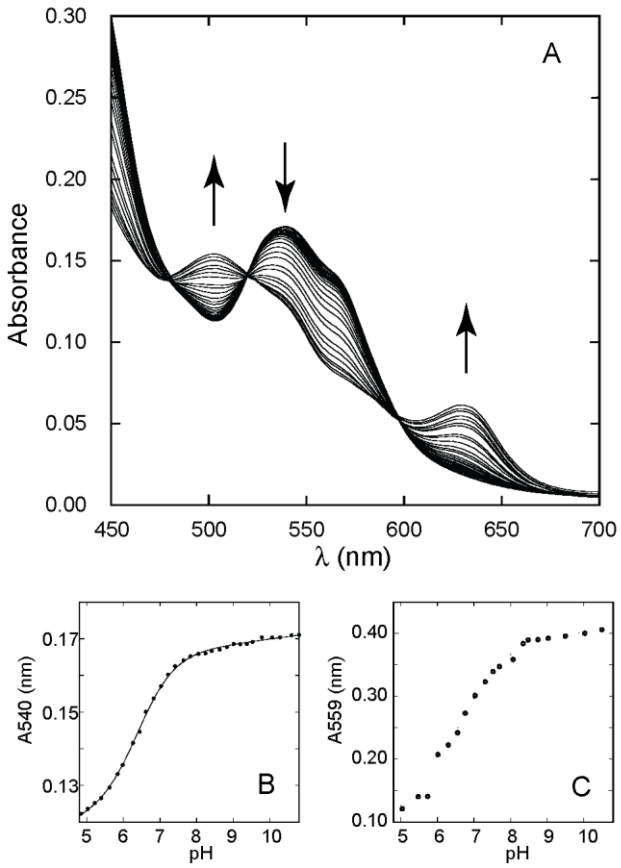

Fig. 3.3 pH titration of rTHB1. (A) The α and β bands of the ferric protein are shown at pH values between pH 10.8 and pH 4.8. The vertical arrows indicate the direction of the change as the pH is lowered. **(B)** Absorbance of the ferric protein at 540 nm as a function of pH. The solid line is the result of fitting the data according to a modified Henderson-Hasselbalch equation assuming a single ionization event (pK_a = 6.48, see text). **(C)** Absorbance of the ferrous protein at 559 nm as a function of pH.

The spectral response in the 4.8 to 10.8 pH range is shown for the visible region in Figure 3.3A. Figure 3.3B presents the pH curve described by the absorbance at 540 nm. The 430–700 nm data, when analyzed by singular value decomposition,[34] yield two principal

abstract vectors. Global fitting[35] returns an apparent pK_a of 6.48 ± 0.07 with Hill coefficient of 0.86 ± 0.03 (where the uncertainties are the errors of the fit) and indicates a transition involving one proton. However, imperfect isosbestic points (482, 522, and 598 nm) and the sloping baselines required to achieve a good fit (Fig. 3.3B) hint at the participation of an additional low-population species or secondary ionization event.

The main spectral component between pH 4.8 and pH 6.5 is consistent with a high-spin, water-bound species.[46] In contrast, the main component between pH 6.5 and pH 10.8 has low-spin character and is not readily recognized. Its appearance eliminates the possibility of a ferric hydroxy complex [46] or a ferric pentacoordinate species[47] and supports coordination of a protein residue to the iron on the distal side. This behavior parallels that of ferric CtrHb.[48]

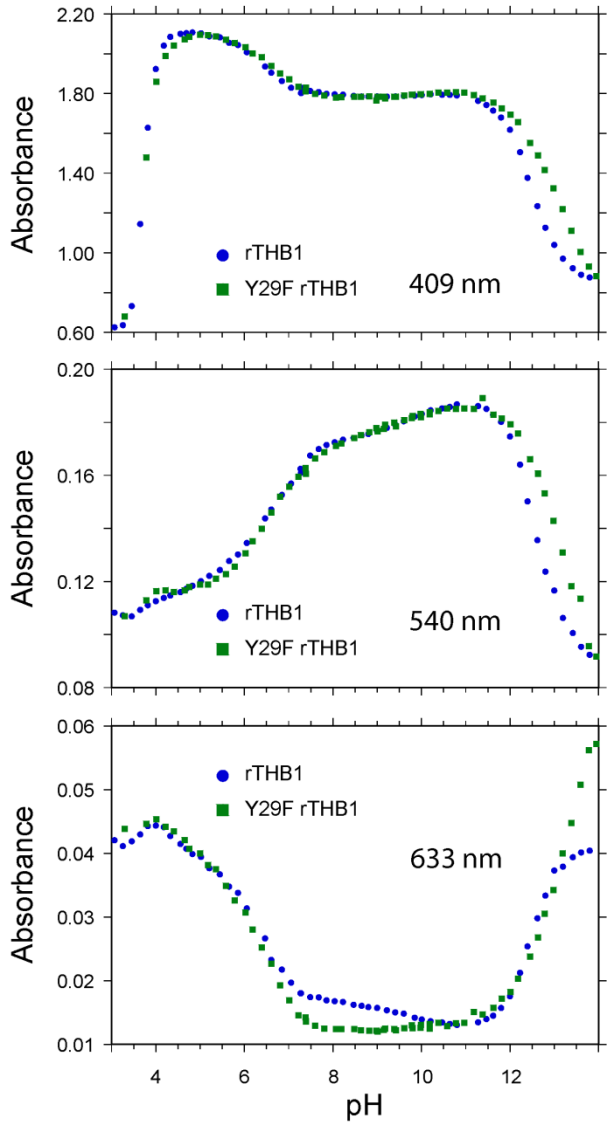

Fig. 3.4 Comparison of the pH titration of ferric wild-type rTHB1 (blue circles) **and Y29F rTHB1** (green squares). The response of Y29F rTHB1 differs from that of the wild-type protein at pH values above 11.5 (where the pH measurement becomes less reliable) and in the 7–10 range, where the high-spin marker (633 nm) of the former is completely absent. The overall similarity of the responses supports that Tyr29 (B10) is not an axial ligand to the iron.

3.4.3 pH dependence of heme axial coordination in ferrous rTHB1

The response of ferrous rTHB1 to pH, shown in Figure 3.3C, is also reminiscent of that observed for CtrHb. Between pH 7 and 10, the protein spectrum is consistent with that of a 6-coordinate low-spin complex.[49] At acidic pH, the spectral features of a 4-coordinate

heme[49] emerge with broad Soret and α-β bands suggesting loose association of the heme with the protein. The intermediate state, presumably a 5-coordinate species with the proximal histidine as sole axial ligand, does not become highly populated although there is evidence for this state at neutral pH (Fig. 3.5). The apparent pK_a for the global 6-coordinate to 4-coordinate transition is ~6.6.

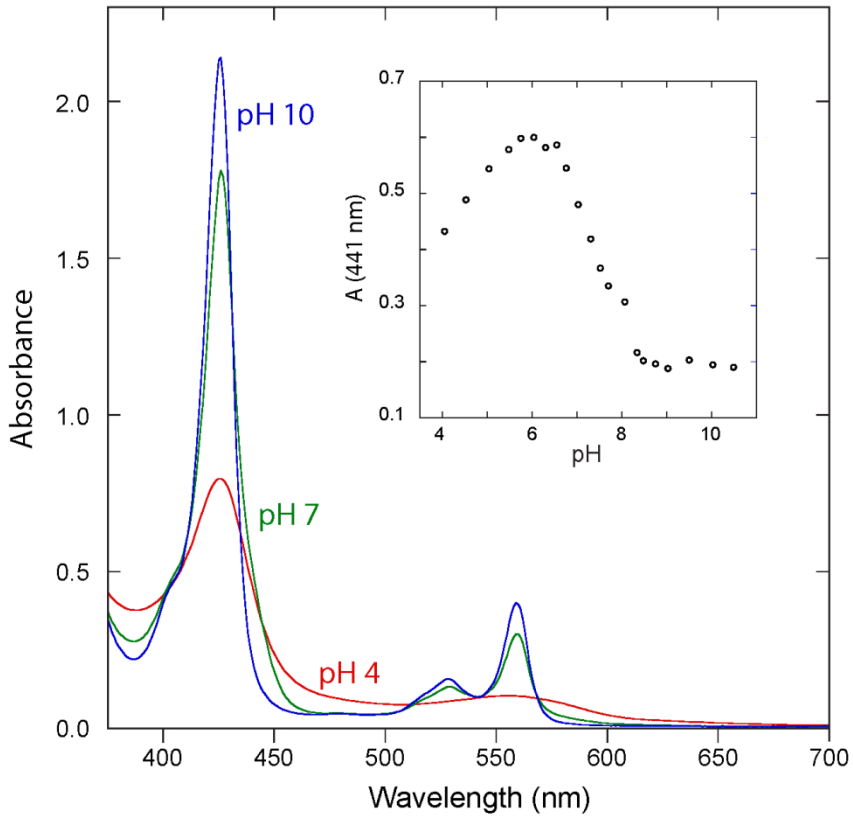

Fig. 3.5 Optical spectrum of ferrous wild-type rTHB1 at three pH values. The intermediate spectrum (green) has a shoulder at ~440 nm and cannot be reproduced with combinations of the other two spectra. This suggests the existence of additional species in solution. The inset shows the absorbance at 441 nm as a function of pH.

3.4.4 Endogenous coordination on the distal side – Optical data

Two plausible candidates for axial coordination on the distal side of the heme are the residues at position B10, as in CtrHb,[48] and E10, as in the two cyanobacterial GlbNs introduced in Figure 1A.[50,51] In THB1, Tyr29 occupies the B10 position, and Lys53 is at E10. To determine the identity of the distal ligand, we first replaced Tyr29 (B10) with a phenylalanine. The Y29F variant binds heme tightly and yields optical spectra (not shown) similar to those of the wild-type protein. In addition, the pH response has transitions in the acidic, neutral, and alkaline regions that match closely those of the wild-type protein (Fig. 3.4). In particular the transition near neutral pH occurs with an apparent pK_a of 6.82 ± 0.05 and a Hill coefficient of 0.97 ± 0.05, obtained by global fitting. The minor perturbations caused by the Y29F replacement suggest that, in ferric wild-type THB1, Tyr B10 is not an axial ligand to the iron.

In contrast, the K53A replacement causes pronounced changes in the optical spectrum and its pH response. At neutral pH K53A rTHB1 has a spectrum (Fig. 3.6) reminiscent of wild-type and Y29F rTHB1 at acidic pH, indicating the presence of a water molecule on the distal side of the heme and absence of a sixth endogenous ligand. There is little change in the spectrum from pH 5 to pH 8. At pH 9 the Soret band, Q band, and charge transfer band begin to decrease as the pH is raised. At pH 10 the charge transfer band has almost disappeared and both the Soret band and the Q band shift to the red (Soret maximum: 406 nm to 408 nm; Q: 502 nm to 534 nm). These data implicate Lys53 (E10) as the distal ligand to the iron responsible for the 6-coordinate low-spin features detected optically in wild-type and Y29F rTHB1. The absence of a 602 nm maximum also suggests that Tyr B10 does not coordinate the iron.[52] Interestingly, the spectra of ferric and ferrous wild-type and Y29F rTHB1 resemble those reported for the Met100Lys variant of

cytochrome *c*-550,[53] with allowance for a blue shift caused by the thioether cross-links in the cytochrome. Resemblance to complexes with N–Fe–N coordination is also noted.[54]

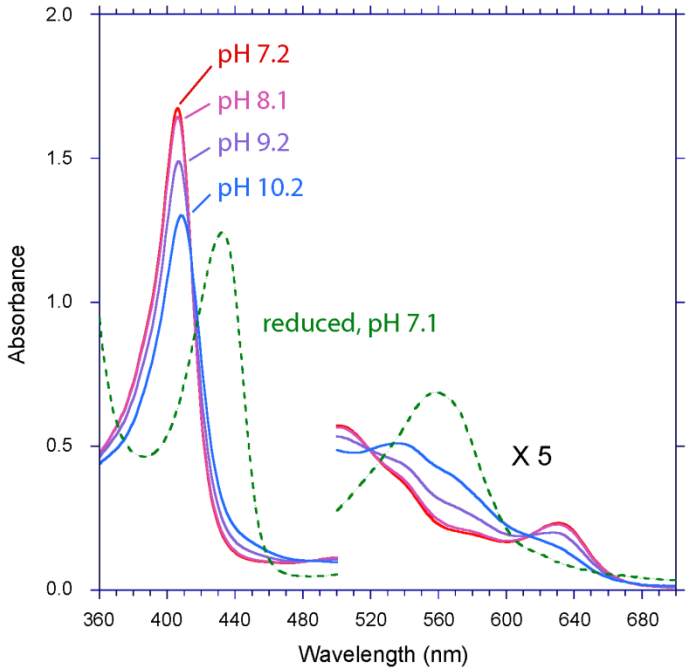

Fig. 3.6 K53A THB1 rough pH titration. The optical spectrum of K53A rTHB1 in the ferric state at four pH values and in the reduced state at pH 7.1. The ferric state undergoes an aquomet–hydroxymet transition at high pH.

3.4.5 Identification of Lys 53 as the distal axial ligand – NMR data

Optical spectra have limited information content, and amino acid replacements can have unanticipated consequences; confirmation of the ligation scheme was therefore pursued by NMR spectroscopy. At pH 7.6, the ^{1}H spectrum of ferric rTHB1, shown in Figure 3.7A, contains moderately shifted resonances supporting a predominant low-spin complex. The spectrum also showed a minor population of low intensity, far-downfield broad resonances characteristic of a high-spin (S = 5/2) complex.[55] In accordance with the absorbance data, this high-spin form increased in population (Fig. 3.7B) upon lowering the pH and was therefore attributed to an aquomet species. As the pH was raised above 8, the broad lines

disappeared, and only the spectrum with comparatively narrow features could be detected (not shown). At pH 7.0, the Y29F variant also displays a predominant low-spin species (Fig. 3.8C). Remarkably, the K53A rTHB1 spectrum at neutral pH contains only the resonances of an aquomet complex (Fig. 3.8D). As the pH is raised to 9.1, a broad spectrum consistent with mixtures of aquomet and hydroxymet forms is obtained (not shown).

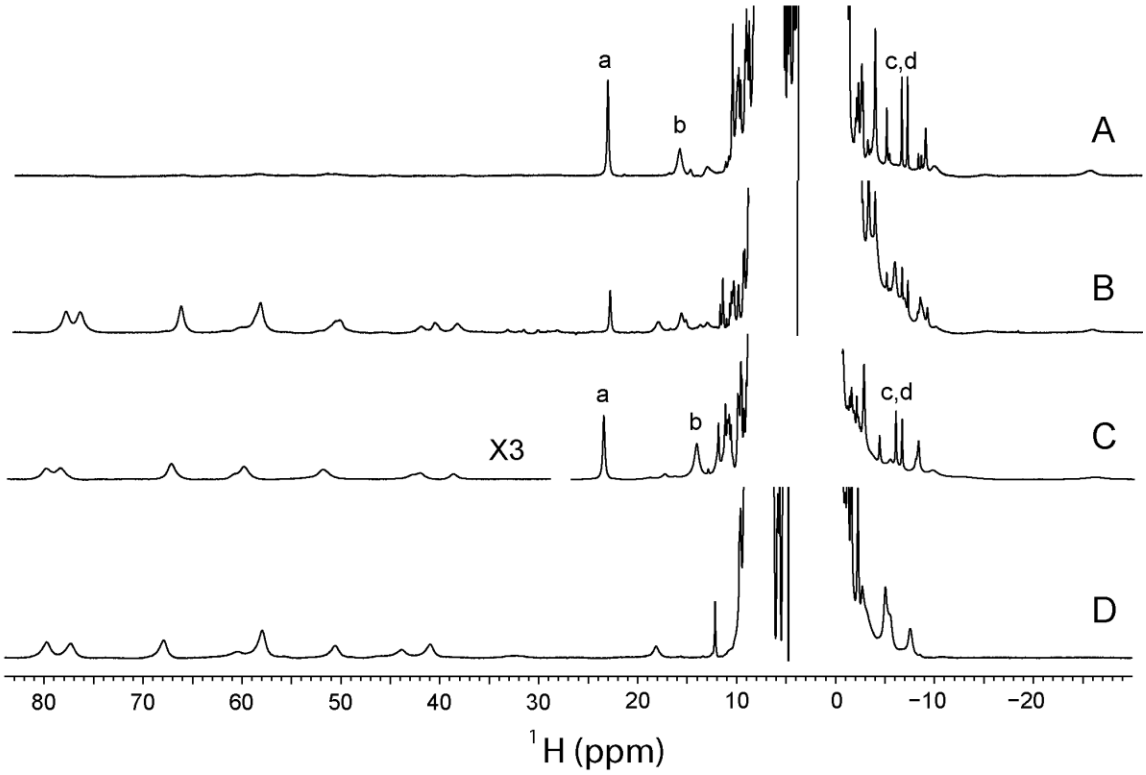

Fig. 3.7 One-dimensional ^{1}H spectra of ferric rTHB1. **(A**), wild-type, pH 7.6 (~9 % high-spin); **(B)**, wild-type, pH 5.4 (intensity ×4 compared to trace A, ~90% high-spin); **(C)**, Y29F variant, pH 7.0 (intensity of downfield region ×3, ~40% high-spin); and **(D)** K53A variant, pH 7.4. Resonances marked a, b, c, d correspond to the 3-CH_3, 8-CH_3, and 2-vinyl β_{trans} and β_{cis} protons from the low-spin wild-type and Y29F species. Data were recorded in 10% ^2H_2O/90% ^1H_2O and 298 K.

In close proximity to the iron, paramagnetic effects can broaden lines and render resonance identification difficult. These effects were attenuated by reduction to the ferrous

state, which was conducted at high pH (9–9.5) to populate the diamagnetic complex according to the optical data. The water-presaturation ^{1}H 1D spectrum of ferrous wild type rTHB1 (Fig. 3.9A) and ferrous Y29F rTHB1 (Fig. 3.9B) at pH 9.5 (10 % $^{2}H_2O$/90% $^{1}H_2O$) and pH* 9.2 (90% $^{2}H_2O$/90% $^{1}H_2O$), respectively, revealed a set of six single-proton resonances between −1.4 and −3.4 ppm. Such large upfield shifts are expected of nuclei above and below the porphyrin macrocycle. These signals were absent from the K53A variant, which displayed broad features (Appendix Fig. A20C) typical of $S > 1/2$ states. *J*-correlation data (DQF-COSY, Fig. 3.10A) collected on Y29F rTHB1 unequivocally traced a –CH–$(CH_2)_4$– system attributed to a lysine. A strikingly similar set of aliphatic resonances has been reported for the Met100Lys variant of cytochrome *c*[56] and lends further support to the ligation of a lysine to the iron. In addition, a resonance corresponding to two labile protons was detected at −7.8 ppm. Strong NOEs to the lysine aliphatic chain (Fig. 3.9B), splitting into a doublet in ^{15}N-labeled samples (Fig. 3.8A), and decoupling by ^{15}N irradiation at ~25 ppm (Appendix Fig. A20) secure assignment to the NζH_2 of the lysine. The chemical shifts of the Lys53 side chain are in Appendix Table A2. We conclude that the distal ligand in ferrous rTHB1 is Lys53, in the first example of a His–Fe–Lys coordination scheme in a hemoglobin.

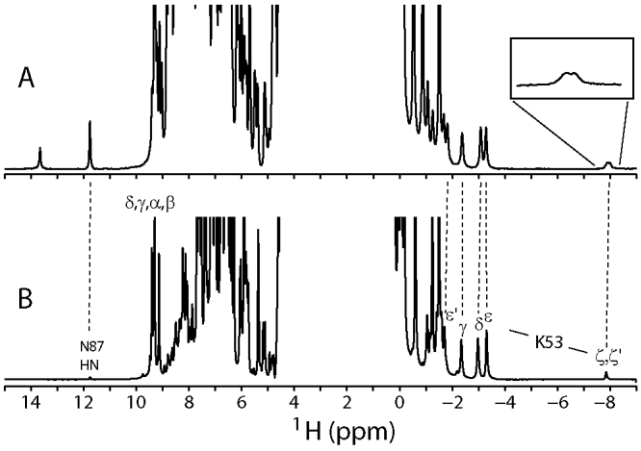

Fig. 3.8 ^{1}H spectra of ferrous rTHB1. One-dimensional spectra of **(A)** ^{15}N-labeled wild-type rTHB1 in 90% H_2O/10% ^2H_2O , pH 9.5, with amide ^{15}N decoupling (120 ppm) during acquisition; **(B)**, Y29F rTHB1 in 10% H_2O/90% ^2H_2O, pH* 9.2; heme meso, Asn87 NH and resolved Lys53 signals are labeled.

The pH titrations of ferric and ferrous wild-type rTHB1 displayed similar apparent pK_a values (6.5–6.6, Fig. 3.3); we reasoned that the axial lysine, which coordinates in the ferrous protein, remains a heme ligand in the ferric state. To test this hypothesis, we sought to measure ESE between the low-spin proteins. A sample of uniformly ^{15}N-labeled ferric wild-type rTHB1 was prepared at pH 9.2 to favor the endogenously hexacoordinate state (Fig. 3.4). Substoichiometric addition of DT resulted in a mixture of ferrous and ferric rTHB1. In fully relaxed ^{1}H-^{15}N HSQC spectra, the downfield-shifted amide NH signals from Asn87 (see below) report on the proportion of reduced and oxidized species. The mixture shown in Appendix Figure A21 originally contained approximately 31% reduced rTHB1. Little oxidation occurred during the course of data acquisition (28% reduced rTHB1 present at the end). Two-dimensional ^{1}H-(N_Z)-^{1}H data were collected to take advantage of the resolved ^{1}H shifts and the apparent slow exchange between the two states. The observation of specific cross peaks connecting corresponding ferrous and ferric amide NH resonances is direct

evidence that under these conditions, an electron transfer event interconverts the redox forms of rTHB1.

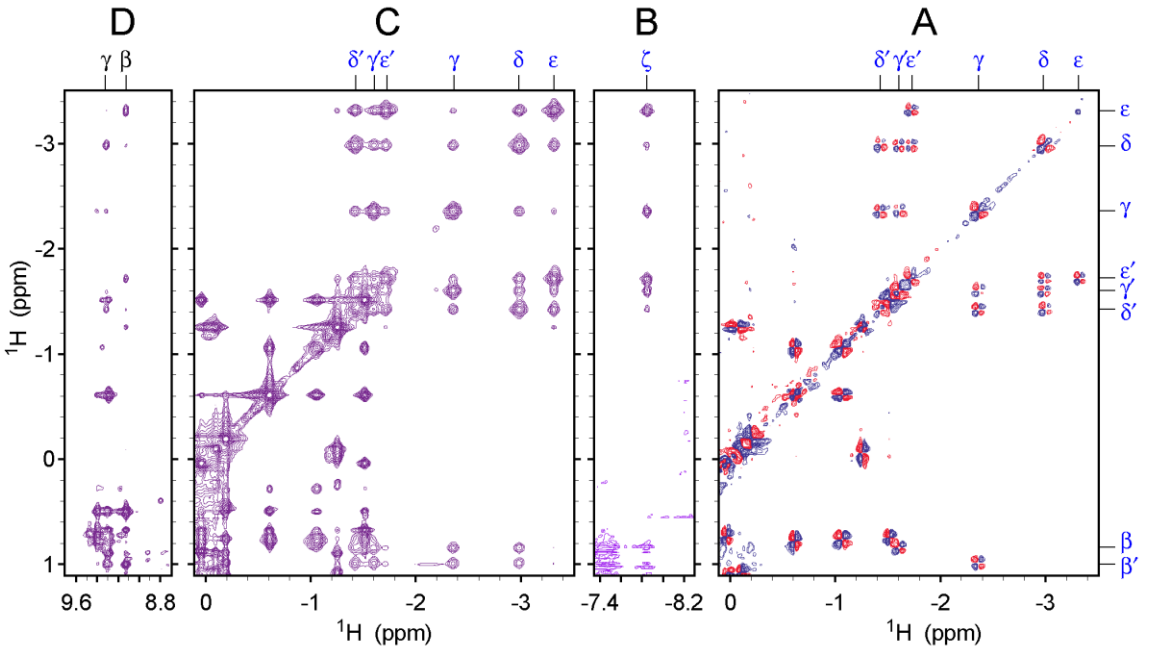

Fig. 3.9 Two-dimensional ^{1}H data collected on ferrous Y29F rTHB1. (A) Upfield portion of the DQF-COSY data. **(B–D)** Regions of the NOESY data mapping the Lys 53 spin system and indicating contact with the heme β and γ meso protons. Data were recorded in 10% ^2H_2O/90% ^1H_2O at 298 K, pH* 9.2. Blue symbols in A, B, and C refer to Lys53 signals. Black symbols in D are for heme meso signals.

In favorable cases, measurement of the cross and diagonal peak intensities as a function of the N_Z mixing time provides data for determining the rate constant of exchange.[56] Population drift and low signal-to-noise ratio prevented a detailed analysis of the exchange process, but an estimate could be obtained from the backbone amide cross peak of Asn87. An effective ESE rate constant was found to be 0.4 s^{-1} at 1.8 mM total protein. Although this number pertains to non-physiological conditions, it indicates that rTHB1 can exchange electrons at a rate about an order of magnitude slower than the *bis*-histidine GlbNs under similar conditions.[44] ESE kinetics have been measured from 10^7 – 10^2 $M^{-1}s^{-1}$ in a

variety of heme proteins including the cytochromes *c* (His-Met, $10^7 – 10^2$ $M^{-1}s^{-1}$), cytochromes b_5 (His-His, $10^5 – 10^4$ $M^{-1}s^{-1}$), and aforementioned GlbNs (His-His, $10^3 – 10^2$ $M^{-1}s^{-1}$). The rather slow kinetics for rTHB1 suggest that structural reorganization may limit the rate of electron transfer.[57] Rapid lysine decoordination or solvent exchange dynamics may explain the slow but detectable ESE, and be responsible for the broad lineshape of the Lys53 N□ H_2. Overall, the data are consistent with Lys53 as reversible distal ligand in both the ferric and ferrous states of rTHB1.

3.4.7 Enzymatic activity of rTHB1 – NOD and peroxidase activity.

NOD activity is a common function of globins that is often imputed to TrHbs. For example, *M. tuberculosis* TrHbN[59] and *T. pyriformis* TrHb1[58] are both likely to serve in the capacity of $NO^{\bullet}$ detoxifiers. Although there are differences in the heme pockets of these proteins, they share the distal hydrogen bond network identified by NMR spectroscopy in cyanomet rTHB1. This network may enhance the superoxide character of the O_2-bound state and to facilitate the NOD reaction. In the case of *C. reinhardtii*, NOD activity may be useful for protection from nitrosative damage and for regulation of processes involving $NO^{\bullet}$. Among the globins of *C. reinhardtii*, THB1 is the smallest, consisting only of the heme domain. It is highly water soluble, and therefore its potential role as a cytoplasmic enzyme must be considered.

To investigate the ability of rTHB1 to undergo multiple NOD turnovers, a simple in-vitro assay was designed that utilizes the optical spectra shown in Figure 3.2 (see Materials and Methods). Figure 3.11A illustrates typical results. At $t = 0$, a molar equivalent of MAHMA-NONOate was added to a sample containing rTHB1-O_2 and the Fd/$NADP^+$ reduction system. An immediate drop in the absorbance at 581 nm and 545 nm registered the disappearance of rTHB1-O_2. At the end of this rapid phase, the spectrum corresponds

to a mixture of ferric rTHB1 and rTHB1-O_2 (66% and 34%, respectively, in this particular experiment). The protein then returned to 100% rTHB1-O_2 under the effect of the enzymatic reduction system and dissolved O_2. Under these conditions, conversion is observed from the ferric state directly to the oxy state without detection of a ferrous intermediate. Also not detected are NO• adducts of the ferric or ferrous state.

Subsequent additions of MAHMA-NONOate lead to the same saw tooth behavior. The proportion of ferric state at the minimum of absorbance varies, with a tendency for an increase over the course of multiple NO• injections. At concentrations of the NO• donor capable of releasing three rather than two times the protein amount, the ferric form binds NO•, giving rise to the altered profile shown in Figure 3.10B. At no point was the ferrous-nitrosyl adduct of rTHB1 detected. The same experiment carried out with horse skeletal muscle Mb gave the profile shown in Figure 3.10C.

To verify that rTHB1 turns over NO• and forms nitrate, the end mixtures were subjected to the Griess assay.[37] The Griess assay depends on the reaction of sulfanilic acid with nitrite to form an activated diazonium salt, ultimately producing the detected azo dye. Under conditions of excess Griess reagents, colorimetric product formation reports on nitrite concentration. In the absence of rTHB1, oxidation of NO• by O_2 generates detectable quantities of nitrite most likely through the NO• + ½ O_2 reaction.[60] In the presence of rTHB1, however, a negligible amount of nitrite is found in solution (Fig. 3.11). This indicates an enzymatic reaction either consuming NO• considerably faster than the enzyme-free processes. Addition of *Aspergillus* NR to convert nitrate to nitrite showed that in the rTHB1 sample, ~90% of NO• released by MAHMA-NONOate was oxidized to nitrate. A comparable yield was obtained with Mb.

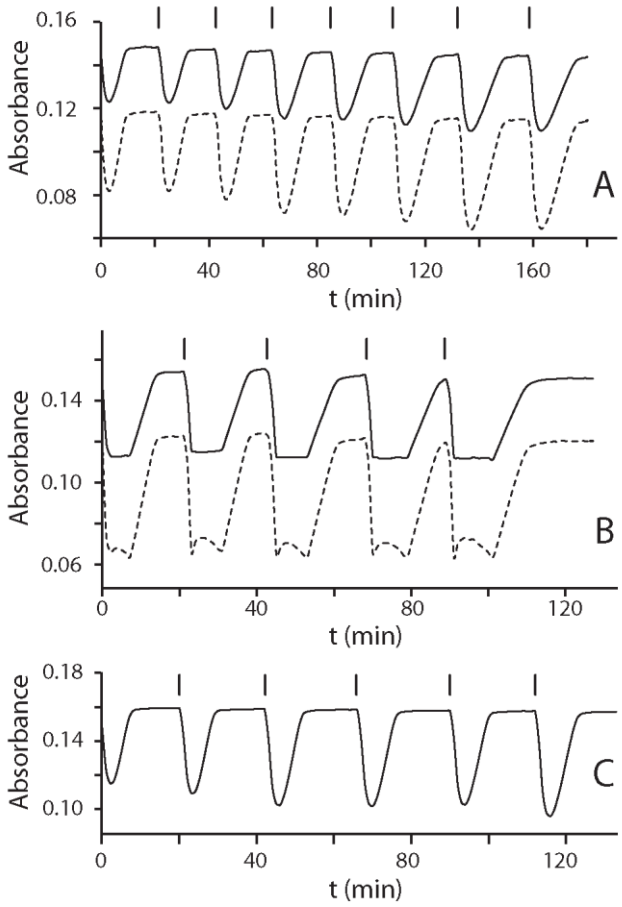

Fig. 3.10 NOD activity of rTHB1 and Mb. The traces illustrate the temporal change in absorbance in the α–β region (500 – 600 nm) of the UV/Vis spectrum. Samples contained ~10 μM protein in 100 mM phosphate buffer, pH 7.1 and a Fd/$NADP^+$ reduction system. (A) Time traces at 545 nm (solid line) and 581 nm (dashed line) upon repeated addition of 1 eq. MAHMA-NONOate to rTHB1-O_2. The first addition occurred at t = 0; subsequent additions are marked by the vertical bars. (B) Same, using 1.5 eq. MAHMA-NONOate. (C) Time trace at 543 nm upon addition of 1 eq. MAHMA-NONOate to oxy Mb. The additional minor phase during the "turnover" period corresponds to buildup and decay of the ferric-nitrosyl adduct.

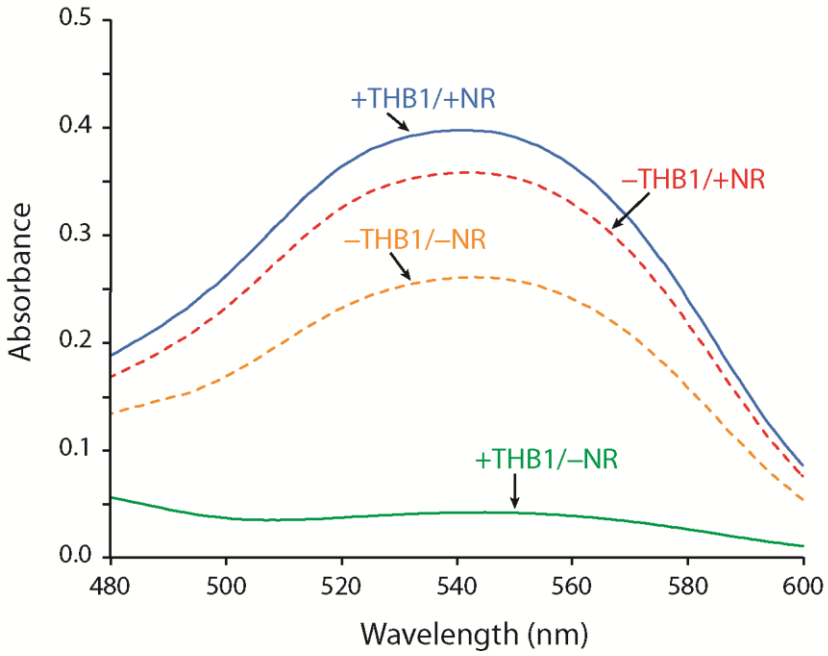

Fig. 3.11 Representative Griess assay results (conditions described in the text). In all cases the same period of time elapsed before quantitation. –THB1/–NR (dashed, orange) illustrates nitrite production in the absence of the globin and the nitrate reductase. –THB1/+NR (dashed, red) illustrates the production of nitrate in the absence of the globin; the amount of nitrate produced by non-enzymatic reactions corresponds to the difference between the two dashed curves. +THB1/–NR (green) shows that the globin prevents the production of nitrite and demonstrates that under the chosen condition, THB1 consumes $NO^{\bullet}$ faster than it disappears non-enzymatically. The amount of nitrate produced by the enzymatic reactions corresponds mostly to the difference between the two solid curves. The +THB1/+NR assay (blue) demonstrates that the globin catalyzes the production of nitrate. Note that the nitrite and nitrate amounts produced in the non-enzymatic reaction depend on the overall experiment time and has no direct relation to the amount of nitrate produced by THB1.

The minimal set of reactions in the NOD assay includes 1) $NO^{\bullet}$ release by MAHMA-NONOate (first order decay, measure independently), 2) $NO^{\bullet}$ reaction with rTHB1-O_2 (Eqs. 2 and 3, considered irreversible), 3) reduction of ferric rTHB1 via reduced Fd, 4) Fd re-reduction, and 5) O_2 binding by ferrous rTHB1 (reversible, measured

independently in the absence of NO•). Although accurate rate constants for NOD activity cannot be obtained with this assay, it is possible to test the plausibility of the mechanism by simulating the kinetic traces corresponding to each NO• addition. Reproduction of the experimental data shown in Figure 3.10A can be achieved with a first phase dominated by the release of NO• by MAHMA-NONOate and a second phase limited by the rate of reduction of Fd by the NADPH system. At high NO• concentration (Fig. 3.10B), reversible NO• binding to ferric rTHB1 must also be included to account for the additional spectral feature.

The simplest interpretation of the data is that rTHB1 can process NO• efficiently in the test tube and that it undergoes no or little damage as it turns over the substrates. This supports that, if O_2 and NO• are simultaneously available to THB1 in the cell, NOD activity is likely. Multiple turnovers, however, require a reducing agent. Reductants such as NADPH and glutathione are not effective with the recombinant protein when used in reasonable concentrations (data not shown). The identity of the reducing agent, dedicated to THB1 or not, is not known.

NOD assays were also performed on the THB1 variants, K53A and Y29F, to determine if altering the distal side of the heme affected the NOD activity of the protein (Fig. 3.12). These experiments show that the activity of the Y29F variant is similar to that of WT (Fig. 3.12A). However, there is a slight decrease in the signal after each NO addition suggesting that the Y29F variant is more susceptible to damage during this process than the WT. Figure 3.12B shows the kinetic trace of the oxy-K53A THB1 variant upon multiple NO additions. The data show the same saw-tooth pattern as WT, but the regeneration of the oxy-protein is much slower for K53A than for the WT. It is known that the distal endogenous ligand of heme-proteins can facilitate heme iron reduction. Therefore, it is likely

that removal of the distal lysine slows the reduction rate in K53A, and thus the rate at which the oxy-protein is able to regenerate.

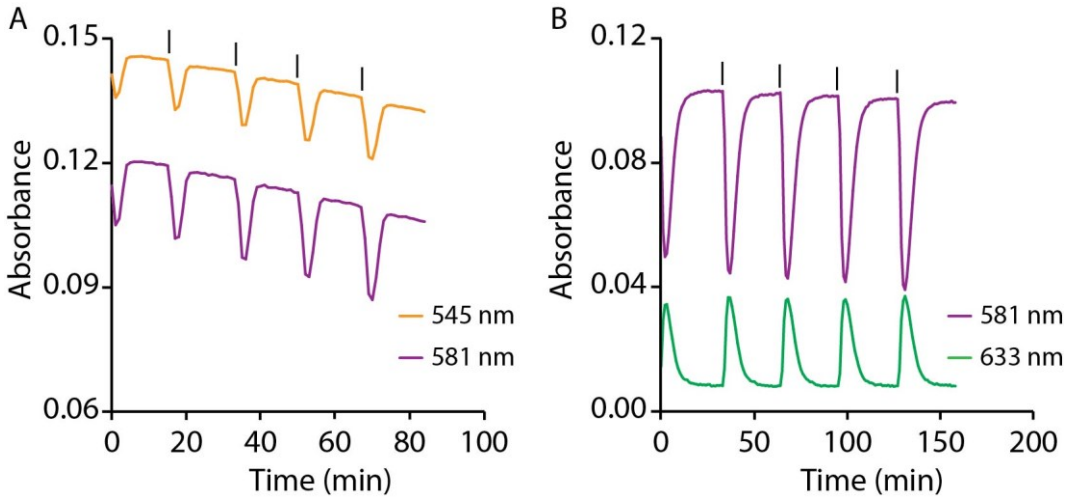

Fig. 3.12 NOD activity of Y29F and K53A THB1 variants. The traces show the change in absorbance over time. Each vertical line represents an addition of NO. Note the difference in scale of the x-axis. **(A)** Y29F variant. Note the decrease in absorbance signal over time, suggesting protein damage. The two wavelengths shown correspond to the α (purple) and β (orange) peaks of the oxy-Y29F THB1 spectrum. **(B)** K53A variant. The 633 nm (green) wavelength corresponds to the charge transfer band seen in the ferric K53A spectrum and serves as a monitor for ferric heme formation during the NOD reaction.

Truncated hemoglobins are also known to exhibit peroxidase activity, converting hydrogen peroxide to water[61]. In GlbN the proximal histidine protects the heme from oxidative damage by hydrogen peroxide[62]. To explore this activity in THB1 5-fold H_2O_2 was added to samples of WT THB1. Optical spectra monitoring the reaction of H_2O_2 show an immediate and significant decrease in the Soret peak within 10 seconds of H_2O_2 addition (Fig. 3.13A). One minute after H_2O_2 addition the heme signal is nearly gone. For THB1 the decrease in the Soret is much more rapid compared to GlbN upon H_2O_2 addition (Fig. 3.13B) The sharp drop in absorbance signal indicates that damage is occurring to the heme.

Additionally, protein damage upon H_2O_2 addition was observed via SDS-PAGE gel electrophoresis, where higher molecular weight species of THB1 are seen (data not shown), similar to those formed in GlbN samples upon H_2O_2 addition[62]. These data suggest that THB1 does not act as a peroxidase.

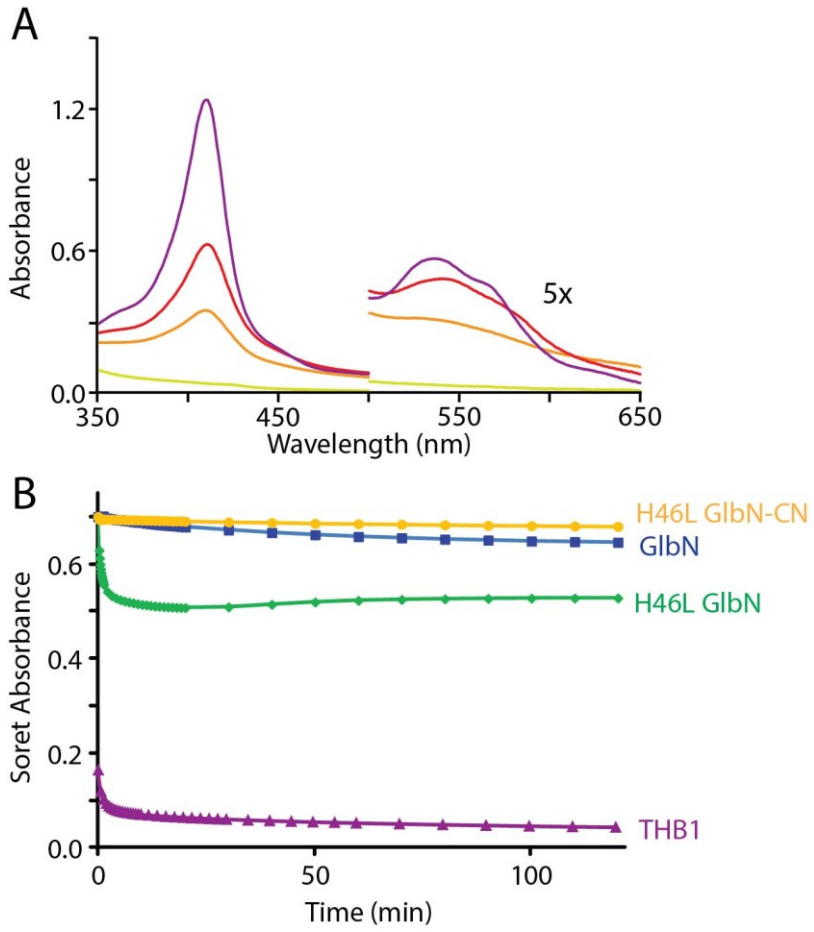

Fig. 3.13 Optical spectra of THB1 upon H_2O_2 addition. (A) Optical spectra of ferric WT THB1 before 5-fold H2O2 addition (purple), and 10 s (red), 1 min (orange), and 240 min (line green) after H_2O_2 addition. **(B)** Kinetics traces following the change in absorbance of the Soret peak after H_2O_2 addition for THB1 (purple), GlbN (yellow), H46L GlbN variant, where the distal His is absent (green), and cyanomet H46L GlbN (yellow).

3.4.8 THB1 levels are linked to the nitrogen source

To complement the structural and chemical data, we pursued the in-vivo characterization of THB1. To this end, we generated an anti-THB1 polyclonal antiserum. In a previous study,[19] expression of THB1 protein was confirmed by the identification through mass spectrometry of two proteolytic fragments from the flagella of the *C. reinhardtii bbs4-1* mutant. One of the peptides corresponds to an N-terminal extension to the truncated globin domain and most of the short α helix. The N-terminal extension is only a few residues long (Fig. 3.1A), and analysis of the THB1 sequence with PredAlgo,[63] a program designed to reveal protein subcellular localization in green algae, does not suggest targeting to a specific organelle of the cell. Based on evidence that the N-terminal extension is expressed and unlikely to be important for protein targeting, this region of the protein was chosen for anti-THB1 antibody production.

Polyclonal antibodies raised against the N-terminal proteolytic fragment (red sequence in Fig. 3.1A) recognize rTHB1 and a protein within whole-cell extracts of *C. reinhardtii* at the molecular weight that corresponds to the full-length THB1 (Appendix Fig. A3.19B, lane 2). The purified polyclonal antibodies appear highly specific; the only other detected band gives a weak response at a molecular weight slightly below 40,000, seen only after prolonged over-exposure (data not shown).

Given the assumption that THB1 interacts in some form with $NO^{\bullet}$, the native function of THB1 may well be linked to cellular activity that either creates $NO^{\bullet}$ or is regulated by the molecule. Nitrogen metabolism is a potential target for THB1 as it is both regulated by $NO^{\bullet}$[17] and can produce $NO^{\bullet}$ through a low-efficiency side-reaction of NR acting on nitrite.[64] Nitrogen usage in *C. reinhardtii* is complicated by the fact that not all laboratory strains metabolize nitrogen in the same way. Both CC-1690 and CC-125 are

commonly used laboratory strains of *C. reinhardtii*; CC-1690 is assumed to be genetically identical to the original Sager 21 gr laboratory strain, but CC-125 carries mutations within both the *NIT1* and *NIT2* genes.[65] The *NIT1* gene encodes the only NR found within *C. reinhardtii*;[66] it is responsible for reducing nitrate to nitrite via an NADPH-dependent reaction. *NIT2* encodes a transcription factor required for expression of genes involved in nitrogen assimilation and is activated by nitrate.[67] A cell with nonfunctional copies of either *NIT1* or *NIT2* is thus prevented from utilizing nitrate as a source for nitrogen. Figure 3.15A shows immunodetection of THB1 in protein extracts from whole cells grown in Sager-Granick "M" medium, a common medium for cell culture of *C. reinhardtii*. THB1 is found in strain CC-1690, but is not detected in strain CC-125. The *NIT1* and *NIT2* mutations in the CC-125 strain can be separated using strains CC-1086 (containing only a mutation to the *NIT2* gene) and CC-2453 (containing only a mutation to the *NIT1* gene.) As seen in Figure 3.14A, only strains with functional versions of the *NIT2* gene express detectable levels of THB1 within the cell.

When nitrate is present in the growth medium, *NIT2* induces expression of the nitrate assimilation pathway. Sager-Granick "M" medium uses 3.75 mM ammonium nitrate as the nitrogen source (i.e., equal amounts ammonium and nitrate). When the "M" medium is modified to contain 7.5 mM ammonium chloride or 7.5 mM potassium nitrate, the amount of THB1 within *C. reinhardtii* strain CC-1690 varies (Fig. 3.14B); when nitrate is removed from the medium there is a marked depletion of THB1 protein from the cell.

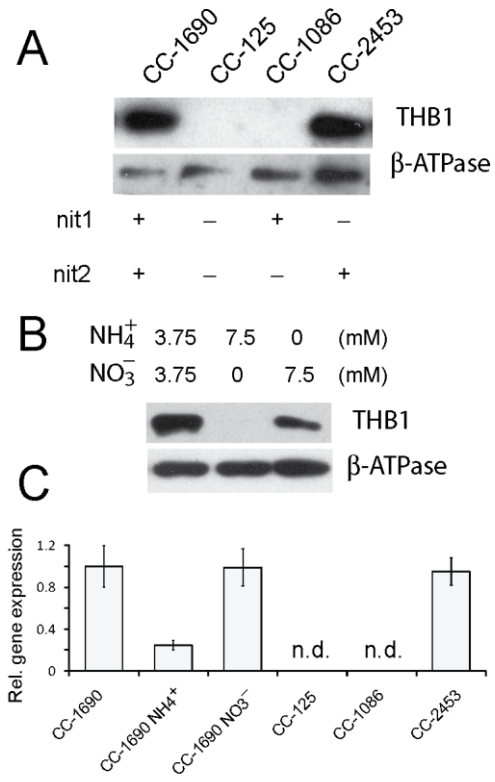

Fig. 3.14 Variation in THB1 protein and gene expression. (A) Western blot of whole cell extracts from *C. reinhardtii* strains CC-1690, CC-125, CC-1086, and CC-2453 probed with antibodies to THB1. All strains were grown in Sager-Granick M medium. The β subunit of the ATP synthase was used as loading control. (B) Western blot of whole cell extracts probed with antibodies to THB1. Cells are from strain CC-1690 grown in Sager-Granick M medium with modifications to the nitrogen source in the media as indicated. The β subunit of the ATP synthase was used as loading control. (C) Transcript abundances of *THB1* relative to *CBLP*, as determined by qPCR. Averages ± standard deviation of three independent experiments performed on a mixture of biological duplicates are shown (nd: not detected). All samples grown in Sager-Granick M medium except "NH_4^+" and "NO_3^-" which are strain CC-1690 grown in ammonium or nitrate media as in part B.

The transcriptional regulation of the *THB1* gene was followed using RNA isolated from these individual strains (Fig. 3.14C). The level of gene expression for the *THB1* gene was undetectable when either strains CC-125 or CC-1086 were analyzed; however, both CC-1690 and CC-2453 (containing functional *NIT2* genes) possessed equivalent levels of the

transcript. The CC-1690 strain reduced its level of *THB1* transcripts when grown in a nitrate-free (7.5 mM ammonium) medium, in agreement with the depletion of the protein seen in the immuno-blot (Fig. 3.14A and B). In sum, these observations are consistent with induced expression of *THB1* being dependent on the presence of nitrate.

3.4.9 Possible THB1 function

The present results strongly suggest that the expression of the *THB1* gene is not constitutive, but rather linked to the source of nitrogen available to the cell. This expression also resembles the expression pattern for NR, which is known to be under the control of the *NIT2* gene product.[66] A minimal interpretation of the data holds that THB1 and NR expressions are linked because THB1 is required to detoxify the $NO^{\bullet}$ released by NR. In addition to lowering $NO^{\bullet}$ levels temporarily and recycling the nitrogen to nitrate, the scavenging activity would diminish the uncatalyzed and random production of nitrite from $NO^{\bullet}$ and O_2. S-nitrosylation of various proteins and other RNS reactions would also be tempered. THB1's role, however, is likely to be more complex. First, $NO^{\bullet}$ can have origins other than NR activity; it is now established that in the absence of dioxygen, many ferrous hemoglobins possess the ability to reduce nitrite to nitric oxide[68] and act as anoxic nitrite reductases.[69] The product of the reaction also includes the ferric protein; as nitrite reductase activity continues to produce $NO^{\bullet}$ and consumes reducing equivalents, the reverse reaction may take over, namely ferric hemoglobin may bind $NO^{\bullet}$ and undergo autoreduction to form nitrous acid and ferrous protein.[70,71] It is possible that physiologic conditions exist where exogenous $NO^{\bullet}$ is present while synthesis of THB1 is dramatically curtailed. Another detoxifying agent would be needed to manage the $NO^{\bullet}$ load. Nevertheless, in the presence of nitrate, regulation of $NO^{\bullet}$ levels by THB1 may have several unexpected downstream

effects, as recent studies have found multiple NO-regulated pathways within *C. reinhardtii*, including copper stress response,[72] hypoxia,[18] and ammonium and nitrate transport.[17,73] In light of the ability of THB1 to process NO•, it can be proposed that THB1 provides a critical link in the regulation of the nitrogen assimilation pathway. Further investigation will be necessary to disentangle the possible roles of THB1 in exogenous versus endogenous NO• regulation.

3.5 Conclusion

We have shown that in THB1 the heme iron has two axial ligands: the proximal histidine and a neutral lysine (Lys53) from the distal helix. The lysine ligand can be displaced by protonation below neutral pH or by exogenous ligands. The structure of the His–Fe–Lys complex is expected to resemble the structure of the *bis*-histidine cyanobacterial TrHb1s. In vitro, THB1 is proposed to be an efficient NO dioxygenase, and its link to nitrogen metabolism, specifically expression of NR, suggests that a similar activity occurs in the cell.

Hemoglobins first appeared over 3 billion years ago in a biosphere substantially different from ours. Without significant atmospheric oxygen and with a host of highly reduced molecules, stringent control of redox chemistry must have been essential to the earliest forms of life. Hbs have been retained since those early days and have remained within the genetic toolbox of organisms across the entire spectrum of life. Many of these Hbs have been proposed to function in roles related to reactive nitrogen.[13,74,75] *C. reinhardtii* is a well-studied model organism[76-78] and exploring the function of TrHbs within this alga will harness a wealth of knowledge to define the role of these proteins. The study of THB1 presented here constitutes a first step toward a comprehensive investigation of photosynthetic Hbs.

Acknowledgements

The authors wish to thank Dr. Karen Beemon for assistance with the gene expression experiments.

This work was supported by the National Science Foundation grants MCB-0843439 and MCB-1330488 to JTJL, by National Institutes of Health grant GM030626 to GW, and by the Robert W. Booth Endowment at UMMS to GW. DBN was supported by National Institutes of Health grant T32 GM080189. LG was supported by National Science Foundation grant DBI-1262985.

3.6 References

(1) Potts, M., Angeloni, S. V., Ebel, R. E., and Bassam, D. (1992) Myoglobin in a cyanobacterium. *Science, 256*, 1690-1691.

(2) Wittenberg, J. B., Bolognesi, M., Wittenberg, B. A., and Guertin, M. (2002) Truncated hemoglobins: A new family of hemoglobins widely distributed in bacteria, unicellular eukaryotes and plants. *Journal of Biological Chemistry, 277*, 871-874.

(3) Hill, D. R., Belbin, T. J., Thorsteinsson, M. V., Bassam, D., Brass, S., Ernst, A., Boger, P., Paerl, H., Mulligan, M. E., and Potts, M. (1996) GlbN (cyanoglobin) is a peripheral membrane protein that is restricted to certain *Nostoc* spp. *Journal of Bacteriology, 178*, 6587-6598.

(4) Couture, M., Chamberland, H., St-Pierre, B., Lafontaine, J., and Guertin, M. (1994) Nuclear genes encoding chloroplast hemoglobins in the unicellular green alga *Chlamydomonas eugametos*. *Moleuclar and General Genetics*, *243*, 185-197.

(5) Pesce, A., Couture, M., Dewilde, S., Guertin, M., Yamauchi, K., Ascenzi, P., Moens, L., and Bolognesi, M. (2000) A novel two-over-two a-helical sandwich fold is characteristic of the truncated hemoglobin family. *EMBO Journal, 19*, 2424-2434.

(6) Couture, M., and Guertin, M. (1996) Purification and spectroscopic characterization of a recombinant chloroplastic hemoglobin from the green unicellular alga *Chlamydomonas eugametos*. *European Journal of Biochemistry, 242*, 779-787.

(7) Vinogradov, S. N., Hoogewijs, D., Bailly, X., Arredondo-Peter, R., Gough, J., Dewilde, S., Moens, L., and Vanfleteren, J. R. (2006) A phylogenomic profile of globins. *BMC Evolutionary Biology, 6*, 31.

(8) Vinogradov, S. N., Tinajero-Trejo, M., Poole, R. K., and Hoogewijs, D. (2013) Bacterial and archaeal globins — A revised perspective. *Biochimica et Biophysica Acta-Proteins Proteomics, 1834*, 1789-1800.

(9) Vazquez-Limon, C., Hoogewijs, D., Vinogradov, S. N., and Arredondo-Peter, R. (2012) The evolution of land plant hemoglobins. *Plant Science, 191*, 71-81.

(10) Anbar, A. D. (2008) Elements and evolution. *Science, 322*, 1481-1483.

(11) Crowe, S. A., Dossing, L. N., Beukes, N. J., Bau, M., Kruger, S. J., Frei, R., and Canfield, D. E. (2013) Atmospheric oxygenation three billion years ago. *Nature, 501*, 535-538.

(12) Gardner, P. R. (2005) Nitric oxide dioxygenase function and mechanism of flavohemoglobin, hemoglobin, myoglobin and their associated reductases. *Journal of Inorganic Biochemistry, 99*, 247-266.

(13) Gardner, P. R. (2012) Hemoglobin, a nitric-oxide dioxygenase. *Scientifica, 2012*.

(14) De Marinis, E., Casella, L., Ciaccio, C., Coletta, M., Visca, P., and Ascenzi, P. (2009) Catalytic peroxidation of nitrogen monoxide and peroxynitrite by globins. *IUBMB Life, 61*, 62-73.

(15) Bowman, L. A., McLean, S., Poole, R. K., and Fukuto, J. M. (2011) The diversity of microbial responses to nitric oxide and agents of nitrosative stress close cousins but not identical twins. *Advances in Microbial Physiology, 59*, 135-219.

(16) Gardner, P. R., Gardner, A. M., Martin, L. A., and Salzman, A. L. (1998) Nitric oxide dioxygenase: an enzymic function for flavohemoglobin. *Proceedings of the National Academy of Sciences, 95*, 10378-10383.

(17) Sanz-Luque, E., Ocana-Calahorro, F., Llamas, A., Galvan, A., and Fernandez, E. (2013) Nitric oxide controls nitrate and ammonium assimilation in *Chlamydomonas reinhardtii*. *Journal of Experimental Botany, 64*, 3373-3383.

(18) Hemschemeier, A., Duner, M., Casero, D., Merchant, S. S., Winkler, M., and Happe, T. (2013) Hypoxic survival requires a 2-on-2 hemoglobin in a process involving nitric oxide. *Proceedings of the National Academy of Sciences, 110*, 10854-10859.

(19) Lechtreck, K. F., Johnson, E. C., Sakai, T., Cochran, D., Ballif, B. A., Rush, J., Pazour, G. J., Ikebe, M., and Witman, G. B. (2009) The *Chlamydomonas reinhardtii* BBSome is an IFT cargo

required for export of specific signaling proteins from flagella. *Journal of Cell Biology, 187*, 1117-1132.

(20) Johnson, E. A., and Lecomte, J. T. (2013) The globins of cyanobacteria and algae. *Advances in Microbial Physiology, 63*, 195-272.

(21) Witman, G. B. (1986) Isolation of *Chlamydomonas* flagella and flagellar axonemes. *Methods in Enzymology, 134*, 280-290.

(22) Craige, B., Brown, J. M., and Witman, G. B. (2013) Isolation of *Chlamydomonas* flagella. *Current Protocols in Cell Biology, 59*, 3.41.41-43.41.49.

(23) Lechtreck, K. F., Brown, J. M., Sampaio, J. L., Craft, J. M., Shevchenko, A., Evans, J. E., and Witman, G. B. (2013) Cycling of the signaling protein phospholipase D through cilia requires the BBSome only for the export phase. *Journal of Cell Biology, 201*, 249-261.

(24) Atteia, A., van Lis, R., Gelius-Dietrich, G., Adrait, A., Garin, J., Joyard, J., Rolland, N., and Martin, W. (2006) Pyruvate formate-lyase and a novel route of eukaryotic ATP synthesis in *Chlamydomonas* mitochondria. *Journal of Biological Chemistry, 281*, 9909-9918.

(25) King, S. M., and Witman, G. B. (1990) Localization of an intermediate chain of outer arm dynein by immunoelectron microscopy. *Journal of Biological Chemistry, 265*, 19807-19811.

(26) Cole, D. G., Diener, D. R., Himelblau, A. L., Beech, P. L., Fuster, J. C., and Rosenbaum, J. L. (1998) *Chlamydomonas* kinesin-II-dependent intraflagellar transport (IFT): IFT particles contain proteins required for ciliary assembly in *Caenorhabditis elegans* sensory neurons. *Journal of Cell Biology,141*, 993-1008.

(27) Chang, C. W., Moseley, J. L., Wykoff, D., and Grossman, A. R. (2005) The LPB1 gene is important for acclimation of *Chlamydomonas reinhardtii* to phosphorus and sulfur deprivation. *Plant Physiology, 138*, 319-329.

(28) Scott, N. L., and Lecomte, J. T. J. (2000) Cloning, expression, purification, and preliminary characterization of a putative hemoglobin from the cyanobacterium *Synechocystis* sp. PCC 6803. *Protein Science, 9*, 587-597.

(29) de Duve, C. (1948) A spectrophotometric method for the simultaneous determination of myoglobin and hemoglobin in extracts of human muscle. *Acta Chemica Scandinavica, 2*, 264-289.

(30) Preimesberger, M. R., Wenke, B. B., Gilevicius, L., Pond, M. P., and Lecomte, J. T. J. (2013) Covalent heme attachment in *Synechocystis* hemoglobin: Implications for facile histidine posttranslational modification. *Biochemistry, 52*, 3478–3488.

(31) Gasteiger, E., Hoogland, C., Gattiker, A., Duvaud, S., Wilkins, M. R., Appel, R. D., and Bairoch, A. (2005) Protein Identification and Analysis Tools on the ExPASy Server, In *The Proteomics Protocols Handbook* (Walker, J. M., Ed.), Humana Press.

(32) Englander, S. W., Calhoun, D. B., and Englander, J. J. (1987) Biochemistry without oxygen. *Analytical Biochemistry, 161*, 300-306.

(33) Hayashi, A., Suzuki, T., and Shin, M. (1973) An enzymic reduction system for metmyoglobin and methemoglobin, and its application to functional studies of oxygen carriers. *Biochimica et Biophysica Acta, 310*, 309-316.

(34) Hendler, R. W., and Shrager, R. I. (1994) Deconvolutions based on singular value decomposition and the pseudoinverse: a guide for beginners. *Journal of Biochemical and Biophysical Methods, 28*, 1-33.

(35) Bilsel, O., Zitzewitz, J. A., Bowers, K. E., and Matthews, C. R. (1999) Folding mechanism of the a-subunit of tryptophan synthase, an a/b barrel protein: global analysis highlights the interconversion of multiple native, intermediate, and unfolded forms through parallel channels. *Biochemistry, 38*, 1018-1029.

(36) Hrabie, J. A., Klose, J. R., Wink, D. A., and Keefer, L. K. (1993) New nitric oxide-releasing zwitterions derived from polyamines. *Journal of Organic Chem, 58*, 1472-1476.

(37) Griess, P. (1879) Bemerkungen zu der Abhandlung der HH Weselsky und Benedikt "Über einige Azoverbindungen." *Chemische Berichte, 12*, 426-428.

(38) Verdon, C. P., Burton, B. A., and Prior, R. L. (1995) Sample pretreatment with nitrate reductase and glucose-6-phosphate dehydrogenase quantitatively reduces nitrate while

avoiding interference by NADP+ when the Griess reaction is used to assay for nitrite. *Analytical Biochemistry, 224*, 502-508.

(39) Johnson, K. A. (2009) Fitting enzyme kinetic data with KinTek Global Kinetic Explorer. *Methods in Enzymology, 467*, 601-626.

(40) Wishart, D. S., Bigam, C. G., Yao, J., Abildgaard, F., Dyson, H. J., Oldfield, E., Markley, J. L., and Sykes, B. D. (1995) ^{1}H, ^{13}C and ^{15}N chemical shift referencing in biomolecular NMR. *Journal of Biomolecular NMR, 6*, 135-140.

(41) Delaglio, F., Grzesiek, S., Vuister, G. W., Zhu, G., Pfeifer, J., and Bax, A. (1995) NMRPipe: a multidimensional spectral processing system based on UNIX pipes. *Journal of Biomolecular NMR, 6*, 277-293.

(42) Goddard, T. D., and Kneller, D. G. (2006) SPARKY 3. *University of California, San Francisco*.

(43) Lecomte, J. T. J., Vu, B. C., and Falzone, C. J. (2005) Structural and dynamic properties of *Synechocystis* sp. PCC 6803 Hb revealed by reconstitution with Zn-protoporphyrin IX. *Journal of Inorganic Biochemistry, 99*, 1585-1592.

(44) Preimesberger, M. R., Pond, M. P., Majumdar, A., and Lecomte, J. T. J. (2012) Electron self-exchange and self-amplified posttranslational modification in the hemoglobins from *Synechocystis* sp. PCC 6803 and *Synechococcus* sp. PCC 7002. *Journal of Biological Inorganic Chemistry, 17*, 599-609.

(45) Cavanagh, J., Fairbrother, W. J., Palmer, A. G. I., and Skelton, N. J. (1996) *Protein NMR Spectroscopy. Principles and Practice*, Academic Press, San Diego, USA.

(46) Antonini, E., and Brunori, M. (1971) *Hemoglobin and myoglobin in their reactions with ligands*, Vol. 12, North-Holland, Amsterdam.

(47) Bogumil, R., Maurus, R., Hildebrand, D. P., Brayer, G. D., and Mauk, A. G. (1995) Origin of the pH-dependent spectroscopic properties of pentacoordinate metmyoglobin variants. *Biochemistry, 34*, 10483-10490.

(48) Das, T. K., Couture, M., Lee, H. C., Peisach, J., Rousseau, D. L., Wittenberg, B. A., Wittenberg, J. B., and Guertin, M. (1999) Identification of the ligands to the ferric heme of

Chlamydomonas chloroplast hemoglobin: Evidence for ligation of tyrosine-63 (B10) to the heme. *Biochemistry, 38*, 15360-15368.

(49) Couture, M., Das, T. K., Lee, H. C., Peisach, J., Rousseau, D. L., Wittenberg, B. A., Wittenberg, J. B., and Guertin, M. (1999) *Chlamydomonas* chloroplast ferrous hemoglobin. Heme pocket structure and reactions with ligands. *Journal of Biological Chemistry, 274*, 6898-6910.

(50) Couture, M., Das, T. K., Savard, P. Y., Ouellet, Y., Wittenberg, J. B., Wittenberg, B. A., Rousseau, D. L., and Guertin, M. (2000) Structural investigations of the hemoglobin of the cyanobacterium *Synechocystis* PCC 6803 reveal a unique distal heme pocket. *European Journal of Biochemistry, 267*, 4770-4780.

(51) Scott, N. L., Falzone, C. J., Vuletich, D. A., Zhao, J., Bryant, D. A., and Lecomte, J. T. J. (2002) The hemoglobin of the cyanobacterium *Synechococcus* sp. PCC 7002: evidence for hexacoordination and covalent adduct formation in the ferric recombinant protein. *Biochemistry, 41*, 6902-6910.

(52) Patel, N., Seward, H. E., Svensson, A., Gurman, S. J., Thomson, A. J., and Raven, E. L. (2003) Exploiting the conformational flexibility of leghemoglobin: a framework for examination of heme protein axial ligation. *Archives of Biochemistry and Biophysics, 418*, 197-204.

(53) Ubbink, M., Campos, A. P., Teixeira, M., Hunt, N. I., Hill, H. A., and Canters, G. W. (1994) Characterization of mutant Met100Lys of cytochrome *c*-550 from *Thiobacillus versutus* with lysine-histidine heme ligation. *Biochemistry, 33*, 10051-10059.

(54) Du, J., Perera, R., and Dawson, J. H. (2011) Alkylamine-ligated H93G myoglobin cavity mutant: a model system for endogenous lysine and terminal amine ligation in heme proteins such as nitrite reductase and cytochrome *f*. *Inorganic Chemistry, 50*, 1242-1249.

(55) La Mar, G. N., Satterlee, J. D., and de Ropp, J. S. (2000) Nuclear magnetic resonance of hemoproteins, In *The Porphyrin Handbook* (Smith, K. M., Kadish, K., and Guilard, R., Eds.), pp 185-298, Academic Press, Burlington, MA.

(56) Jeener, J., Meier, B. H., Bachmann, P., and Ernst, R. R. (1979) Investigation of exchange processes by two-dimensional NMR spectroscopy. *Journal of Chemical Physics, 71*, 4546-4553.

(57) Mispelter, J., Momenteau, M., and Lhoste, J.-M. (1993) Heteronuclear magnetic resonance. Applications to biological and related paramagnetic molecules. *Biological Magnetic Resonance, 12*, 299-355.

(58) Igarashi, J., Kobayashi, K., and Matsuoka, A. (2011) A hydrogen-bonding network formed by the B10-E7-E11 residues of a truncated hemoglobin from *Tetrahymena pyriformis* is critical for stability of bound oxygen and nitric oxide detoxification. *Journal of Biological Inorganic Chemistry, 16*, 599-609.

(59) Ouellet, H., Ouellet, Y., Richard, C., Labarre, M., Wittenberg, B., Wittenberg, J., and Guertin, M. (2002) Truncated hemoglobin HbN protects *Mycobacterium bovis* from nitric oxide. *Proceedings of the National Academy of Sciences, 99*, 5902-5907.

(60) Ignarro, L. J., Fukuto, J. M., Griscavage, J. M., Rogers, N. E., and Byrns, R. E. (1993) Oxidation of nitric oxide in aqueous solution to nitrite but not nitrate: comparison with enzymatically formed nitric oxide from L-arginine. *Proceedings of the National Academy of Sciences, 90*, 8103-8107.

(61) Ouellet, H., Ranguelova, K., LaBarre, M., Wittenberg, J. B., Wittenberg, B. A., Magliozzo, R. S., and Guertin, M. (2007) Reaction of *Mycobacterium tuberculosis* truncated hemoglobin O with hydrogen peroxide: Evidence for peroxidatic activity and formation of protein-based radicals. *Journal of Biological Chemistry, 282*, 7491-7503.

(62) Nothnagel, H. J., Preimesberger, M. R., Pond. M. P., Winer, B. Y., Adney, E. M., and Lecomte, J. T. J. (2011) Chemical reactivity of *Synechococcus* sp. PCC 7002 and *Synechocystis* sp. PCC 6803 hemoglobins: covalent heme attachement and bishistidine coordination. *Journal of Biological Inorganic Chemistry, 16*, 539-552.

(63) Tardif, M., Atteia, A., Specht, M., Cogne, G., Rolland, N., Brugiere, S., Hippler, M., Ferro, M., Bruley, C., Peltier, G., Vallon, O., and Cournac, L. (2012) PredAlgo: A new subcellular

localization prediction tool dedicated to green algae. *Molcular Biology and Evolution, 29*, 3625-3639.

(64) Sakihama, Y., Nakamura, S., and Yamasaki, H. (2002) Nitric oxide production mediated by nitrate reductase in the green alga *Chlamydomonas reinhardtii*: an alternative NO production pathway in photosynthetic organisms. *Plant & Cell Physiology, 43*, 290-297.

(65) Kubo, T., Abe, J., Saito, T., and Matsuda, Y. (2002) Genealogical relationships among laboratory strains of *Chlamydomonas reinhardtii* as inferred from matrix metalloprotease genes. *Current Genetics, 41*, 115-122.

(66) Fernandez, E., Schnell, R., Ranum, L. P., Hussey, S. C., Silflow, C. D., and Lefebvre, P. A. (1989) Isolation and characterization of the nitrate reductase structural gene of *Chlamydomonas reinhardtii. Proceedings of the National Academy of Sciences, 86*, 6449-6453.

(67) Camargo, A., Llamas, A., Schnell, R. A., Higuera, J. J., Gonzalez-Ballester, D., Lefebvre, P. A., Fernandez, E., and Galvan, A. (2007) Nitrate signaling by the regulatory gene NIT2 in *Chlamydomonas*. *Plant Cell, 19*, 3491-3503.

(68) Petersen, M. G., Dewilde, S., and Fago, A. (2008) Reactions of ferrous neuroglobin and cytoglobin with nitrite under anaerobic conditions. *Journal of Inorganic Biochemistry, 102*, 1777-1782.

(69) Sturms, R., DiSpirito, A. A., and Hargrove, M. S. (2011) Plant and cyanobacterial hemoglobins reduce nitrite to nitric oxide under anoxic conditions. *Biochemistry, 50*, 3873-3878.

(70) Addison, A. W., and Stephanos, J. J. (1986) Nitrosyliron(III) hemoglobin: autoreduction and spectroscopy. *Biochemistry, 25*, 4104-4113.

(71) Fernandez, B. O., Lorkovic, I. M., and Ford, P. C. (2004) Mechanisms of ferriheme reduction by nitric oxide: nitrite and general base catalysis. *Inorganic Chemistry, 43*, 5393-5402.

(72) Zhang, L. P., Mehta, S. K., Liu, Z. P., and Yang, Z. M. (2008) Copper-induced proline synthesis is associated with nitric oxide generation in Chlamydomonas reinhardtii. *Plant & Cell Physiology, 49*, 411-419.

(73) de Montaigu, A., Sanz-Luque, E., Galvan, A., and Fernandez, E. (2010) A soluble guanylate cyclase mediates negative signaling by ammonium on expression of nitrate reductase in *Chlamydomonas*. *Plant Cell*, *22*, 1532-1548.

(74) Perazzolli, M., Romero-Puertas, M. C., and Delledonne, M. (2006) Modulation of nitric oxide bioactivity by plant haemoglobins. *Journal of Experimental Botany, 57*, 479-488.

(75) Reeder, B. J. (2010) The redox activity of hemoglobins: from physiologic functions to pathologic mechanisms. *Antioxidants and Redox Signaling, 13*, 1087-1123.

(76) Harris, E. H. (2001) *Chlamydomonas* as a model organism. *Annual Reviews - Plant Physiology, 52*, 363-406.

(77) Merchant, S. S., Prochnik, S. E., Vallon, O., Harris, E. H., Karpowicz, S. J., Witman, G. B., Terry, A., Salamov, A., Fritz-Laylin, L. K., Marechal-Drouard, L., Marshall, W. F., Qu, L. H., Nelson, D. R., Sanderfoot, A. A., Spalding, M. H., Kapitonov, V. V., Ren, Q., Ferris, P., Lindquist, E., Shapiro, H., Lucas, S. M., Grimwood, J., Schmutz, J., Cardol, P., Cerutti, H., Chanfreau, G., Chen, C. L., Cognat, V., Croft, M. T., Dent, R., Dutcher, S., Fernandez, E., Fukuzawa, H., Gonzalez-Ballester, D., Gonzalez-Halphen, D., Hallmann, A., Hanikenne, M., Hippler, M., Inwood, W., Jabbari, K., Kalanon, M., Kuras, R., Lefebvre, P. A., Lemaire, S. D., Lobanov, A. V., Lohr, M., Manuell, A., Meier, I., Mets, L., Mittag, M., Mittelmeier, T., Moroney, J. V., Moseley, J., Napoli, C., Nedelcu, A. M., Niyogi, K., Novoselov, S. V., Paulsen, I. T., Pazour, G., Purton, S., Ral, J. P., Riano-Pachon, D. M., Riekhof, W., Rymarquis, L., Schroda, M., Stern, D., Umen, J., Willows, R., Wilson, N., Zimmer, S. L., Allmer, J., Balk, J., Bisova, K., Chen, C. J., Elias, M., Gendler, K., Hauser, C., Lamb, M. R., Ledford, H., Long, J. C., Minagawa, J., Page, M. D., Pan, J., Pootakham, W., Roje, S., Rose, A., Stahlberg, E., Terauchi, A. M., Yang, P., Ball, S., Bowler, C., Dieckmann, C. L., Gladyshev, V. N., Green, P., Jorgensen, R., Mayfield, S., Mueller-Roeber, B., Rajamani, S., Sayre, R. T., Brokstein, P., Dubchak, I., Goodstein, D., Hornick, L., Huang, Y. W., Jhaveri, J., Luo, Y., Martinez, D., Ngau, W. C., Otillar, B., Poliakov, A., Porter, A., Szajkowski, L., Werner, G., Zhou, K., Grigoriev, I. V., Rokhsar, D. S., and Grossman, A. R. (2007) The

Chlamydomonas genome reveals the evolution of key animal and plant functions. *Science, 318*, 245-250.

(78) Terashima, M., Specht, M., and Hippler, M. (2011) The chloroplast proteome: a survey from the *Chlamydomonas reinhardtii* perspective with a focus on distinctive features. *Current Genetics, 57*, 151-168.

(79) Arnold, K., Bordoli, L., Kopp, J., and Schwede, T. (2006) The SWISS-MODEL workspace: a web-based environment for protein structure homology modelling. *Bioinformatics, 22*, 195-201.

Chapter 4

Structure of *Chlamydomonas reinhardtii* THB1, a group 1 truncated hemoglobin with a rare histidine–lysine heme ligation

* This chapter was previously published in *Acta Crystallographica F* (**Rice, S.L.**, *et al.*, 2015) Figure 4.2 and Tables 4.2,4.3, and 4.5 were contributed by coauthors, all other results in this chapter represent original work. For this dissertation, modifications were made to the text and additional figures were added (Figures 4.2 and 4.4-4.6 and Table 4.5).

Author Contributions

Selena L. Rice: purified protein, performed crystal screens, assisted in freezing crystals, performed structural analysis, and wrote the paper

Lauren E. Boucher: collected data at Brookhaven National Lab X25 beamline, processed and analyzed data, and built the model

Jamie L. Schlessman: froze crystals, provided advice on protein crystallization techniques

Jürgen Bosch: collected data at Brookhaven National Lab X25 beamline, processed and analyzed data

Juliette T.J. Lecomte: designed research and wrote the paper

4.1 Abstract

THB1 is one of several group 1 truncated hemoglobins (TrHb1s) encoded in the genome of the unicellular green alga *Chlamydomonas reinhardtii*. THB1 expression is under the control of NIT2, the master regulator of nitrate assimilation, which also controls the expression of the cell's only nitrate reductase, NIT1. *In vitro* and physiologic evidence suggests that THB1 converts nitric oxide generated by NIT1 into nitrate. To aid in the elucidation of the function and mechanism of THB1, we solved the structure of the protein in the ferric state. THB1 resembles other TrHb1s, but also exhibits distinct features associated with the coordination of the heme iron by a histidine (proximal) and a lysine (distal). The new structure illustrates the versatility of the TrHb1 fold, suggests factors that stabilize the axial ligation of a lysine, and highlights the difficulty of predicting the identity of the distal ligand, if any, in this group of proteins.

4.2 Introduction

THB1 is a cytosolic hemoglobin expressed by the green alga *Chlamydomonas reinhardtii*. Sequence analyses place it within the "truncated" lineage of the hemoglobin superfamily, specifically in Group 1 of this ancient branch[1]. Group 1 truncated hemoglobins (TrHb1s) are present in a wide range of unicellular organisms and plants[2,3,4]. Little physiological information is available for these proteins, and their function is generally not known. THB1 is one of the few exceptions for which *in vivo* and *in vitro* data are being collected systematically. Occurrence in a model alga makes THB1 an excellent candidate for further study aimed at understanding the chemistry and molecular evolution of TrHb1s.

THB1 is linked to *C. reinhardtii* nitrogen metabolism[5]. The *THB1* gene is regulated by NIT2, a transcription factor that controls expression of the nitrate reductase gene (*NIT1* or *NIA1*) and other genes involved in nitrate assimilation. Accordingly, THB1 is absent from strains of *C. reinhardtii* cells with non-functional *NIT2*; furthermore, the protein is detectable only when the growth medium contains nitrate[5]. Isolation of THB1 from *C. reinhardtii* cells confirms that the protein contains a *b* heme as its native cofactor[6]. *In vitro* studies show that ferrous recombinant THB1 binds exogenous ligands such as dioxygen, nitric oxide, and carbon monoxide, and is capable of efficient nitric oxide dioxygenase (NOD) activity when provided with oxygen and a suitable reduction system[5]. NOD activity is a plausible function of THB1 in the cytoplasm of *C. reinhardtii*, where it would eliminate nitrite-induced nitric oxide produced by NIT1[7]. Indirect and reversible inhibition of NIT1 by nitric oxide[8] suggests that NIT1 and THB1 constitute a cognate pair[9] with THB1 using NIT1 as its native reductase and preventing full reduction of the NIT1 catalytic site[10].

In solution at neutral pH, recombinant THB1 is a "hexacoordinate" hemoglobin in both the ferric and ferrous states, i.e., the heme iron has two axial ligands contributed by the

protein. One of these is the proximal histidine, His77, a strictly conserved residue of functional hemoglobins. The other ligand, identified in ferrous THB1 by amino acid replacement and nuclear magnetic resonance (NMR) spectroscopy, is Lys53[5]. The histidine–lysine heme ligation scheme is rare, observed only in a few cytochrome *c* proteins[11,12]. In THB1, hexacoordination may serve to facilitate electron transfer[6] and attenuate the kinetics of exogenous ligand binding. In the present work we describe the structure of THB1 with the distal lysine bound to the ferric heme and assess the structural factors associated with this rare form of heme coordination.

4.3 Materials and Methods

Recombinant THB1 was expressed and purified as described previously[5]. In brief, THB1 accumulated in inclusion bodies during overexpression in *Escherichia coli*. The inclusion bodies were solubilized with 8 *M* urea and the apoprotein was partially purified and refolded by gel filtration chromatography. Hemin was added in excess to generate the ferric holoprotein, which was further purified by anion exchange chromatography and lyophilized.

4.3.1 Crystallization

Lyophilized THB1 was solubilized in 5 m*M* Tris pH 7.1 and made to a stock concentration of ~30 mg/mL. Solubilized THB1 was mixed with buffer containing 0.1 *M* glycine, pH 9.5, with varying concentrations of ammonium sulfate (1.6 *M* to 2.1 *M*) and different amounts of glycerol (0%–20%) in a 4:2 ratio (protein:mother liquor) and incubated at room temperature. Red, hexagonal crystals of ferric THB1 first appeared after ~2 weeks in 0.1 *M* glycine, pH 9.5, 1.8 *M* ammonium sulfate, 0%, 10%, or 20% glycerol. Single crystals from the 20% glycerol condition were flash-cooled in liquid nitrogen for data collection.

Table 4.1 Crystallization

	Crystals 1 and 2
Method	Vapor diffusion, hanging drop
Plate type	Hampton Research, VDX 24-well
Temperature (K)	298
Protein concentration	30 mg/mL
Buffer composition of protein solution	0.1 *M* glycine, pH 9.5
Composition of reservoir solution	1.8 *M* ammonium sulfate, 20% glycerol, 0.1 *M* glycine
Volume and ratio of drop	6 μL, 4:2 protein:mother liquor
Volume of reservoir	1 mL

4.3.2 Data collection and processing

Data from two crystals were collected to solve the THB1 structure using multi crystal SAD phasing. One dataset was collected on a home source at Johns Hopkins University using an Agilent SuperNova sealed tube with a wavelength of 1.54 Å. A second high-resolution dataset was collected at the National Synchrotron Light Source (NSLS) on beamline X25 and served as the native dataset. Anomalous data were processed and scaled using the *CrysAlis*^{Pro} software of Agilent; the native data were processed using *XDSGUI* as a front end to *XDS/XSCALE/XDSCONV*[13]. SIRAS phasing using both datasets was performed using hkl2map[14] as a front end for *SHELXC/D/E*[15] to identify two Fe sites, determine initial phases, and for subsequent autotracing. *SHELXE* placed 224 residues into electron density, yielding an almost complete trace of the model assuming two peptides within the unit cell.

Table 4.2 Data collection and processing

Values for the outer shell are given in parentheses

	Native	Anomalous
Data set name	JL01-4_5	xs0378a_max
Diffraction source	NSLS beamline X25	sealed tube
Wavelength (Å)	1.1 Å	1.54 Å
Temperature (K)	100	110
Detector	PSI Pilatus 6*M*	Agilent ATLAS CCD
Crystal-detector distance (mm)	350	100
Rotation range per image (°)	0.3	0.3
Total rotation range (°)	105	242
Exposure time per image (s)	0.5	45
Space group	$P6_122$	$P6_122$
a, *b*, *c* (Å)	144.51, 144.51, 79.91	144.62, 144.62, 78.80
α, β, γ (°)	90, 90, 120	90, 90, 120
Mosaicity (°)	0.097	–
Resolution range (Å)	47.3–1.893 (1.961–1.893)	50.0–3.0 (3.11–3.0)
Total No. of reflections	408679 (27314)	195664 (14343)
No. of unique reflections	39522 (3849)	36655 (3666)
Completeness (%)	99.86 (98.97)	99.3 (99.5)
Redundancy	10.3 (7.1)	5.3 (3.9)
$\langle I/\sigma(I)\rangle$	13.81 (0.96) #	12.39 (3.08)
$R_{meas.}$	0.08576	–
$CC_{1/2}$	0.999 (0.78)	–
CC*	1 (0.936)	–
Overall *B* factor from Wilson plot (Å^2)	39.20†	–
SIRAS phasing		
Resolution (Å)		50–3.5
No. of heavy atoms in asymmetric unit		2
Heavy atom type		Fe
<FOM> (initial/after *SHELXE*)		0.243/0.615

#[16,17,18]

† No anomalies.

4.3.3 Structure solution and refinement

A single round of *Buccaneer*[19,20] in *CCP4*[21] resulted in complete assignment of residues based on the recombinant THB1 sequence. *Coot*[22] and *phenix.refine*[23] were used for subsequent rounds of model building and refinement, respectively. The heme ligands (HEM) were placed using *Coot*. Final refinement was performed using TLS groups, which were

automatically determined via *PHENIX*. The quality of the structure was validated via *MolProbity*[24], and modelling and refinement statistics are presented in Table 4.3.

Table 4.3 Structure solution and refinement

Values for the outer shell are given in parentheses

Resolution range (Å)	47.3–1.9 (1.94–1.9)
Completeness (%)	99.7
σ cutoff	$F > 1.36\ \sigma(F)$
No. of reflections, working set	39472 (2608)
No. of reflections, test set	1993 (125)
Final R_{cryst}	0.187 (0.378)
Final R_{free}	0.218 (0.386)
No. of non-H atoms	
Protein	1931
Ligand	86
Water	209
Total	2226
R.m.s. deviations	
Bonds (Å)	0.010
Angles (°)	1.12
Average *B* factors (Å^2)	
Protein	51.1
Ligand	39.7
Water	51.2
Ramachandran plot	
Most favoured (%)	100
Allowed (%)	0

4.3.4 NMR data collection

NMR data were collected at a proton frequency of 600 MHz on a Bruker Avance or Avance II spectrometer equipped with a cryoprobe. Probe temperature was 298 K. Samples were (1) ^{15}N-labeled THB1 (~1.4 mM) in 25 mM borax buffer pH 9.5, reduced with 7.5 mM dithionite, and (2) ^{15}N-labeled CtrHb (~1.4 mM) in 100 mM borax buffer pH 10, reduced with 6 mM dithionite, both under argon. Following reduction, THB1 and CtrHb solutions (~300 □ L) were transferred into NMR Shigemi tubes and sealed with Parafilm; samples prepared in this manner remained completely reduced over the course of data acquisition. The solvent was 90% H_2O, 10% D_2O. ^{1}H spectra in Fig. 4.X were acquired with ^{15}N-decoupling (^{15}N frequency centered in the amide region, 118–120 ppm). Under these conditions, incomplete decoupling of the Lys E10 NζH_2 protons is observed for THB1 (Fig. 4.7). The flip-back WATERGATE NOESY spectrum in Fig. 4.7 was collected on the same CtrHb sample with a mixing time of 80 ms and ^{15}N decoupling.

4.4 Results and discussion

As purified from the *E. coli* host, the recombinant *C. reinhardtii* THB1 polypeptide has a cleaved initial methionine, is 135 residues in length (Table 4.4), and lacks the N-terminal acetylation detected in the native protein[5]. Under the chosen conditions, THB1 crystallized in space group $P6_122$. The crystallographic asymmetric unit contained only two protein molecules, leading to a large water content (70.3%) and a high Matthews coefficient of 4.14 Å^3/Da, as calculated in *CCP4* using *Matthews – cell content analysis*[21].

Table 4.4 Macromolecule production information

Source organism	*Chlamydomonas reinhardtii*
DNA source	Synthesized gene (DNA 2.0)
Expression vector	pJExpress414
Expression host	*Escherichia coli*
Complete amino acid sequence of the construct produced	AADTAPADSLYSRMGGEAAVEKAVDVFYERIVADPQLAP FFANVDMKKQRRKQVAFMTYVFGGSGAYEGRDLGASH RRLIREQGMNHHHFDLVAAHLDSTLQELGVAQELKAEA MAIVASARPLIFGTGEAGAAN
UniProt identifier	A8JAR4
Ligand	*b* heme (HEM)
Formula weight	15180.9 Da

4.4.1 Ferric THB1 structure – backbone

The structure was solved to a resolution of 1.9 Å (PDB ID: 4XDI, Table 4.3). The electron density was insufficient to define the position of N-terminal residues A^2AD (chain A) and A^2ADT (chain B), and C-terminal residues $AGAAN^{136}$ (chain A) and $TGEAGAAN^{136}$ (chain B). Chain B is composed of seven helical elements (Fig. 4.1A). These are labelled A–H (D absent) as customary for hemoglobins and span residues 13–15 (A), 18–34 (B), 39–42 (C), 47–62 (E), 73–84 (F), 88–104 (G), and 109–127 (H) according to DSSP[25]. Chain A contains the same secondary structure elements, except for a distorted A helix. The two chains align with an rmsd of 0.53 Å over 119/123 Cα pairs (interatomic distance threshold of 2 Å), the largest deviations being located in turns and loops. The B factors are generally high, with elevated values at the termini and mostly in the EF loop and GH turn (chain A). Chain B has higher values on average and noticeably at the beginning of

the B helix and the CE turn. The flexible structure of the first thirteen residues is consistent with the high affinity of recombinant THB1 for antibodies raised against the corresponding peptide[5].

THB1 has the expected TrHb1 features of short or imperfectly formed A helix and long EF loop[26]. The 3_{10} C helix is capped at the N-terminus with a side chain (Asp35) to backbone (Gln37) H-bond as observed in several related proteins[27]. Also conserved is an N-terminal capping box initiating the G helix. In THB1, this motif involves the side chain of His90 (acceptor for the backbone NH of Asn87) and the side chain of Asn87 (acceptor for the backbone NH of His89 and donor for the backbone O of Gly85) and is readily detected in solution[5]. The H helix has a distortion at the level of Ser122 (H14) and toward its C-terminal end.

4.4.2 Ferric THB1 structure – side chains

The structure contains no unusual rotamers. The largest $\chi 1$ deviations are observed for Glu131 in chain A and Glu110 in chain B. Asp46 (chain B) was modelled with two orientations. There is no apparent explanation for these features.

4.4.3 Ferric THB1 structure – heme geometry, axial ligands, and environment

Figure 4.1C shows the electron density of the heme group of chain A. A similar density is obtained for chain B. The average B factor is higher for the macrocycle of heme B (~40 $Å^2$) than for that of heme A (~34 $Å^2$). No evidence for heme disorder (specifically, density corresponding to protein molecules containing the cofactor rotated by 180° about the α–γ axis) was detected at this resolution. An analysis of the macrocycle geometries by normal coordinate decomposition[28] reveals an out-of-plane displacement of ~1 Å,

contributed almost equally by saddling and ruffling modes with opposite signs. This is in contrast to other TrHb1s, which tend to be ruffled[26]. The 2-vinyl groups adopt the *trans* orientation (as defined in[29]) (average $\tau = 174°$, Cβ pointing toward 1-CH_3) whereas the 4-vinyl adopts an out-of-plane *cis* orientation (average $\tau = -29°$, Cβ pointing toward 5-CH_3 and the proximal side). The 2-vinyl has a comparatively elevated B factor at the Cβ position. The heme propionates also have relatively elevated B factors compared to the macrocycle atoms, but are nevertheless well defined. On the proximal side, several water molecules are associated with the carboxyl groups. On the distal side, the 6-propionate interacts with Lys49 (E6) and the 7-propionate with Arg52 (E9) (Fig. 4.1C). These interactions shield the distal heme cavity from solvent penetration.

The distinguishing feature of ferric THB1 is the heme axial coordination Figure 4.1A,B. As expected on the basis of sequence alignment and prior NMR data, one ligand to the iron is the conserved proximal histidine, His77 (referred to as F8). His77 adopts χ1 and χ2 values (averages of −56° and 89°, respectively) such that its heterocycle plane is nearly perpendicular (85°) to the heme plane, and its projection nearly lines up with the β–δ meso direction. This staggered geometry, which minimizes steric clashes with the heme pyrrole nitrogens and allows greater movement of the iron, is typical of TrHbs[26,30,31].

The structure demonstrates unambiguously that Lys53 (E10) is the distal ligand to the iron in the ferric state. This side chain has B factors comparable to those of the heme group to which it is coordinated. The axial lysines are extended with *trans* (t) χ1, χ2 and χ3 dihedral angles. Coordination is made possible by a *gauche*+ (p) χ4, which brings the Nζ atom within 2.2 Å of the Fe atom and forming a Cε–Nζ–Fe angle of ~118°, consistent with

sp^3 geometry for the nitrogen. No water molecule was found in the heme pocket of either molecule in the asymmetric unit.

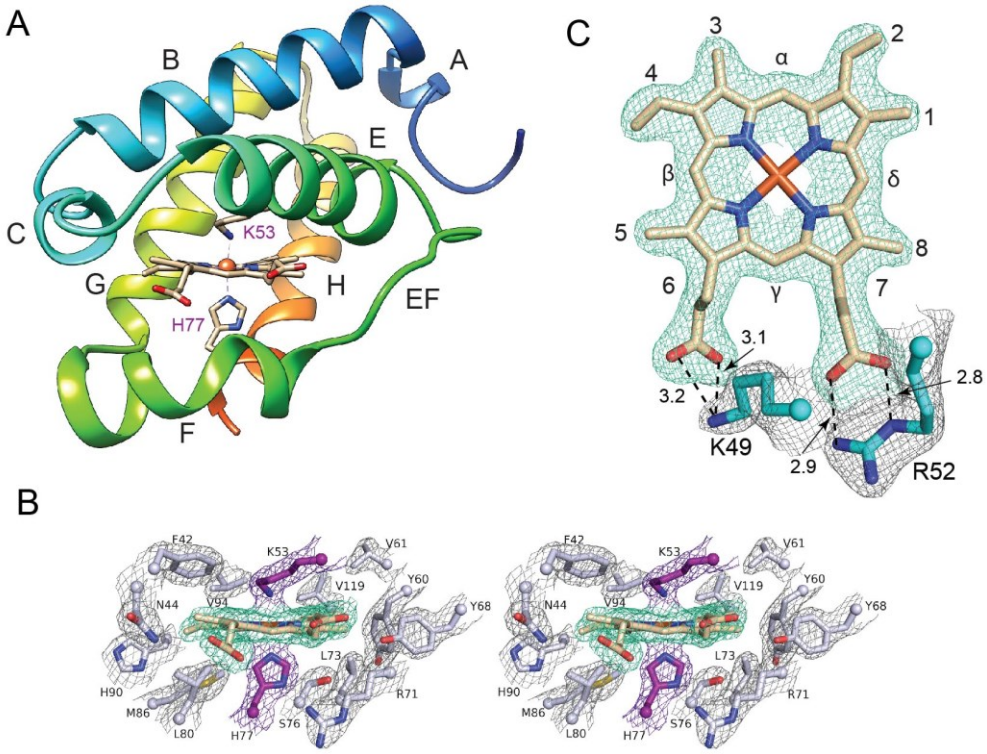

Fig. 4.1 Crystal structure and electron density of heme, propionates, and heme pocket side chains. (A) Ribbon diagram of THB1 (chain B). Helical segment identified by DSSP (Kabsch and Sander, 1983) span residues 13–15 (A), 18–34 (B), 39–42 (C), 47–62 (E), 73–84 (F), 88–104 (G), and 109–127 (H). **(B)** Stereo view (wall-eyed) of the electron density map (1.0 σ, chain A) of the heme, its axial ligands (Lys53 and His77) and several residues within 4 Å of the heme group (Cα depicted with a ball). **(C)** Electron density map (1.0 σ) of the heme and the residues forming well-defined ionic interactions with the propionates (Lys49 and Arg52, Cα depicted with a ball). Distances are in Å.

Residues in contact with the heme are essentially as expected for a TrHb1[27]. Of note are Phe41 (C7), Leu73 (F4), Leu80 and Met86 in the FG turn, Phe91 (G5), and Ile126 (H18) on the proximal side and Phe42 (CD1), Phe57 (E15), and Val94 (G8) on the distal side.

These residues form a largely hydrophobic environment protecting the heme from solvent. It is likely that the stability of lysine coordination despite the requirement of deprotonation is aided by this apolar environment and the preferential interactions of residues E6 and E9 with the propionates.

4.4.4 Comparison to solution structure in the ferrous state

Nuclear magnetic resonance (NMR) data collected on ferrous THB1 at alkaline pH show clear evidence for the ligation of a distal lysine[5]. Electron self-exchange experiments support that the ligands to the iron are identical in the two redox states. In addition, the ^{1}H-^{1}H coupling constants and nuclear Overhauser effects along the lysine side chain[5] are consistent with the dihedral angles modelled in the ferric state. The dipolar contacts detected between the side chain and the heme group are also in agreement with the X-ray structure. This suggests minimal reorganization of the heme cavity structure upon changes in oxidation state.

4.4.5 Comparison to *bis*-histidine TrHb1s

The structure of THB1 can be compared to those of the hexacoordinate TrHb1s (GlbNs) from the cyanobacteria *Synechococcus* sp. PCC 7002 (PDB ID 4MAX) and *Synechocystis* sp. PCC 6803 (PDB ID 1RTX). Automatic alignment using UCSF *Chimera* (Pettersen *et al.*, 2004) matches large sections of the B, C, F, G, and beginning of H helices with deviations below 2 Å (Appendix Table AX, Fig. 4.2A,D). Within the globally optimized superposition, the heme planes are close to each other and the largest deviations are observed for the E helix (Fig. 4.3).

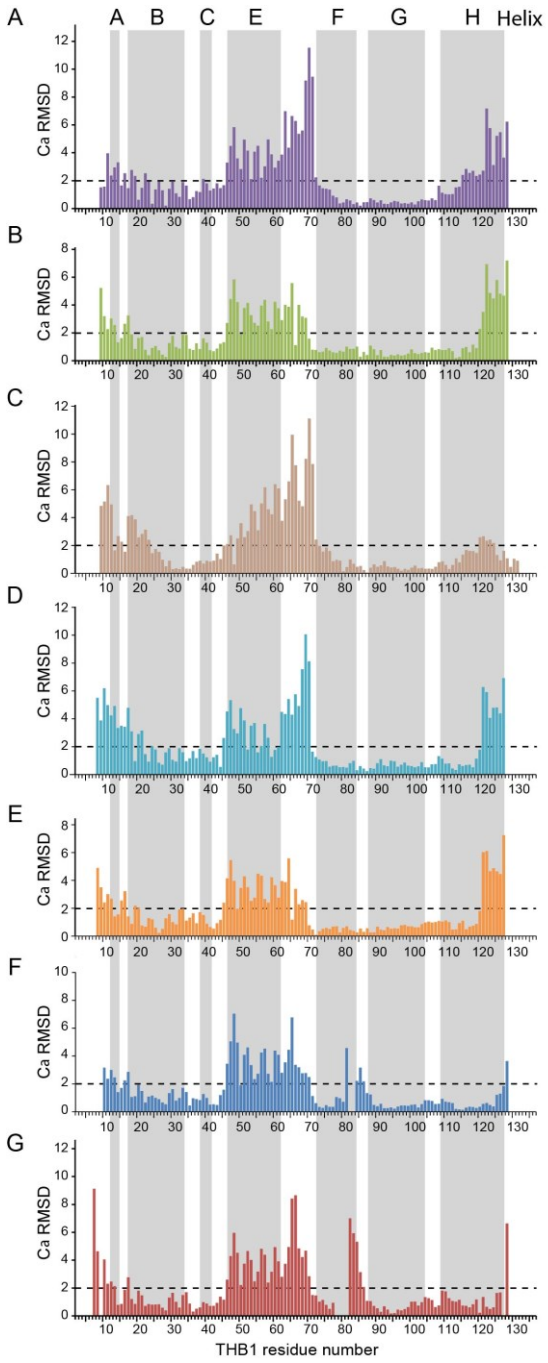

Fig. 4.2 Cα r.m.s.d. as a function of position for the overlay of several trHbs. (A) THB1 with *Synechococcus* GlbN in the *bis*-histidine state, **(B)** THB1 with *Synechococcus* GlbN in the cyanide-bound state, **(C)** *Synechococcus* GlbN in the *bis*-histidine state with the same in the cyanide bound state, **(D)** THB1 with *Synechocystis* GlbN in the *bis*-histidine state, **(E)** THB1 with *Synechocystis* GlbN in the cyanide-bound state, **(F)** THB1 with *C. eugametos* CtrHb in the cyanide bound state, and **(G)** THB1 with *M. tuberculosis* HbN in the oxy state. The dashed line indicates the 2 Å threshold for the matched pair count.

In THB1, the B and E helices have a crossing angle of 56° and a centroid separation of 9.8 Å, whereas in *Synechococcus* GlbN, the angle is 58° and distance 8.7 Å. The E and F helices of THB1 cross with an angle of 53° and are at a distance of 12.5 Å, to be compared with the 52° and 14.9 Å values observed in *Synechococcus* GlbN. Matching the E helices of the two proteins requires a rotation about the helical axis, which introduces a 34° angle between the heme planes.

Tyr B10 plays a special role in many TrHb1s[27,32,33]. The reconfiguration of the B and E helix orientation in THB1 compared to GlbN is accompanied with differences in the position of Tyr B10, which maintains the same rotameric state in all three proteins but points inside the heme cavity in THB1 as opposed to outside in GlbN (Fig. 4.3).

The position of Phe E15 (a residue that is thought to gate access to the heme pocket in other TrHb1s[34]) is also affected. In THB1, the side chain dihedral angles are –85° and −49° and the aromatic ring is under pyrrole B. In *Synechococcus* GlbN, the side chain points between the 2-vinyl and the 3-CH_3 and has dihedral angles of −166° and 105°. Of the residues in contact with the heme group, Phe42 (CD1, actually last residue of the C helix) has the most conserved orientation. All other residues vary significantly. For example, in accordance with the distribution of backbone rmsd, the end of the H helix provides distinct contacts, with THB1 Ile126 (H18) taking the place of GlbN Val121 (H20).

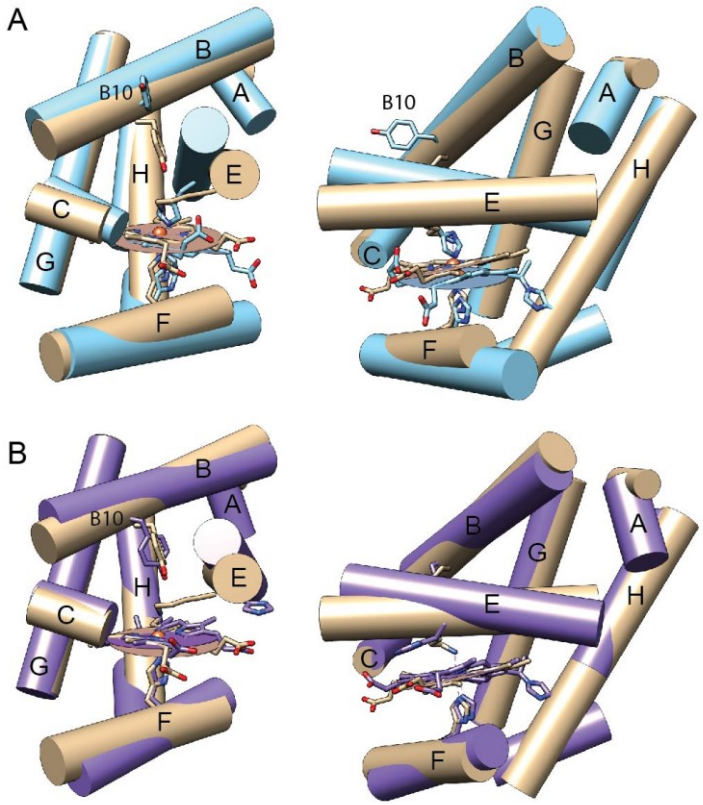

Fig. 4.3 Overlay of THB1 with *Synechococcus* GlbN (A) in the *bis*-histidine state (4MAX) and **(B)** the cyanide-bound state (4L2M). THB1 is in sand colour. Also represented are Tyr B10, the axial His46 and His70 of GlbN along with the cross-linked His117, and the axial Lys53 and His77 of THB1. Linkers between helices are omitted for clarity.

4.4.6 Structural plasticity, exogenous ligand binding, and comparison to other states

In our initial NMR study[5] we collected data on the cyanomet complex (THB1-CN). In this form of the protein, cyanide displaces Lys53 as the distal ligand to the ferric iron. The structure of this complex was partially characterized with special attention to the distal cavity and comparison to other cyanomet forms of TrHb1s. Signals were assigned to the OηH of Tyr29 (B10) and the $N\varepsilon H_2$ of Gln50 (E7) and Gln54 (E11). These three residues

constitute the distal H-bond network first identified in *C. eugametos* CtrHb-CN (PDB ID 1DLY)[35]. Similarity extends to *Synechocystis* GlbN-CN (PDB ID 1S69) and *Synechococcus* GlbN-CN (PDB ID 4L2M). *C. eugametos* CtrHb-CN has a lysine at position E10 and is therefore the most relevant. In the cyanide bound state, Lys E10 interacts with the 7-propionate. It is reasonable to expect the same interaction in THB1 with exogenous ligand bound and assume that the $\chi 1$ dihedral angle would change to *gauche*$^-$ (m) followed by all *trans* dihedrals to reach the propionate.

The NMR data of THB1-CN are well resolved and revealed the population of protein form with heme rotated by 180° around the α–γ meso axis. This isomer accounts for approximately 15% of the sample. The two forms of the protein typically yield distinct NMR spectra even when the complex is diamagnetic. No evidence for a second form was identified in the spectra of the ferrous state and it is possible that the population of the minor isomer is not detectable.

At the time of writing, no crystal structure of THB1 with an exogenous ligand bound is available. However, through comparison of related TrHb1 structures, the overall rearrangement necessary to achieve the bound conformation can be envisioned. This is illustrated by superimposing the structures of THB1 and cyanomet *Synechococcus* GlbN-CN (Fig. 4.3B). In hexacoordinate THB1, the configuration of the B and E helix is such that Tyr B10 is positioned closer to its expected position in the cyanide complex. In fact, the alignment of THB1 with *Synechococcus* GlbN in the cyanide bound state (Fig. 2*b,* Fig. S1*b*) is comparable to the alignment with the *bis*-histidine complex, (rmsd of ~0.97 Å over 82 Cα pairs). For comparison, each of these alignments is arguably better than the alignment of the *bis*-histidine and cyanide bound states of *Synechococcus* GlbN with each other, if one ignores the post-translationally modified H helix (Appendix Table A5, Fig. S1*c*). Within GlbN-CN,

the B and E helices have a crossing angle of 52° and an inter-centroid distance of 9.3 Å. The E and F helices are characterized by a 45° crossing angle and a 11.8 Å distance. Alignments of THB1 with *Synechocystis* GlbN and *C. eugametos* CtrHb in the cyanide bound state, and *Mycobacterium tuberculosis* HbN in the oxy state are also similar (Appendix Table A5, Fig. 4.2E,F,G, Fig. 4.4). We conclude that THB1 has structural traits of both the His–His and the His–diatomic complexes. The structure illustrates that the long loops of TrHb1s, in particular the EF loop[36,37], allow helices to adopt a broad range of relative orientations.

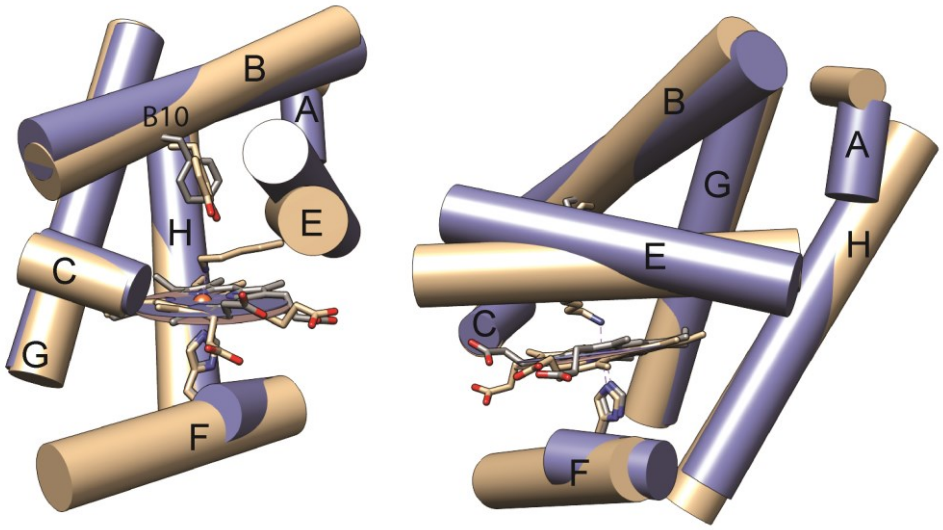

Fig. 4.4 Superimposition of THB1 (sand) **and *C. eugametos* CtrHb in the cyanide bound state** (purple)**.** Note the position of Tyr B10. Unlike GlbN, CtrHb and THB1 do not attach the heme covalently through a histidine at the end of the H helix, and the structural overlap in this region is high.

TrHb1 structures that have a distal exogenous ligand (e.g., cyanide) share the presence of tunnels providing access to the heme cavity. Analysis of the structure of THB1 with coordinated lysine using the program Mole 2.0[38] reveals no large tunnel. However, both chains present a narrow pore. One end of this pore is located where the N-terminus of the B helix meets the GH turn and the other end is between the G and H helices, at the level

of the heme group (Fig. 4.5). In chain B, Phe91 blocks further extension of the pore. Constriction shortens the tunnel by one helical turn in chain A. The positioning of this narrow tunnel is reminiscent of the long tunnel in *C. eugametos* TrHb1[39].

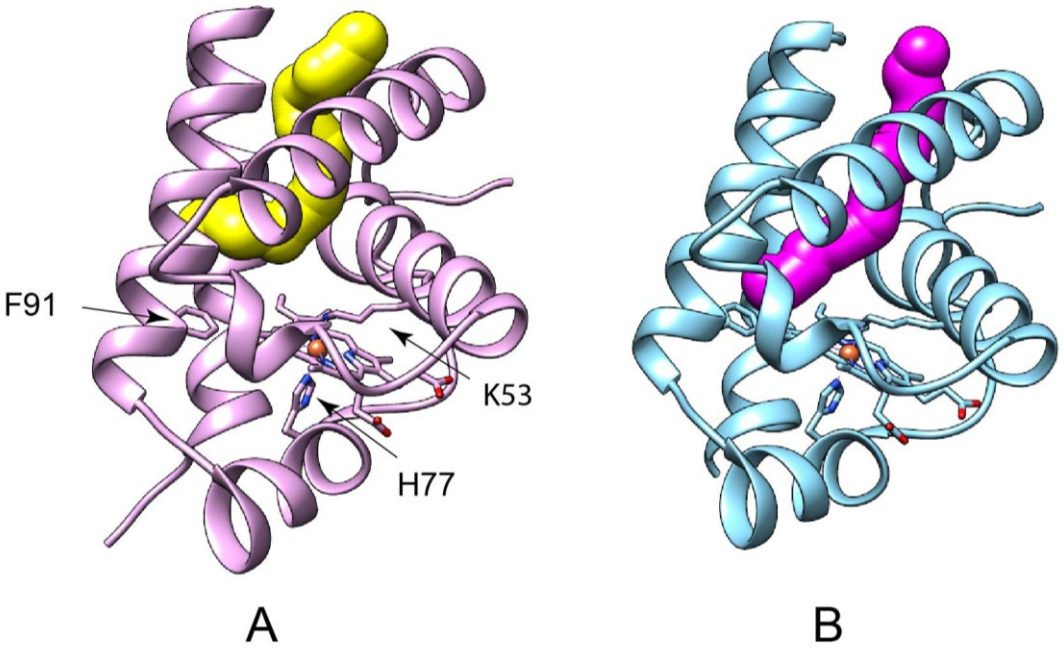

Fig. 4.5 Pores in the structure of THB1 chainA **(A)** and chain B **(B)** as calculated with MOLE 2.0 (interior threshold of 1.15 Å). The pores extend from the B/GH interface to the heme. Also shown are Lys53 (E10), His77 (F8), and Phe91 (G5).

4.4.7 Other instances of lysine coordination

Lysine coordination is rare, likely because of the high energetic cost associated with the deprotonation of the amino group at physiological pH. It has been reported in two forms, either in combination with an axial histidine (as in misfolded iso-1-cytochrome *c*[40], a variant cytochrome c_{550}[41], and nitrite reductase/quinol dehydrogenase complex[12]) or a water molecule (as in nitrite reductase[12]). Ferric M100K cytochrome c_{550} at neutral pH has similar spectroscopic properties to native cytochrome c_{550} at alkaline pH and thus is used as a mimic for the alkaline form seen in several *c* cytochromes[41]. The X-ray structure (Fig. 4.6A, PDB

ID 2BH5) shows that both of the axial ligands are found in loops. The "proximal" histidine (His19) has a staggered orientation with imidazole ring projection oriented along α-γ meso axis. The "distal" lysine (Lys100) has a χ_1 angle of 111° more than three standard deviations from the average value and practically eclipsed with the Cα–C bond. Angle $\chi 3$ (−133°) is also unusual, reinforcing that a strained conformation is necessary to achieve coordination. In addition, the heme pocket contains a water molecule within H-bonding distance of the amino group of Lys100.

Another example of His–Lys coordination is provided by the cytochrome c nitrite reductase complex (Fig. 4.6B, PDB ID 2J7A). This large complex is composed of four cytochrome *c* nitrite reductase molecules, NrfA, and two molecules of its electron donor, NrfH (cytochrome *c* quinol dehydrogenase). There are 28 heme groups in the assembly[12]. Two of the *c* hemes in this symmetrical complex (hemes 4H/H*) have His–Lys coordination and are located in the $NrfH_2A_4$ interface, where the proximal histidine (His140) residue and heme are from NrfH and the distal lysine (Lys331) is from a β-strand located in NrfA. Heme 4 has a proximal histidine with a staggered orientation, aligned along the α–γ axis as in M100K cytochrome c_{550} (perpendicular to the orientation in THB1). The distal lysine has mttt dihedral angles, which orient the side chain practically perpendicular to the heme plane. The interfacial position of hemes 4H/H* makes it likely that they are important for electron transfer from NrfH to NrfA and for the stability of the complex[12,42].

Cytochrome *c* nitrite reductase (NrfA) has a second *c* heme with lysine coordination (Fig. 4.6C). Heme $1A^i/A^e$ is coordinated by a proximal lysine (Lys151), located on a turn between two helices, with no ligand on the distal side[12]. Unlike the distal lysine of heme 4H/H* of NrfH or THB1 the proximal lysine has mmtm dihedral angles. In this case as well, the side chain is nearly perpendicular to the heme plane, but the distance between

Lys151 Cα and the heme Fe is ~7 Å compared to ~8 Å for Lys331. As in M100K cytochrome c_{550}, a water molecule is within H-bond distance of the amino group. Heme $1A^i/A^e$ is the active site of NrfA, where nitrite is converted into ammonia and thus the coordination of the heme is critical for the function of the protein. The redox potential of the high-spin heme $1A^i/A^e$ has been estimated at −50 mV[41] in *Desulfovibrio vulgaris* NrfA. The large number of heme groups, most of which have bis-histidine coordination, complicates these measurements[43] so that limited mechanistic information is available.

It is interesting that the available examples of lysine ligation all involve *c* hemes, except THB1, and that one of these *c* heme examples is interfacial. Thus, attachment of the heme group to a fixed position with respect the polypeptide or the lysine is not a requirement. The structures also show no common geometry for the lysine side chain, which can be parallel (THB1), at angle (M100K cytochrome c_{550}) or perpendicular (nitrite reductase) to the heme plane (Fig. 4.6). There is no trend in the dihedral angles or the secondary structure of the segment bearing the lysine (Table 4.6). It is interesting that the previously available examples of lysine ligation all involve *c* hemes. THB1 demonstrates that covalent attachment of the heme group to a fixed position with respect the polypeptide or the lysine is not a requirement. The amino group of the lysine may or may not form an H-bond to a distal residue or a water molecule (Fig. 4.6, Table 4.5). Nevertheless, two common features emerge, in that the coordinating lysine is generally not directly accessible to bulk solvent and stable, alternative states are expected to cause clashes and require substantial structural rearrangement.

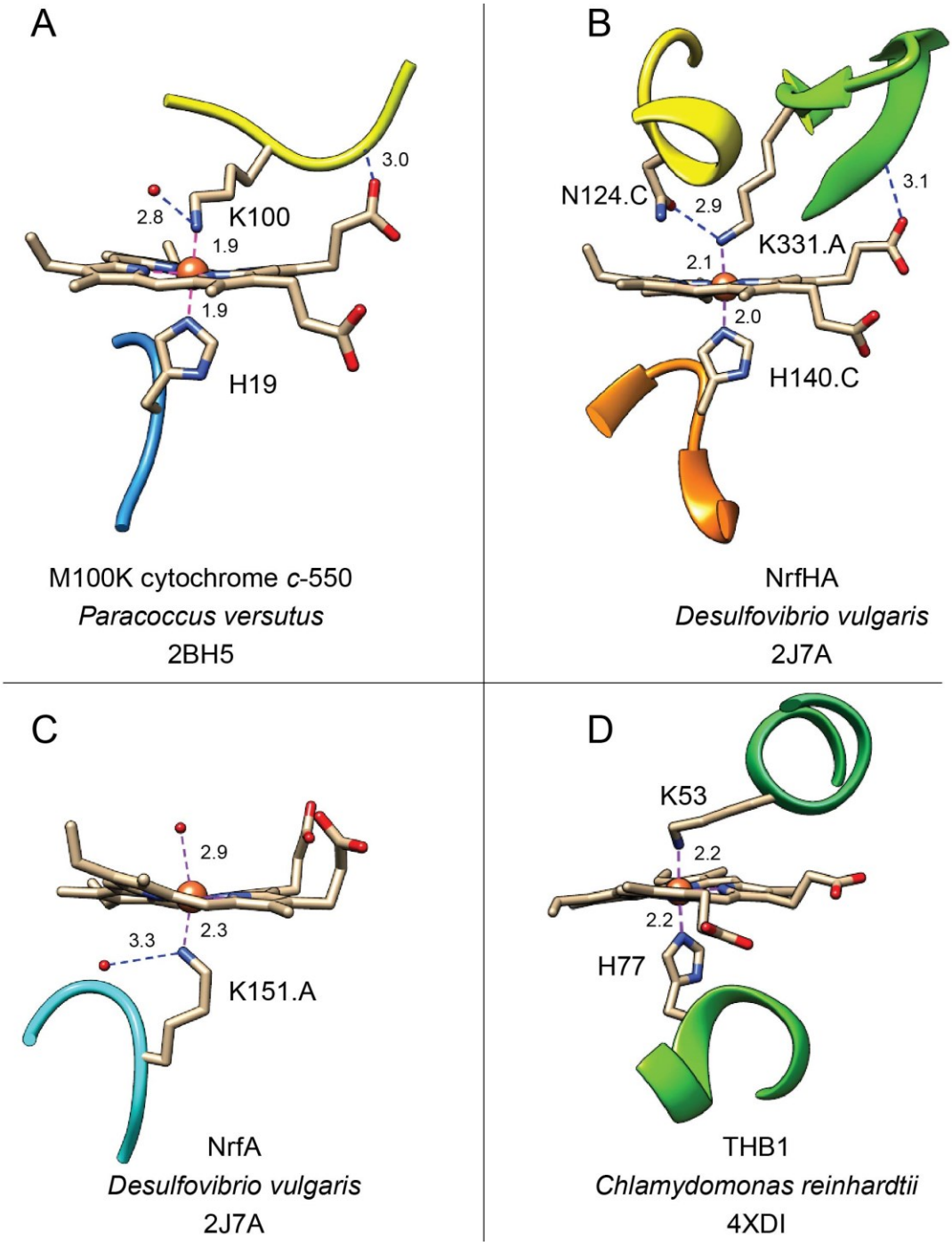

Fig. 4.6 Available examples of lysine coordination. Distances are in Å.

Table 4.5 Geometry of coordinating lysines

Protein	Structure	2° structure	Lys χ1–4	Cε–Nζ–Fe	Nζ–Fe (Å)	$N\zeta H_2$ H-bond
THB1 His77–Lys53	4XDI	α-helix	tttp	118°	2.23	no
M100K cyt c_{550} His19–Lys100	2B5H	loop	111°, t, −133°, t	129°	1.89	water
nitrite reductase NrFHA His140.C–Lys331.A	2J7A	β-strand	mttt	116 ± 5°	2.17 ± 0.06[a]	Asn124.C
nitrite reductase NrFHA Lys151.A–H_2O	2J7A	turn	mmtm	123 ± 6°	2.20 ± 0.09	water

[a]Average over all chains.

4.4.8 Structural predictions

Many TrHb1s have a lysine at position E10, but not all Lys E10 coordinate the iron. Two examples are ferric *M. tuberculosis* HbN[44] and *Paramecium caudatum* HbN[34]. In both instances, a water molecule takes the place of Lys E10. So far, TrHb1 structures with exogenous ligand bound resemble each other closely (Appendix Table A5) and thus using any of these structures as a template with programs such as *SWISS-MODEL*[45] to represent a TrHb1 of unknown structure is likely to yield acceptable results. However, a "hexacoordinate" template (be it with axial His E10 or Lys E10) may also generate plausible structures. Interestingly, an acceptable hexacoordinate model of *C. eugametos* TrHb1 (CtrHb) can be prepared from THB1. Finally, *C. reinhardtii* has other TrHb1s, two of which have been mentioned in the literature, THB2[9] and THB8[46]. Both of these proteins have a lysine at

E10 and it is possible to construct acceptable models of THB2 and THB8 using the coordinates of THB1 and *SWISS-MODEL*[45]. Experimental data will be required to establish heme coordination in these homologous proteins.

4.5 Conclusion

The structure of THB1 illustrates that the TrHb1 fold adjusts to accommodate different distal heme ligands and emphasizes the difficulty in predicting whether a protein side chain or a water molecule coordinates the iron. Thus, structural determination by NMR or X-ray crystallography is a necessity to characterize the heme environment and rationalize the chemical properties of these proteins.

Acknowledgements

The authors thank Maxime Siegler for the collection of the anomalous data set and Eric Johnson for useful comments. The work was supported by funding from The Bloomberg Family Foundation (J.B.), the NIH Chemistry-Biology Interface Training Grant (T32 GM080189) (L.E.B.), the NIH Cellular and Molecular Biology Training Grant (T32 GM007231) (S.L.R.), a Predoctoral Fellowship from the Johns Hopkins Malaria Research Institute (L.E.B.), and the National Science Foundation (MCB 1330488) (J.T.J.L.).

4.6 References

(1) Wittenberg, J. B., Bolognesi, M., Wittenberg, B. A., and Guertin, M. (2002) Truncated hemoglobins: A new family of hemoglobins widely distributed in bacteria, unicellular eukaryotes and plants. *Journal of Biological Chemistry. 277*, 871-874.

(2) Vinogradov, S. N., Bailly, X., Smith, D. R., Tinajero-Trejo, M., Poole, R. K. and Hoogewijs, D. (2013) Microbial eukaryote hemoglobins. *Advances in Microbial Physiology, 63*, 391-446.

(3) Vinogradov, S. N., Fernandez, I., Hoogewijs, D. and Arredondo-Peter, R. (2011) Phylogenetic relationships of 3/3 and 2/2 hemoglobins in Archaeplastida genomes to bacterial and other eukaryote hemoglobins. *Molecular Plant, 4*, 42-58.

(4) Vinogradov, S. N., Tinajero-Trejo, M., Poole, R. K., and Hoogewijs, D. (2013) Bacterial and archaeal globins — A revised perspective. *Biochimica Biophysica Acta-Proteins Proteomics 1834*, 1789-1800.

(5) Johnson, E. A., Rice, S. L., Preimesberger, M. R., Nye, D. B., Gilevicius, L., Wenke, B. B., Brown, J. M., Witman, G. B., and Lecomte, J. T. J. (2014) Characterization of THB1, a *Chlamydomonas reinhardtii* truncated hemoglobin: Linkage to nitrogen metabolism and identification of lysine as the distal heme ligand. *Biochemistry, 53*, 4573-4589.

(6) Johnsons, E. A. and Lecomte, J. T. J. (2014) Characterization of the truncated hemoglobin THB1 from protein extracts of *Chlamydomonas reinhardtii. F1000Research, 3*.

(7) Maia, L. B. and Moura, J. J. (2015) Nitrite reduction by molybdoenzymes: A new class of nitric oxide-forming nitrite reductases. *Journal of Biological Inorganic Chemistry, 20*, 403-433.

(8) Sanz-Luque, E., Ocana-Calahorro, F., Llamas, A., Galvan, A. and Fernandez, E. (2013) Nitric oxide controls nitrate and ammonium assimilation in *Chlamydomonas reinhardtii. Journal of Experimental Botany, 64*, 3373-3383.

(9) Sanz-Luque, E., Ocana-Calahorro, F., de Montaigu, A., Chamizo-Ampudia, A., Llamas, A., Galvan, A. and Fernandez, E. (2015) THB1, a truncated hemoglobin, modulates nitric oxide levels and nitrate reductase activity. *Plant Journal, 81*, 467-479.

(10) Stewart, J. J. and Coyne, K. J. (2011) Analysis of raphidophyte assimilatory nitrate reductase reveals unique domain architecture incorporating a 2/2 hemoglobin. *Plant Molecular Biology, 77*, 565-575.

(11) Ferrer, J. C., Guillemette, J. G., Bogumil, R., Inglis, S. C., Smith, M. and Mauk, A. G. (1993) Identification of Lys97 as an iron ligand in one form of alkaline yeast iso-1-ferricytochrome *c*. *Journal of the American Chemical Society, 115*, 7507-7508.

(12) Rodrigues, M. L., Oliveira, T. F., Pereira, I. A. and Archer, M. (2006) X-ray structure of the membrane-bound cytochrome *c* quinol dehydrogenase NrfH reveals novel haem coordination. *EMBO Journal, 25*, 5951-5960.

(13) Kabsch, W. (2010) *XDS*. *Acta Crystallogr D Biol Crystallogr, 66*, 125-132.

(14) Pape, T. and Schneider, T. R. (2004) *HKL2MAP*: A graphical user interface for macromolecular phasing with *SHELX* progams. *Journal of Applied Crystallography, 37*, 843-844.

(15) Sheldrick, G. M. (2010) Experimental phasing with *SHELX/C/D/E*: combining chain tracing with density modification. *Acta Crystallographica Section D: Biological Crystallography, 66*, 479-485.

(16) Luo, Z., Rajashankar, K. and Dauter, Z. (2014) Weak data do not make a free lunch, only a cheap meal. *Acta Crystallographica Section D: Biological Crystallography, 70*, 253-260.

(17) Karplus, P. A. and Diederichs, K. (2012) Linking crystallographic model and data quality. *Science, 336*, 1030-1033.

(18) Diederichs, K. and Karplus, P. A. (2013) Better models by discarding data? *Acta Crystallographica Section D: Biological Crystallography, 69*, 1215-1222.

(19) Cowtan, K. (2006) The *Buccanneer* software for automated model building. 1. Tracing protein chains. *Acta Crystallographica Section D: Biological Crystallography, 62*, 1002-1011.

(20) Cowtan, K. (2008) Fitting moleculare fragments into electron density. *Acta Crystallographica Section D: Biological Crystallography, 64*, 83-89.

(21) Winn, M. D., Ballard, C. C., Cowtan, K. D., Dodson, E. J., Emsley, P., Evans, P. R., Keegan, R. M., Krissinel, E. B., Leslie, A. G. W., McCoy, A., McNicholas, S. J., Murshudov, G. N., Pannu, N. S., Potterton, E. A., Powell, H. R., Read, R. J., Vagin, A. and Wilson, K. S. (2011) Overview of the *CCP4* suite and current developments. *Acta Crystallographica Section D: Biological Crystallography, 67*, 235-242.

(22) Emsley, P., Lohkamp, B., Scott, W. G. and Cowtan, K. (2010) Features and development of *Coot*. *Acta Crystallographica Section D: Biological Crystallography, 66*, 486-501.

(23) Adams, P. D., Afonine, P. V., Bunkoczi, G., Chen, V. B., Davis, I. W., Echols, N., Headd, J. J., Hung, L. W., Kapral, G. J., Grosse-Kunstleve, R. W., McCoy, A. J., Moriarty, N. W., Oeffner, R., Read, R. J., Richardson, D. C., Richardson, J. S., Terwilliger, T. C. and Zwart, P. H. (2010) *PHENIX*: A comprehensive Python-based system for macromolecular structure solution. *Acta Crystallographica Section D: Biological Crystallography, 66*, 213-221.

(24) Chen, V. B., Arendall, W. B. I., Headd, J. J., Keedy, D. A., Immormino, R. M., Kapral, G. J., Murray, L. W., Richardson, J. S. and Richardson, D. C. (2010) *MolProbity*: All-atom structure validation for macromolecular crystallography *Acta Crystallographica Section D: Biological Crystallography, 66*, 12-21.

(25) Kabsch, W. and Sander, C. (1983) Dictionary of protein secondary structure: Pattern recognition of hydrogen-bonded and geometrical features. *Biopolymers, 22*, 2577-2637.

(26) Wenke, B. B., Lecomte, J. T., Heroux, A. and Schlessman, J. L. (2014) The 2/2 hemoglobin from the cyanobacterium *Synechococcus* sp. PCC 7002. *Proteins, 82*, 528-534.

(27) Vuletich, D. A. and Lecomte, J. T. J. (2006) A phylogenetic and strucutral analysis of truncated hemoglobins. *Journal of Molecular Evolution, 62*, 196-210.

(28) Jentzen, W., Ma, J. G. and Shelnutt, J. A. (1998) Conservation of the conformation of the porphyrin macrocycle in hemproteins. *Biophysical Journal, 74*, 753-763.

(29) Marzocchi, M. P. and Smulevich, G. (2003) Relationship between heme vinyl conformation and the protein matrix in peroxidases. *Journal of Raman Spectroscopy, 34*, 725-736.

(30) Samuni, U., Ouellet, Y., Guertin, M., Friedman, J. M. and Yeh, S. R. (2004) The absence of proximal strain in the truncated hemoglobins from *Mycobacterium tuberculosis*. *Journal of the American Chemical Society, 126*, 2682-2683.

(31) Nothnagel, H. J., Preimesberger, M. R., Pond. M. P., Winer, B. Y., Adney, E. M., and Lecomte, J. T. J. (2011) Chemical reactivity of *Synechococcus* sp. PCC 7002 and *Synechocystis* sp. PCC 6803 hemoglobins: covalent heme attachement and bishistidine coordination. *Journal of Biological Inorganic Chemistry, 16*, 539-552.

(32) Nardini, M., Pesce, A., Milani, M. and Bolognesi, M. (2007) Protein fold and structure in the truncated (2/2) globin family. *Gene, 398*, 2-11.

(33) Pesce, A., Bolognesi, M. and Nardini, M. (2013) The diversity of 2/2 (truncated) globins. *Advances in Microbial Physiology, 63*, 49-78.

(34) Daigle R, Guertin M, Lagüe P (2009) Structural characterization of the tunnels of *Mycobacterium tuberculosis* truncated hemoglobin N from molecular dynamics simulations. *Proteins, 75*, 735–747.

(35) Pesce, A., Couture, M., Dewilde, S., Guertin, M., Yamauchi, K., Ascenzi, P., Moens, L., and Bolognesi, M. (2000) A novel two-over-two α-helical sandwich fold is characteristic of the truncated hemoglobin family. *EMBO Journal, 19*, 2424-2434.

(36) Dellarole, M., Roumestand, C., Royer, C. and Lecomte, J. T. J. (2013) Volumetric properties underlying ligand binding in a monomeric hemoglobin: A high-pressure NMR study. *Biochimica et Biophysica Acta-Proteins and Proteomics, 1834*, 1910-1922.

(37) Pond, M. P., Majumdar, A. and Lecomte, J. T. J. (2012) Influence of heme post-translational modification and distal ligation on the backbone dynamics of a monomeric hemoglobin. *Biochemistry, 51*, 5733-5747.

(38) Berka, K., Hanák, O., Sehnal, D., Banáš, P., Navrátilová, V., Jaiswal, D., Ionescu, C.-M., Svobodová Vařeková, R., Koča, J. and Otyepka, M. (2012) MOLE*online* 2.0: Interactive web-based analysis of biomacromolecular channels. *Nucleic Acids Research, 40*, W222-W227.

(39) Milani, M., Pesce, A., Ouellet, Y., Ascenzi, P., Guertin, M. and Bolognesi, M. (2001) *Mycobacterium tuberculosis* hemoglobin N displays a protein tunnel suited for O_2 diffusion to the heme. *EMBO Journal, 20*, 3902-3909.

(40) Bandi, S. and Bowler, B. E. (2011) Probing the dynamics of a His73-heme alkaline transition in a destabilized variant of yeast iso-1-cytochrome *c* with conformationally gated electron transfer methods. *Biochemistry, 50*, 10027-10040.

(41) Ubbink, M., Campos, A. P., Teixeira, M., Hunt, N. I., Hill, H. A. and Canters, G. W. (1994) Characterization of mutant Met100Lys of cytochrome *c*-550from *Thiobacillus versutus* with lysine-histidine heme ligation. *Biochemistry, 33*, 10051-10059.

(42) Todorovic, S., Rodrigues, M. L., Matos, D., and Pereira, I. A. C. (2012) Redox properties of lysine- and methionine-coordinated hemes ensure downhill electron transfer in $NrfH_2A_4$ nitrite reductase. *Journal of Physical Chemistry B, 116*, 5637-5643.

(43) Doyle, R. M., Marritt, S. J., Gwyer, J. D., Lowe, T. G., Tikhonova, T. V., Popov, V. O., Cheesman, M. R., and Butt, J. N. (2013) Contrasting catalytic profiles of multiheme nitrite reductases containing CxxCK heme binding motifs. *Journal of Biological Inorganic Chemistry, 18*, 655-667.

(44) Couture, M., Das, T. P., Lee, H. C., Peisach, J., Rousseau, D. L., Wittenberg, B. A., Wittenberg, J. B., and Guertin, M. (1999) *Chlamydomonas* chloroplast ferrous hemoglobin: Heme pocket structure and reactions with ligands. *Journal of Biological Chemistry, 274*, 6898-6910.

(45) Arnold, K., Bordoli, L., Kopp, J. and Schwede, T. (2006) The SWISS-MODEL workspace: A web-based environment for protein structure homology modelling. *Bioinformatics, 22*, 195-201.

(46) Hemschemeier, A., Duner, M., Casero, D., Merchant, S. S., Winkler, M., and Happe, T. (2013) Hypoxic survival requires a 2-on-2 hemoglobin in a process involving nitric oxide. *Proceedings of the National Academy of Sciences U. S. A. 110*, 10854-10859.

Chapter 5

Concluding Remarks

In Chapter 2 of this work I showed that it was possible to engineer a covalent cross-link between a histidine residue and one of the heme vinyls in the truncated hemoglobin, CtrHb. The engineered cross-link is based on the posttranslational modification found in GlbN that forms upon heme reduction. I demonstrated that it was possible to engineer the PTM in a globin that is structurally similar to GlbN, but has a different amino acid sequence (CtrHb). Upon reduction of the cyanomet CtrHb variants ECL data indicated that both variants form the PTM, although to varying degrees. It is possible that in CtrHb the binding of cyanide slightly alters the orientation of the heme providing a more favorable relative geometry between the reactants, thereby facilitating the PTM reaction. Together, these data demonstrated that the main factors involved in the PTM reaction are the presence of a reactive residue close enough to reach a heme vinyl and a ferrous heme.

Chapter 3 provides an initial characterization of the eukaryotic truncated hemoglobin, THB1. Optical data of this protein show that THB1 has a distal endogenous ligand that binds the heme at neutral and alkaline pH, but is also capable of binding common Hb ligands. In other words, the distal ligand is labile, similar to the distal histidine in GlbN. Analysis of optical spectra and pH titration data for the THB1 variants Y29F and K53A strongly suggested that the distal ligand of THB1 is Lys53(E10). This is the first known instance of a hemoglobin with His-Lys heme coordination. In THB1 the distal lysine is necessary for efficient reduction of the

heme. THB1 is able to convert nitric oxide to nitrate (NOD) in vitro. NOD experiments using the K53A variant suggest that while the distal lysine is not involved in the NOD reaction, it does facilitate re-reduction of the heme iron after the reaction is complete. Unlike the distal histidine in GlbN, the distal lysine of THB1 does not protect the protein from hydrogen peroxide damage[1], suggesting that THB1 is not involved in H_2O_2 detoxification.

The x-ray crystallographic study of ferric THB1 described in Chapter 4 confirmed that the distal ligand of THB1 is Lys53(E10). The crystal structure shows that THB1 has the common trHb fold. When overlayed with the structures of other trHbs the position of the backbone of THB1 is actually more similar to that of proteins with exogenously bound ligands (4L2M, 1DLY), most notably in the position of the E helix. The larger distance between the B and E helices in THB1 is likely needed to accommodate the longer lysine side chain in the heme pocket. THB1 adds to the short list of heme proteins with a lysine bound heme. Based on the few known structures of these proteins there does not seem to be any commonalities in the coordinating lysine geometry or surrounding protein environment. The only similarity between these proteins is the fact that the heme is shielded from solvent. Thus, further investigations are needed to determine the factors that allow for lysine-heme ligation.

In summary I have added to our knowledge of the GlbN PTM, showing that it can be engineered in a trHb other than GlbN. This strongly suggests that the main determinant of PTM formation is the relative geometry of the reactive groups and highlights the possibility of using this PTM to increase heme affinity in blood substitutes. Given the relative ease of the reaction the question is raised of why this

His-vinyl cross-link is not seen in Hbs more often. Analysis of protein structures containing *b* heme shows a low incidence of histidines near the heme vinyls[2]. This suggests that given the affinity of the histidine imidazole ring for heme, there has been evolutionary pressure to remove extraneous histidines in the heme pocket to prevent incorrect heme-binding and protein misfolding.

Additionally, I have optically characterized a new eukaryotic trHb, THB1, and shown that this protein can bind exogenous ligands despite having a lysine as a distal endogenous ligand. This novel Hb heme ligation illustrates the plasticity of the hemoglobin fold and the work presented here highlights how the identity of the distal ligand cannot be determined from the protein sequence.

By increasing our knowledge of the factors behind PTM formation and characterizing new axial ligation schemes we come closer to understanding the methods by which proteins control heme reactivity. This will allow us to better harness the reactivity of heme and improve our ability engineer heme-proteins with specific functions[3,4].

5.1 References

(1) Nothnagel, H. J., Preimesberger, M. R., Pond. M. P., Winer, B. Y., Adney, E. M., and Lecomte, J. T. J. (2011) Chemical reactivity of *Synechococcus* sp. PCC 7002 and *Synechocystis* sp. PCC 6803 hemoglobins: covalent heme attachment and bishistidine coordination. *Journal of Biological Inorganic Chemistry, 16*, 539-552.

(2) Preimesberger, M. R., Wenke, B. B., Gilevicius, L., M., Pond, and Lecomte, J. T. J. (2013) Facile heme vinyl posttranslational modification in a hemoglobin. *Biochemistry, 52*, 3478-3488.

(3) Smith, A. T., Doyle, W. A., Dorlet, P., and Ivancich, A. (2009) Spectrocopic evidence for an engineered, catalytically active Trp radical that creates the unique reactivity of lignin peroxidase. *Proceedings of the National Academy of Sciences U. S. A, 106*, 16084-16089.

(4) Alayash, A. I. (2014) Blood substitutes: Why haven't we been more successful? *Trends in Biotechnology, 32*, 177-185.

Appendix

Chapter 2 Supplementary Figures

Supplementary NMR data provided by coauthors and kept for clarity.

Fig. A1: Portions of ^{1}H-^{1}H NOESY/DQF-COSY spectra for heme vinyl assignments in WT cyanomet CtrHb (major isomer) and vinyl orientation diagram

Fig. A2: Portions of ^{1}H-^{1}H NOESY/DQF-COSY spectra for heme vinyl assignments in WT cyanomet CtrHb (minor isomer) and vinyl orientation diagram

Fig. A3: Aromatic region of a ^{1}H-^{1}H TOCSY spectrum collected on WT cyanomet CtrHb

Fig. A4: Portions of ^{1}H-^{1}H NOESY/DQF-COSY spectra for heme vinyl assignments in T111H cyanomet CtrHb (major isomer) and vinyl orientation diagram

Fig. A5: Portions of ^{1}H-^{1}H NOESY/DQF-COSY spectra for heme vinyl assignments in T111H cyanomet CtrHb (minor isomer) and vinyl orientation diagram

Fig. A6: Aromatic region of a ^{1}H-^{1}H TOCSY spectrum collected on T111H cyanomet CtrHb

Fig. A7: Portions of ^{1}H-^{1}H NOESY/DQF-COSY spectra for heme vinyl assignments in L75H cyanomet CtrHb (major isomer) and vinyl orientation diagram

Fig. A8: Portions of ^{1}H-^{1}H NOESY/DQF-COSY spectra for heme vinyl assignments in L75H cyanomet CtrHb (minor isomer) and vinyl orientation diagram

Fig. A9: Structural summary of heme orientational isomers in wild-type, T111H, and L75H cyanomet CtrHbs

Fig. A10: ^{1}H-^{15}N long-range HMQC spectral overlay of wild-type, T111H, and L75H cyanomet CtrHbs

Fig. A11: ^{1}H NMR spectra following DT reduction of cyanide bound wild-type CtrHb

Fig. A12: ^{1}H NMR spectra following DT reduction of cyanide bound T111H CtrHb

Fig. A13: ^{1}H NMR spectra following DT reduction of cyanide bound L75H CtrHb

Fig. A14: Portions of ^{1}H-^{1}H NOESY/DQF-COSY spectra for heme assignments in T111H cyanomet CtrHb-A^{4} (covalent product)

Fig. A15: Portions of ^{1}H-^{1}H NOESY/DQF-COSY spectra for heme assignments in L75H cyanomet CtrHb-B (covalent product)

Fig. A16: Spectral evidence for an additional heme methyl group in L75H-CtrHb-B

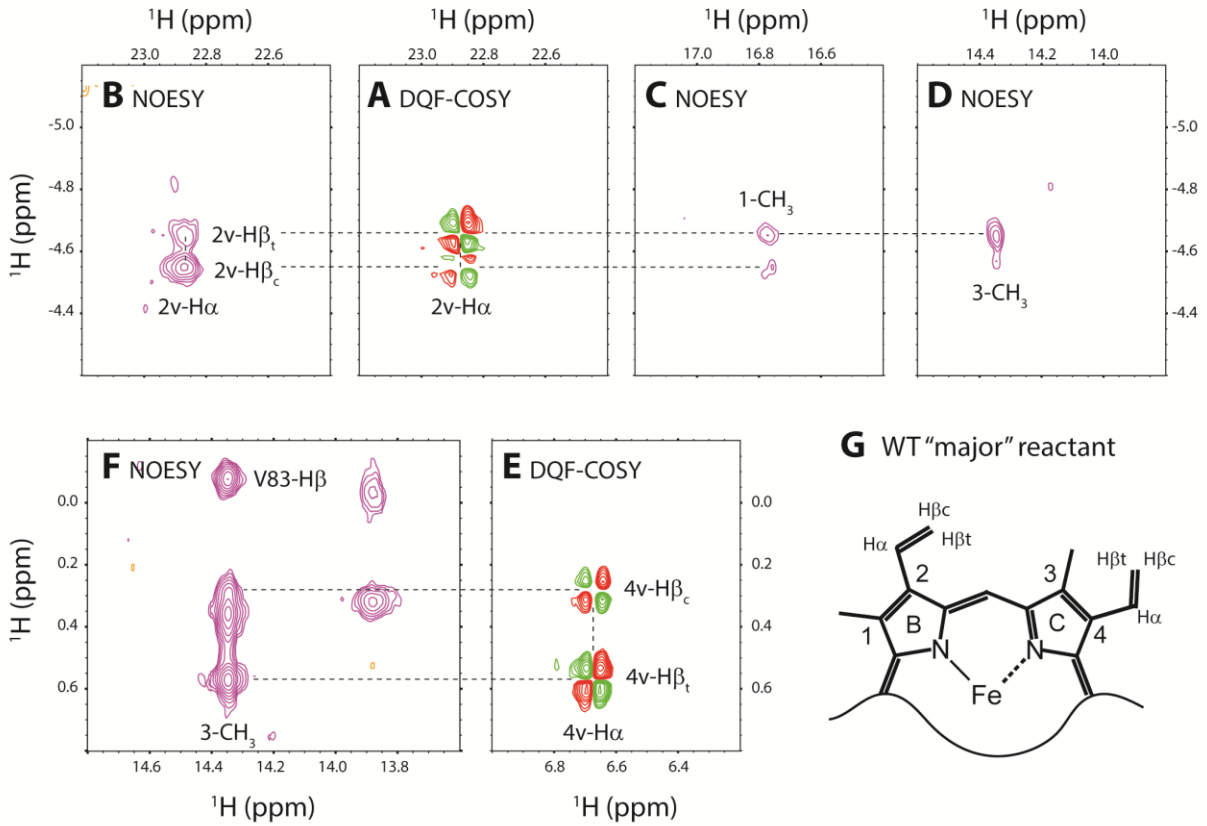

Fig. A1 Portions of ^{1}H-^{1}H NOESY/DQF-COSY spectra for heme vinyl assignments in WT cyanomet CtrHb (major isomer) and vinyl orientation diagram. (A) *J*-coupled protons corresponding to the 2-vinyl group. **(B)** Intra-vinyl NOEs of the 2-vinyl group support 2-β_{cis} and 2-β_{trans} assignments. **(C)** The 2-vinyl β protons exhibit weak NOEs to the heme 1-CH_3. **(D)** The 2-vinyl β_{trans} proton is within dipolar contact with the heme 3-CH_3. Together, these connectivities support a *cis*-like orientation for the 2-vinyl group. **(E)** *J*-coupled protons corresponding to the 4-vinyl group. **(F)** The 4-vinyl β protons exhibit strong NOEs to the heme 3-CH_3 indicating it adopts a *trans*-like orientation. **(G)** Cartoon model depicting the orientations of vinyl groups within cyanomet WT CtrHb.

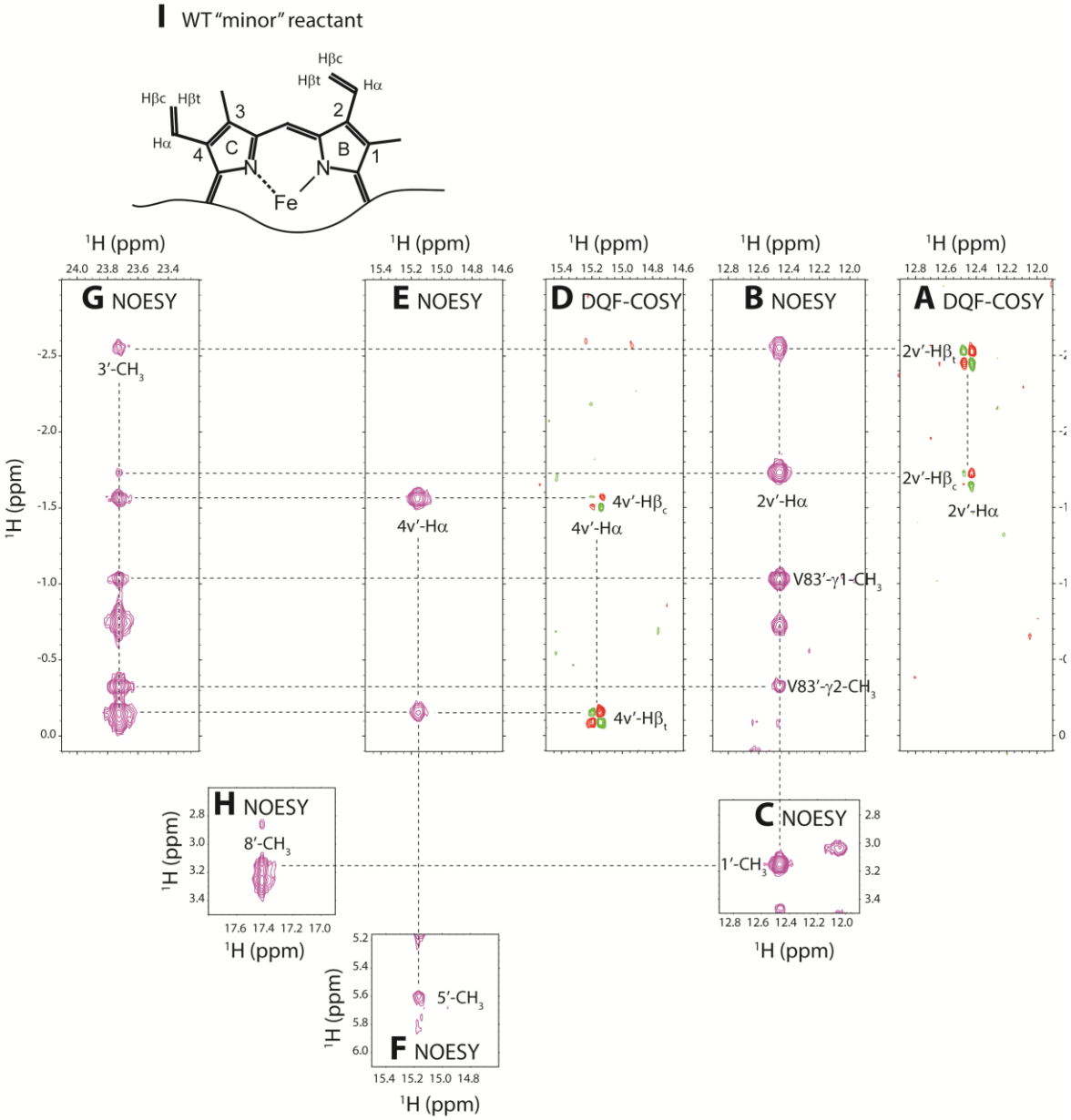

Fig. A2 Portions of ^{1}H-^{1}H NOESY/DQF-COSY spectra for heme vinyl assignments in cyanomet WT CtrHb (minor isomer) and vinyl orientation diagram. **(A)** *J*-coupled protons assigned to the 2-vinyl group. **(B)** The 2-vinyl Hα has strong NOEs to the neighboring Hβs. **(C)** The 2-vinyl Hα also shows a strong contact to the heme 1-CH_3. **(D)** *J*-correlated signals assigned to the 4-vinyl group. **(E)** The 4-vinyl Hβs exhibit strong intra-vinyl NOE to the Hα. **(F)** The 4-vinyl Hα is in dipolar contact with the heme 5-CH_3. **(G)** The 2- and 4-vinyl Hβs are proximal to the heme 3-CH_3. **(H)** The heme 8-CH_3 shows an NOE to the 1-CH_3. The heme connectivity pattern is thus: 8-CH_3 ↔ 1-CH_3 ↔ 2-vinyl ↔ 3-CH_3 ↔ 4-vinyl ↔ 5-CH_3. **(I)** Cartoon model depicting vinyl orientations in cyanomet wild-type CtrHb.

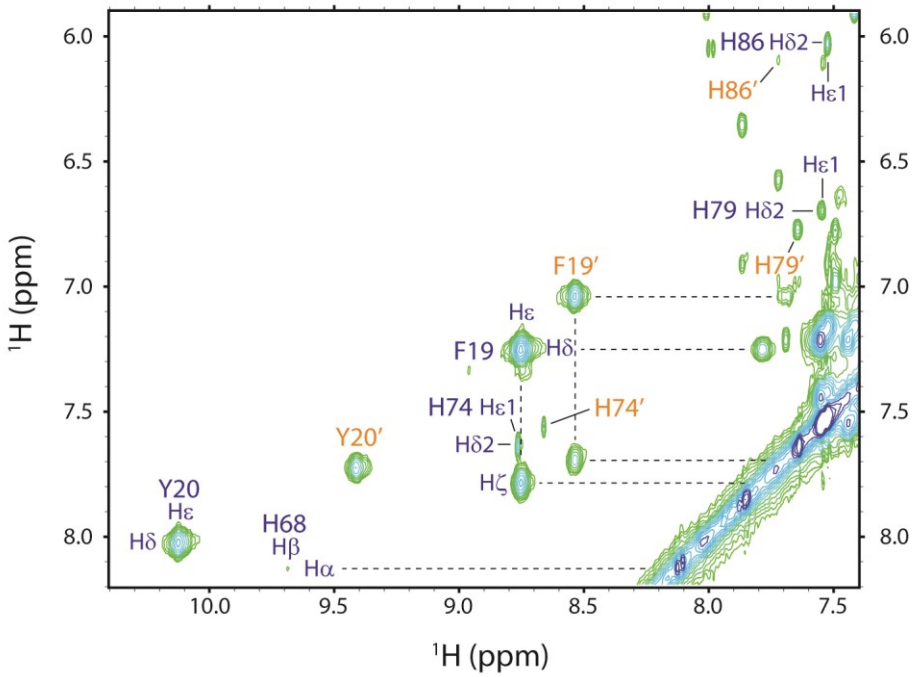

Fig. A3 Downfield aromatic region of a ^{1}H-^{1}H TOCSY spectrum collected on cyanomet WT CtrHb. Assignments for some key heme pocket residues [H68 (His F8), Y20 (Tyr B10), and F19 (Phe B9)] and additional histidines are included. Peaks corresponding to the major heme orientational isomer are labeled in blue; peaks assigned to the minor heme orientational isomer are labeled in orange and denoted with prime.

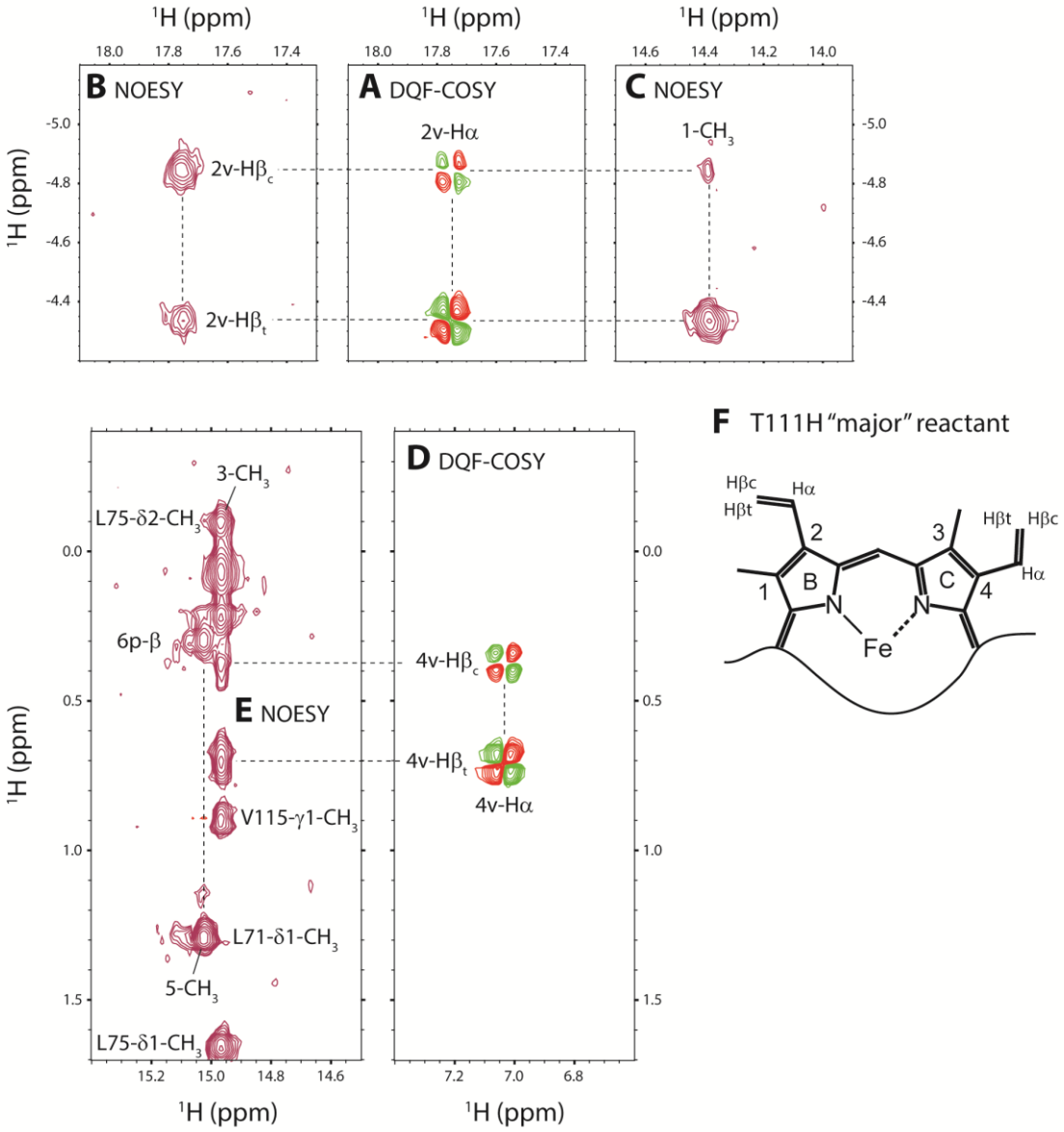

Fig. A4 Portions of ^{1}H-^{1}H NOESY/DQF-COSY spectra for heme vinyl assignments in cyanomet T111H CtrHb (major isomer) and vinyl orientation diagram. **(A)** *J*-coupled AMX spin system assigned to the heme 2-vinyl group. **(B)** Intra-vinyl NOEs confirm the 2-β_{cis} and 2-β_{trans} proton assignments. **(C)** Strong NOE contacts between the 2-Hβs and the heme 1-CH_3 group orient the 2-vinyl in the *trans* conformation. These data support distinct 2-vinyl orientations between WT and T111H CtrHbs. **(D)** *J*-coupled signals corresponding to the heme 4-vinyl substituent. **(E)** NOEs between the 4-vinyl Hβs and the heme 3-CH_3 indicate that the former adopts a *trans* orientation, as observed for WT CtrHb. **(F)** Heme cartoon depicting the vinyl orientations consistent with NOE data.

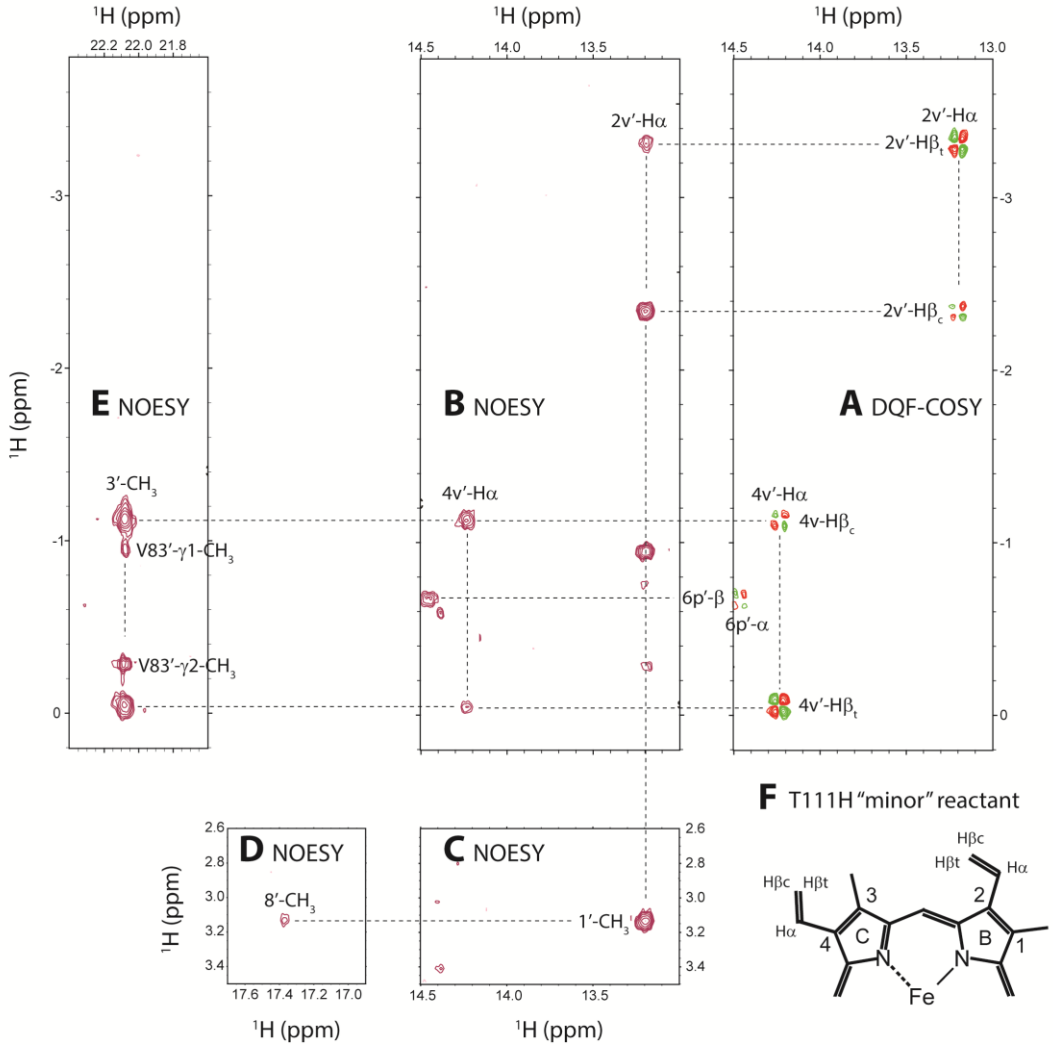

Fig. A5 Portions of ^{1}H-^{1}H NOESY/DQF-COSY spectra for heme vinyl assignments in T111H cyanomet CtrHb (minor isomer) and vinyl orientation diagram. **(A)** *J*-correlated signals corresponding to the 2- and 4-vinyl groups. **(B)** Corresponding region displaying the intra-vinyl NOEs, confirming the assignment of β_{cis} and β_{trans} protons. **(C)** The 2-vinyl Hα displays a strong dipolar contact to the heme 1-CH_3 group supporting a 2-vinyl *cis* orientation. **(D)** A weak NOE was detected between the heme 1- and 8-CH_3. **(E)** The 4-vinyl β protons both show strong contacts to the heme 3-CH_3, indicative of the 4-vinyl group adopting a *trans* orientation. **(F)** Cartoon depiction of the heme vinyl group orientations.

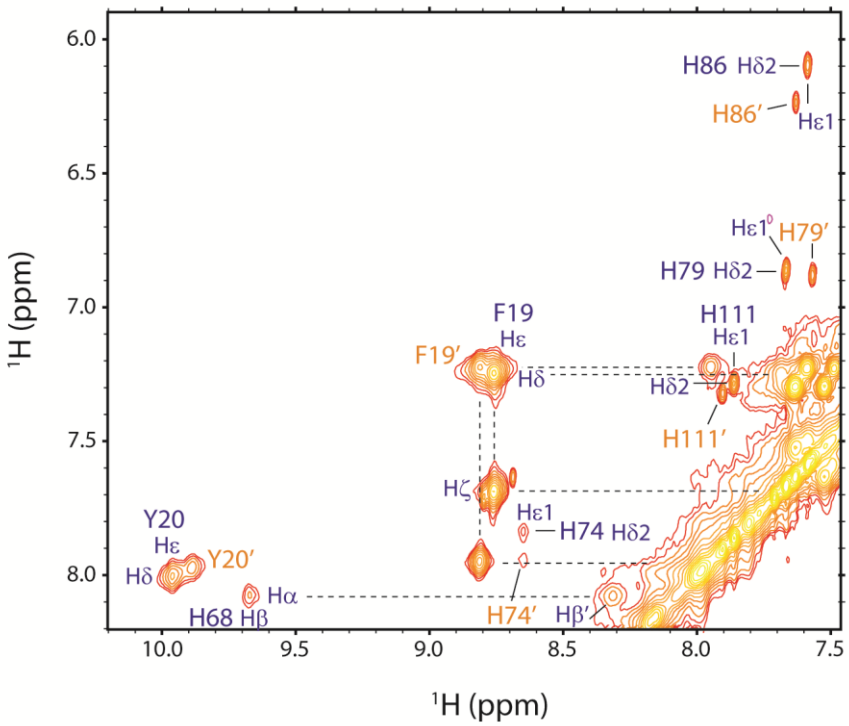

Fig. A6 Downfield aromatic region of a ^{1}H-^{1}H TOCSY spectrum collected on cyanomet T111H CtrHb. Detectable histidine signals, along with distal heme pocket residues [Y20 (Tyr B10), F19 (Phe B9)] are labeled (major orientational isomer = blue, minor isomer = orange). Note the presence of the His111 Hε1 ↔ Hδ2 correlations. Interestingly, there is a closer chemical shift similarity between major and minor heme isomers in T111H CrHb compared to the WT CtrHb.

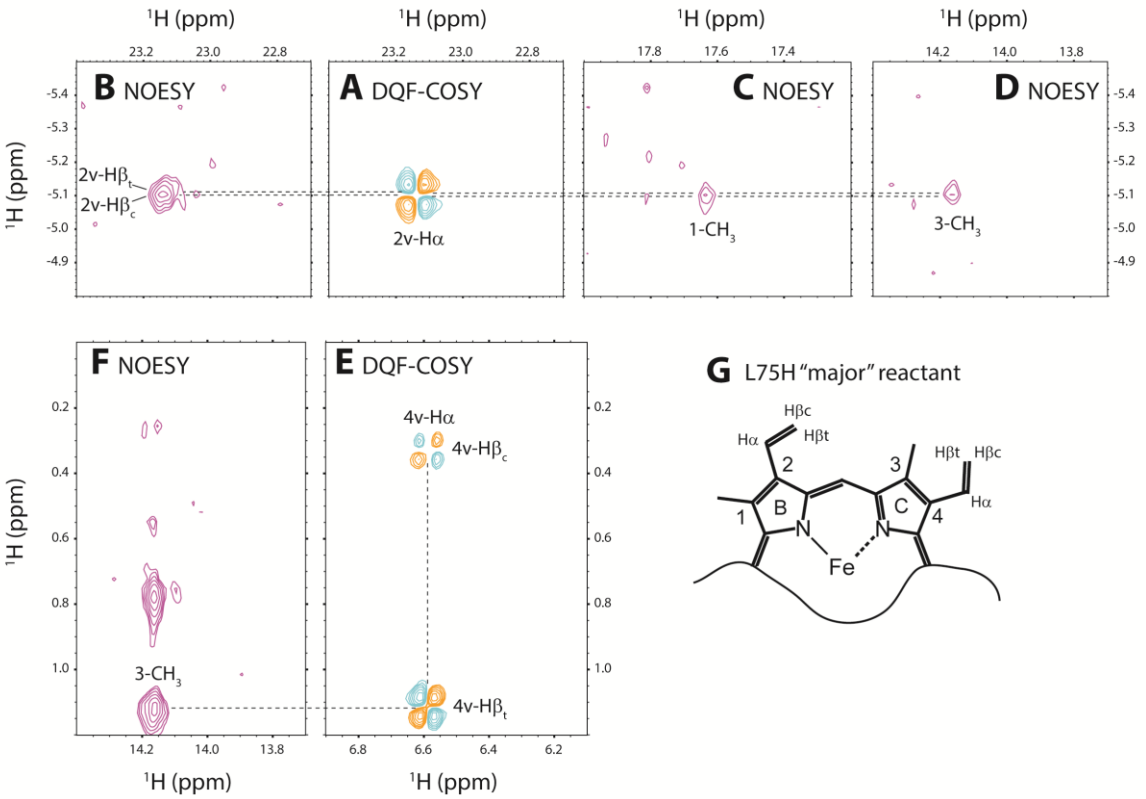

Fig. A7 Portions of ^{1}H-^{1}H NOESY/DQF-COSY spectra for heme vinyl assignments in cyanomet L75H CtrHb (major isomer) and vinyl orientation diagram. (A) *J*-correlations exhibited between the 2-vinyl Hβs (overlapped) and the 2-vinyl Hα. **(B)** Corresponding region showing NOEs between the 2-vinyl Hβs and Hα. **(C)** The 2-vinyl Hβs are in weak dipolar contact with the heme 1-CH_3. **(D)** The 2-vinyl Hβs also show weak NOEs to the heme 3-CH_3 group, supporting a *cis* configuration. **(E)** DQF-COSY cross-peaks assigned to the heme 4-vinyl β_{cis}, β_{trans} and α protons. **(F)** The 4-vinyl Hβ_{trans} exhibits a strong NOE contact to the heme 3-CH_3 group, indicative of a 4-vinyl *trans* geometry. **(G)** Cartoon model showing the heme 2- and 4-vinyl orientations consistent with NMR data.

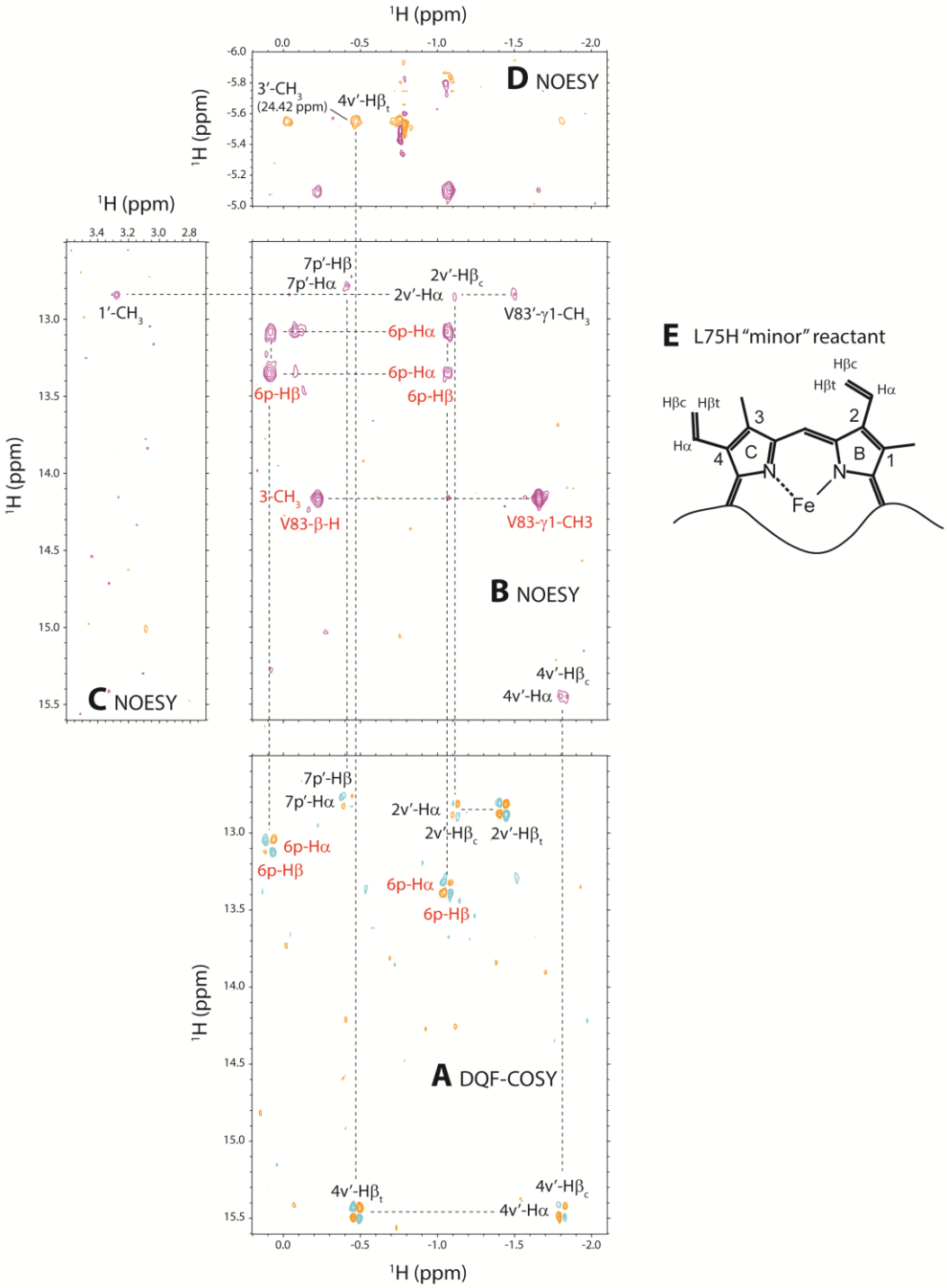

Fig. A8 Portions of ^{1}H-^{1}H NOESY/DQF-COSY spectra for heme vinyl assignments in L75H cyanomet CtrHb (minor isomer) and vinyl orientation diagram. **(A)** *J*-correlations between the α and β protons of the heme 2- and 4-vinyl groups (black labels). Signals annotated with red labels derive from the L75H cyanomet CtrHb major heme isomer. **(B)** Corresponding region of the NOESY spectrum, highlighting intra-heme vinyl NOEs (labels as in A). **(C)** The 2-vinyl H α exhibits a dipolar contact to the heme 1-methyl. Because the Hβs do not show such effects, the data support a 2-vinyl *cis* orientation. **(D)** The 4-vinyl β *trans* proton shows a strong NOE to the heme 3-CH_3 (folded). This strong contact defines a 4-vinyl *trans* orientation. **(E)** Heme structural model depicting vinyl orientations consistent with NOE data.

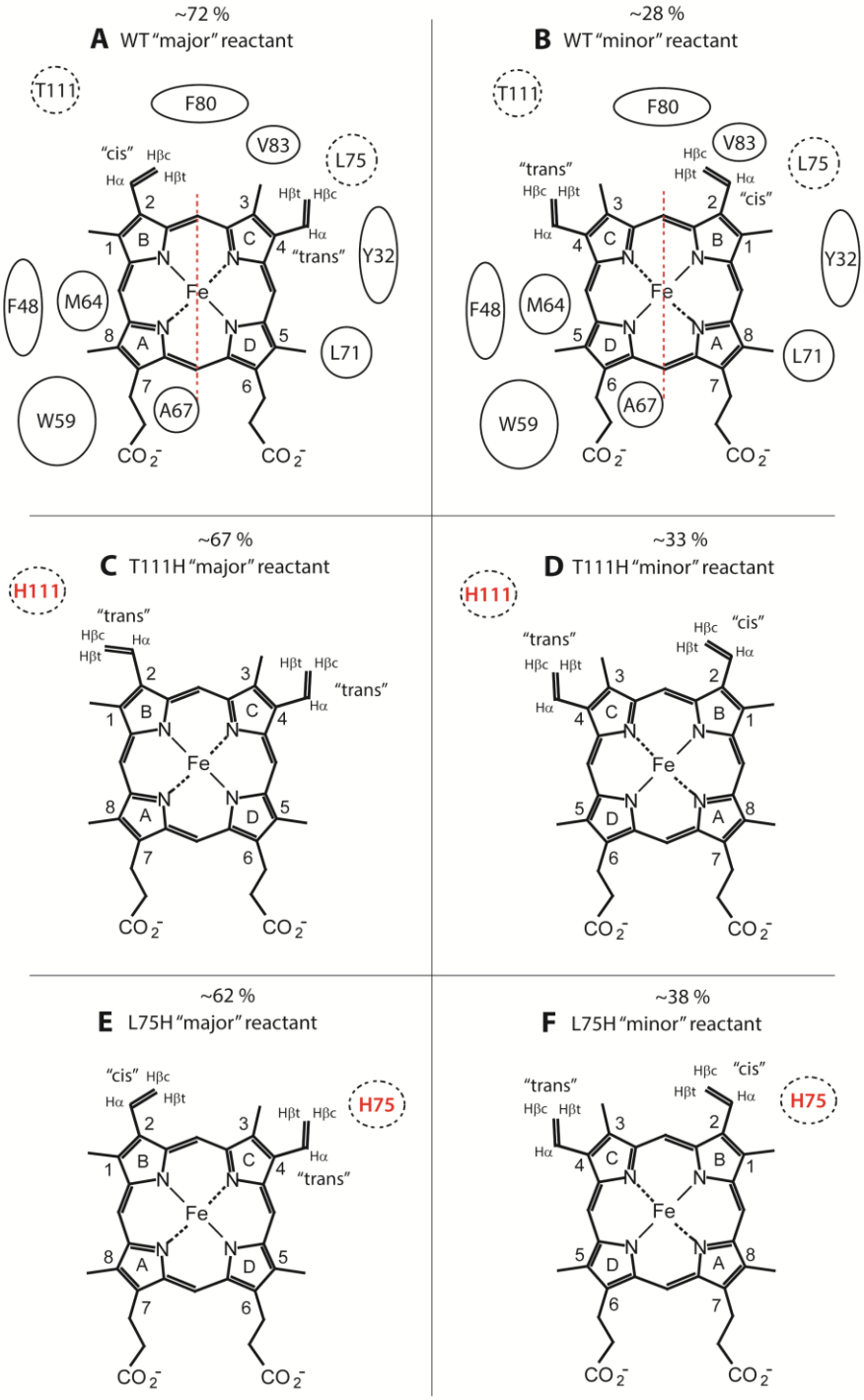

Fig. A9 Structural summary of heme orientational isomers in wild-type (A, B), T111H (C, D), and L75H (E, F) cyanomet CtrHbs. The relative populations of each isomer, as estimated from integration of resolved ^{1}H 1D peak, are given in percent. These populations did not change appreciably over the course of data collection indicating extremely slow exchange. For the WT CtrHb major and minor isomers (top row), several residues in proximity to the heme are depicted as ellipses. Within the left column (major heme isomers), the T111H variant displays a distinct heme 2-vinyl orientation with respect to WT and L75H CtrHbs. The minor heme isomers (right column) all displayed similar intra-heme NOEs, which supports a common vinyl configuration. In each depiction, the proximal histidine is above the page toward the reader.

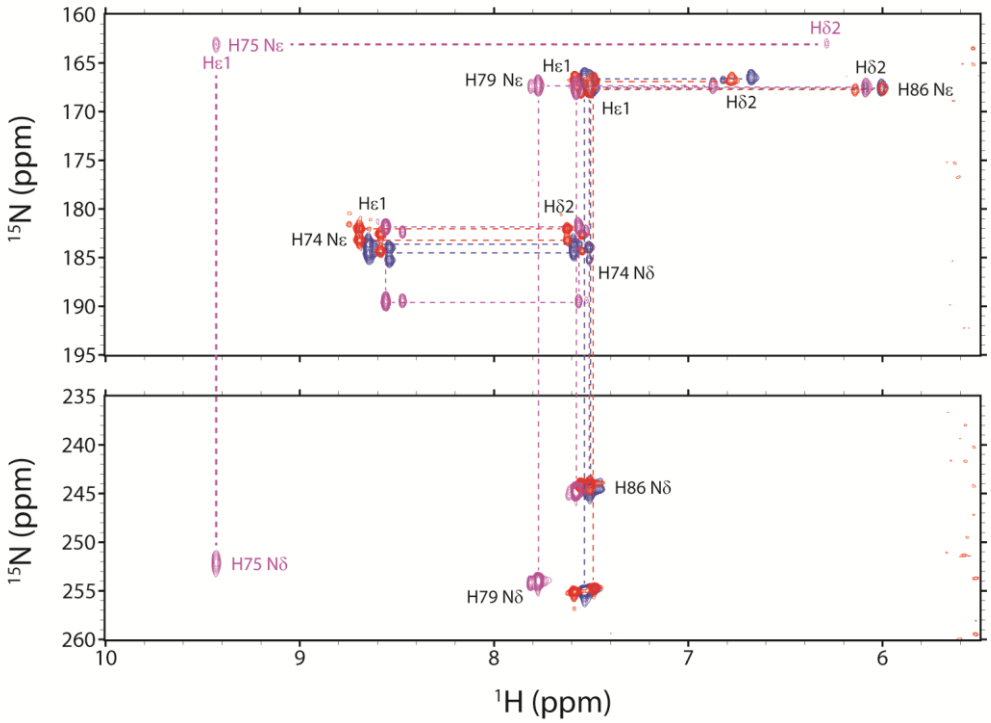

Fig. A10 ^{1}H-^{15}N long-range HMQC ($1/2J_{NH}$ ~ 22 ms) spectral overlay of WT, T111H, and L75H cyanomet CtrHbs. All non-proximal histidine residues (H74, H79, and H86) are assignable in cyanomet WT CtrHb (blue peaks, black labels). For the T111H variant (red peaks), resonances corresponding to H74, H79, and H86 overlay well with the wild-type, but additional signals corresponding to H111 are not observed, likely because of exchange broadening. On the other hand, the L75H variant (magenta peaks) exhibits a new, highly shifted set of resonances attributable to H75 (magenta labels), in addition to minimally perturbed H74, H79, and H86 signals. The unusual chemical shifts observed for H75 protons are consistent with its close proximity to the paramagnetic (S = 1/2) heme.

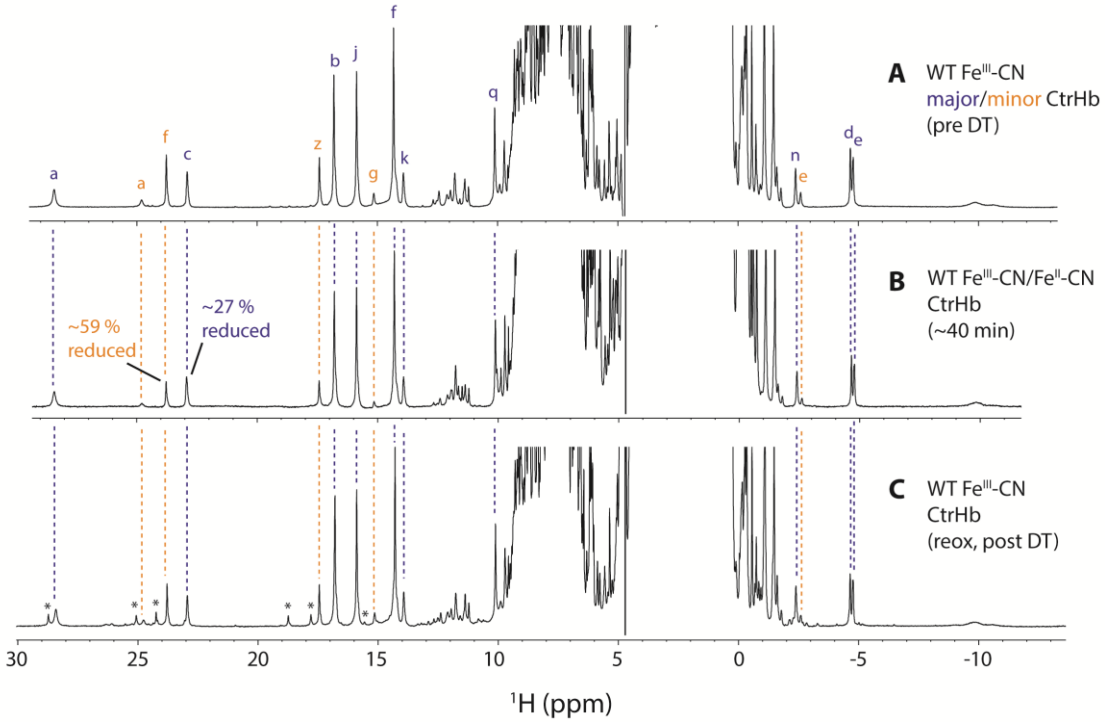

Fig. A11 ^{1}H NMR spectra monitoring DT reduction of cyanide bound WT CtrHb (^{15}N amide decoupled). (A) Cyanomet (Fe^{III}-CN) ^{15}N-labeled protein spectrum prior to DT reduction. Assignments for select heme and protein ^{1}H signals are included. Peaks are labeled as in Fig. 2 of the main text: a, Tyr20 OηH; b, heme 1-CH_3; c, heme 2-vinyl Hα; d, e, heme 2-vinyl $H\beta_{cis}$, $H\beta_{trans}$; f, heme 3-CH_3; g, heme 4-vinyl Hα; j, heme 5-CH_3; k, heme 6-propionate Hα, Hα'; n, heme 7-propionate Hβ; q, Tyr20 CεHs; z, heme 8-CH_3. The major heme orientational isomer (blue labels) occurs at a ~2.6:1 ratio over the minor isomer (orange labels). **(B)** Mixture of cyanomet (Fe^{III}-CN, paramagnetic) and ferrous cyanide (Fe^{II}-CN, diamagnetic) proteins ~40 min following reduction with 6 mM DT. The dashed lines connect remaining cyanomet signals. Assuming no damage occurred to the protein, the decrease in cyanomet peak intensities indicates that approximately 27% of the major isomer was reduced. Interestingly, the minor isomer displays increased susceptibility to reduction (~59% reduced), suggesting that the major and minor heme orientational isomers differ in their ability to stabilize exogenous cyanide in the ferrous state. **(C)** Following ~6 h DT reduction, the sample was completely reoxidized. The predominant forms detected were identical to those observed prior to reduction indicating minimal reaction (dashed lines). However, an additional minor species is detected (asterisks) in an indication of heme side reaction. A–C. Sample conditions: pH ~7.1, 10 % D_2O, 298 K.

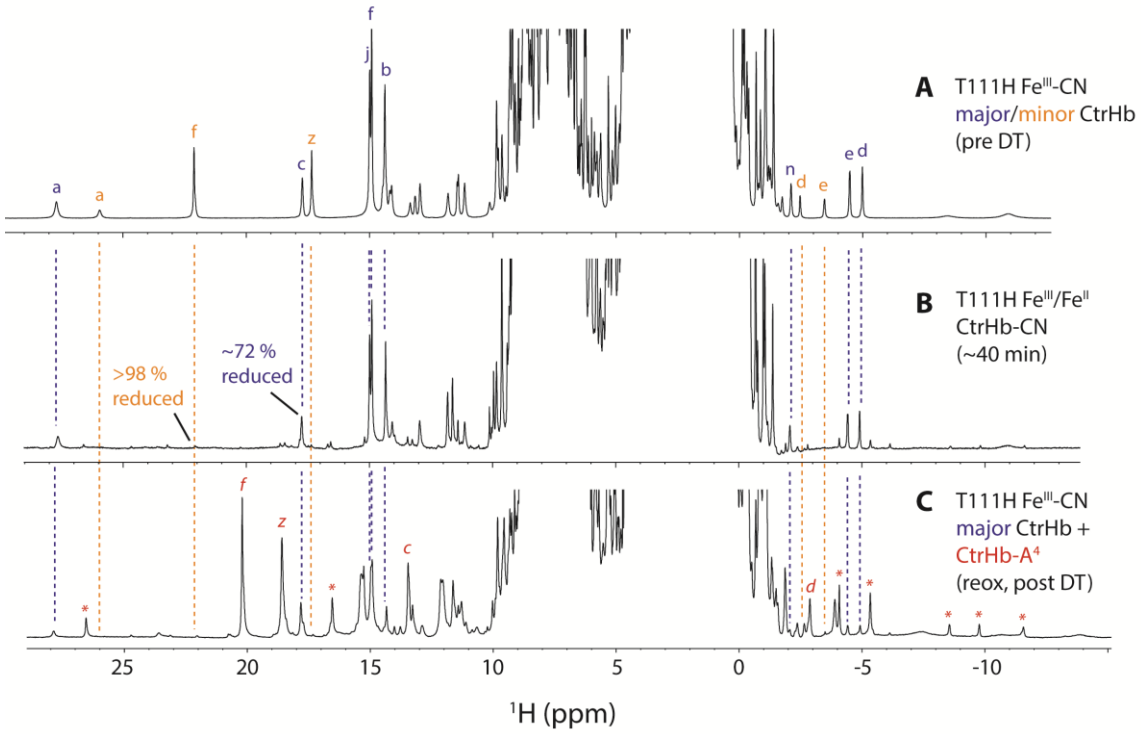

Fig. A12 ^{1}H NMR spectra following DT reduction of cyanide bound T111H CtrHb. (A) Cyanomet (Fe^{III}-CN) protein spectrum before DT reduction. Assignments for select heme and protein ^{1}H signals are included. Peaks are labeled as in Fig. 2 of the main text: a, Tyr20 OηH; b, heme 1-CH_3; c, heme 2-vinyl Hα; d, e, heme 2-vinyl $H\beta_{cis}$, $H\beta_{trans}$; f, heme 3-CH_3; j, heme 5-CH_3; n, heme 7-propionate Hβ; z, heme 8-CH_3. The major heme orientational isomer (blue labels) occurs at a ~2:1 ratio over the minor isomer (orange labels). **(B)** Mixture of cyanomet (Fe^{III}-CN, paramagnetic) and ferrous cyanide (Fe^{II}-CN, diamagnetic) T111H proteins ~40 min following reduction with 6 mM DT. The dashed lines connect remaining cyanomet signals. Under the assumption of no protein damage, the decrease in cyanomet peak intensities indicates that approximately 72% of the major isomer was reduced. In contrast, virtually none of the cyanomet minor isomer remains. Therefore, as in WT CtrHb, the T111H minor heme orientational isomer displays an enhanced susceptibility to DT reduction when compared to the major isomer. However, both isomers of T111H CtrHb are reduced more readily than WT CtrHb. **(C)** Following ~7 h DT reduction, the sample was completely reoxidized. The predominant form (~60%, red labels) corresponds to the major reaction product (cyanomet T111H CtrHb-A^4). Additionally, the unreacted major isomer is observed (blue dashed lines). At least one other form (red asterisks) is noted. This form was not studied further, but we note that the shifts do not suggest formation of T111H CtrHb-A^2. Sample conditions: pH ~7.1, 10 % D_2O, 298 K.

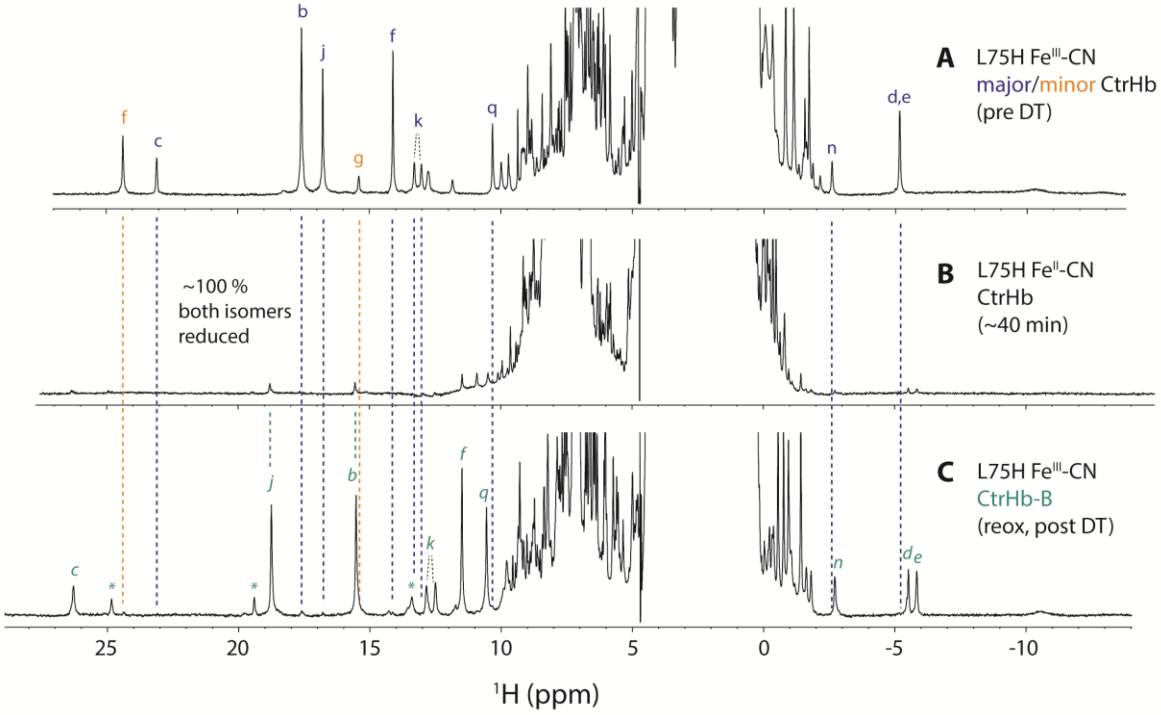

Fig. A13 ^{1}H NMR spectra following DT reduction of cyanide bound L75H CtrHb. (A) Cyanomet (Fe^{III}-CN) protein spectrum prior to DT reduction (100% D_2O, pH* = 7.4). Assignments for select heme and protein ^{1}H signals are included. Peaks are labeled as in Fig. 2 of the main text: a, Tyr20 OηH; b, heme 1-CH_3; c, heme 2-vinyl Hα; d, e, heme 2-vinyl $H\beta_{cis}$, $H\beta_{trans}$; f, heme 3-CH_3; g, heme 4-vinyl Hα; j, heme 5-CH_3; k, heme 6-propionate Hα, Hα'; n, heme 7-propionate Hβ; q, Tyr20 CεHs; z, heme 8-CH_3. The major heme orientational isomer (blue labels) occurs at a ~3:2 ratio over the minor isomer (orange labels). **(B)** The sample was exchanged into H_2O (pH 7.3) and reduced with ~8 mM dithionite. After ~40 min, the sample contained no detectable resonances attributable to either the major or minor cyanomet reactants. Thus, unlike both T111H and WT cyanomet CtrHbs, the L75H variant is completely reduced to the ferrous cyanide bound form. **(C)** Following ~2 h DT reduction, the sample was completely reoxidized and exchanged back into D_2O (pH* 7.2). Both major and minor isomer reactant resonances had essentially vanished (orange and blue dashed lines) but a new set of resonances, corresponding to > 90% of the sample was observed and attributed to the primary product: L75H cyanomet CtrHb-B (cyan labels). A minor product (< 10%, cyan asterisks) was also detected but not examined in this work. Preliminary evidence (lr-HMQC) suggests the minor product in L75H is H75 Nε2–2-Cα linkage. All data were collected at 298 K.

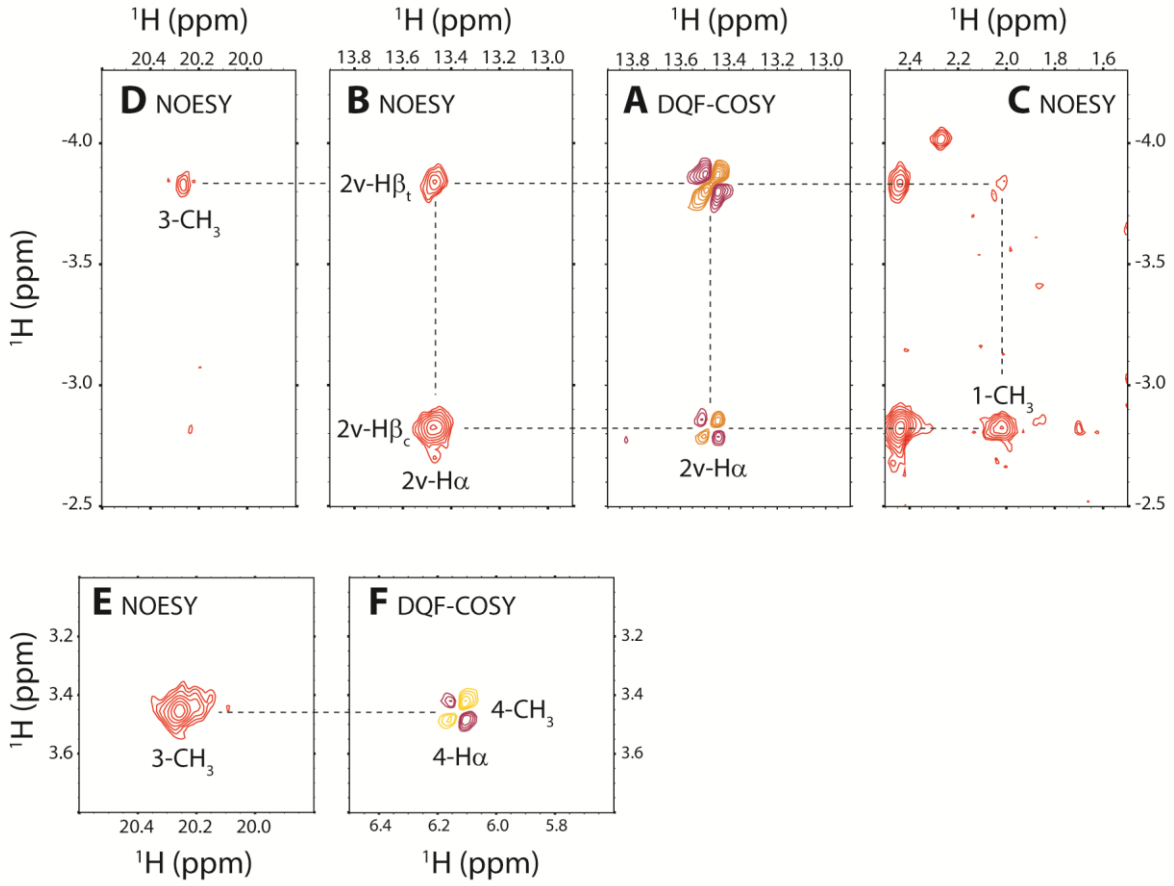

Fig. A14 Portions of ^{1}H-^{1}H NOESY/DQF-COSY spectra for heme assignments in cyanomet T111H CtrHb-A^4 (covalent adduct). **(A)** *J*-correlated resonances assigned to the 2-vinyl Hα and Hβs. **(B)** Corresponding region showing NOEs in support of the 2-vinyl Hβ$_{cis}$ and Hβ$_{trans}$ assignments. **(C)** The 2-vinyl Hβ$_{cis}$ is in dipolar contact with the heme 1-CH_3. **(D)** The 2-vinyl Hβ$_{trans}$ displays an NOE to the heme 3-CH_3. Together, these data support a *cis* or "twist" configuration for the 2-vinyl group. No additional vinyl group was detected. **(E)** The 3-CH_3, which typically displays NOEs to the heme 4-vinyl, instead showed a strong contact with a methyl group (~3.4 ppm), in agreement with a modification at the heme 4-substituent. **(F)** The tentative 4-heme methyl group displayed a *J*-correlation to a signal at (~6.1 ppm), suggesting the modification of the vinyl CαH=CβH_2 group into a CαH-CβH_3 substituent.

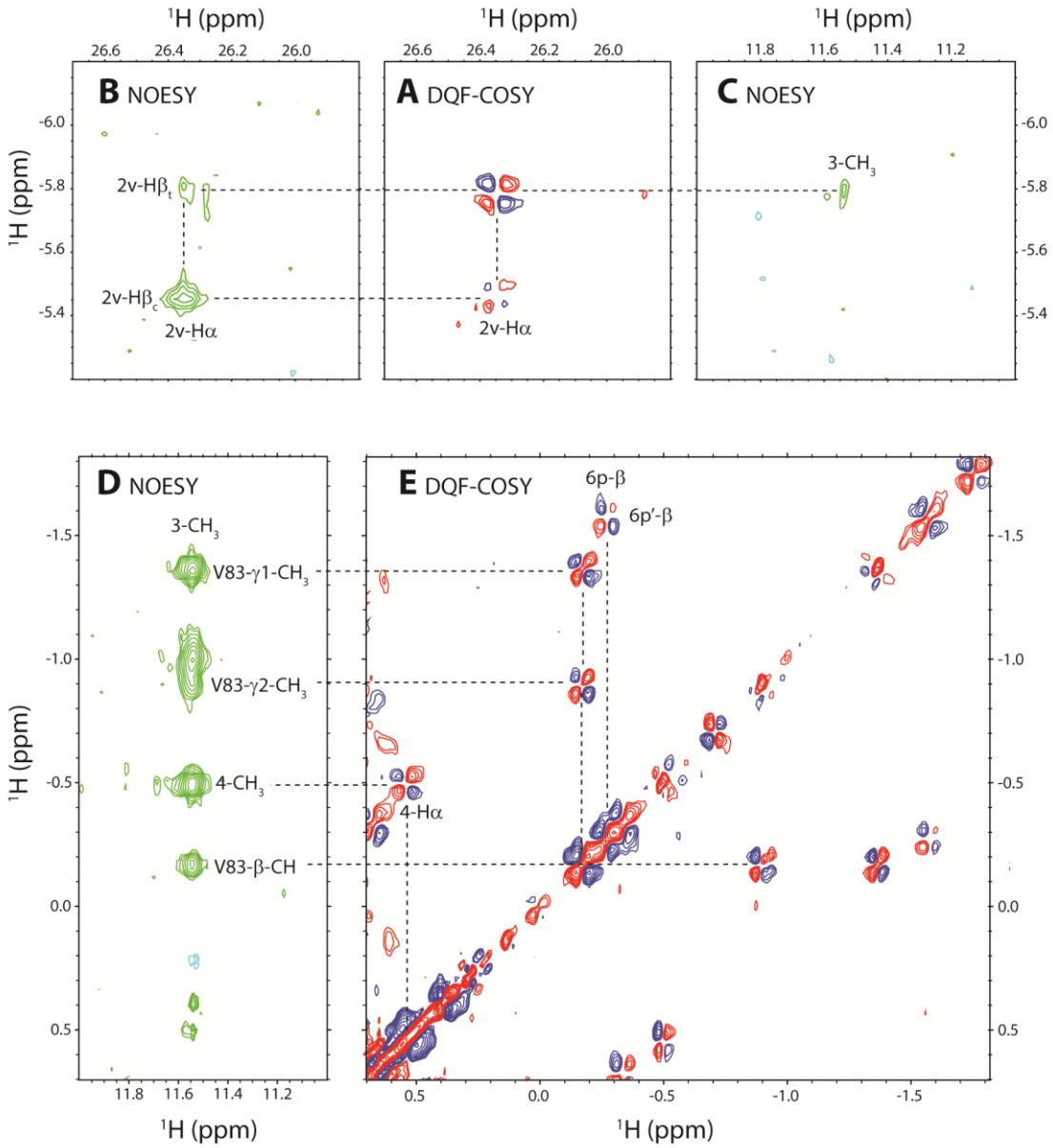

Fig. A15 Portions of ^{1}H-^{1}H NOESY/DQF-COSY spectra for heme assignments in L75H cyanomet CtrHb-B (covalent product). **(A)** *J*-correlations exhibited between 2-vinyl protons. **(B)** Corresponding region showing NOEs in support of 2-vinyl Hβ_{cis} and Hβ_{trans} assignments. **(C)** The 2-vinyl Hβ_{trans} displays a weak NOE to the heme 3-CH_3. The intra-heme connectivities are consistent with the 2-vinyl group adopting a *cis* or "twist" orientation. **(D)** The upfield methyl protons (−0.5 ppm) *J*-correlated to His75 in the ^{15}N histidine-selective lr-HMQC spectrum (Fig. 5, main text) displays a strong NOE to the heme 3-CH_3. This contact, along with the absence of a second vinyl system in DQF-COSY data, indicates that the 4-substituent has undergone modification. **(E)** The heme 4-CβH_3 displays a single *J*-correlation assigned to the heme 4-CαH.

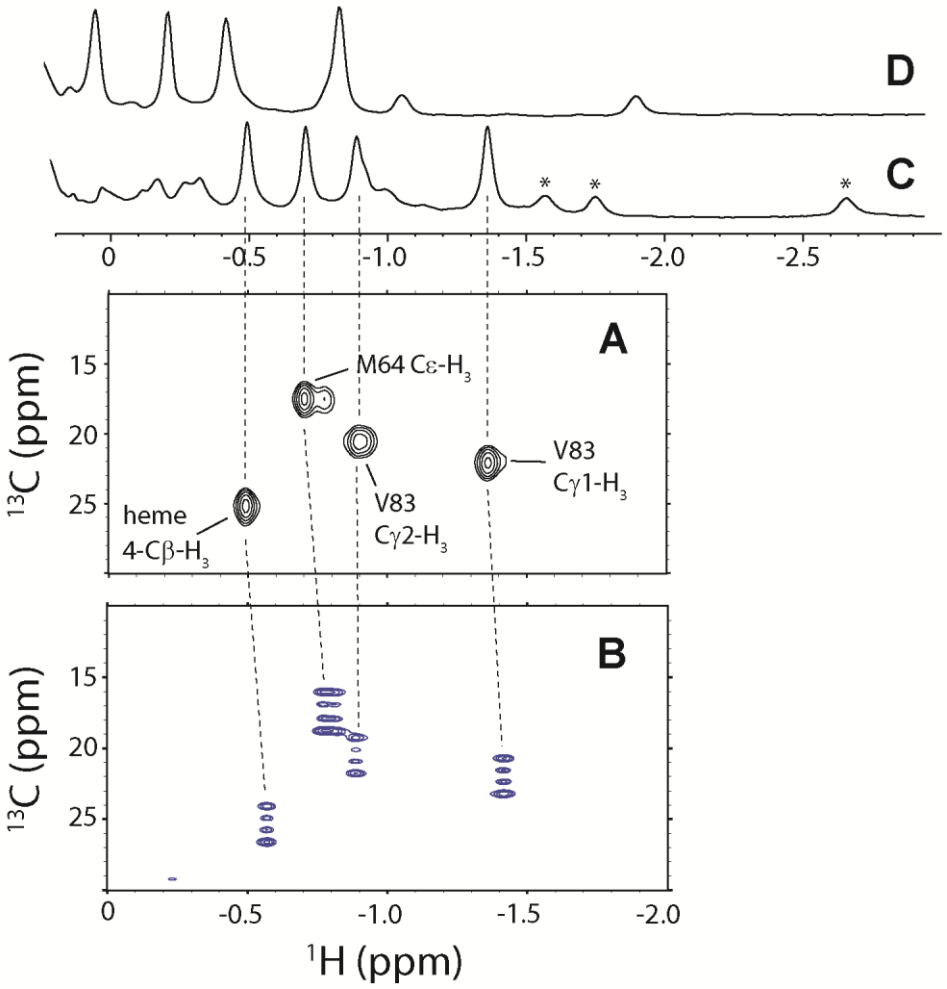

Fig. A16 Identification of the resolved peak at a ^{1}H shift of −0.49 ppm as a methyl group. (A) The ^{1}H-^{13}C HMQC data shown in Fig. 6. **(B)** The corresponding coupled ^{1}H-^{13}C HSQC data clearly showing a 3:1:1:3 quartet at −0.49 ppm. **(C)** The ^{1}H 1D data at 298 K. **(D)** The ^{1}H 1D data at 313 K. The region shown contains the methyl groups of Val83 and Met64. All four methyl groups are highly sensitive to temperature (Curie effect) as illustrated in (D). (A) and (B) were collected on different samples and different spectrometers. Slight changes in temperature and pH explain the small shifts in the proton dimension. For comparison, the peaks marked with asterisks correspond to heme propionate signals with single proton intensity.

Chapter 3 Supplementary Tables and Figures

Supplementary NMR and Western blot data provided by coauthors

Table A1 qPCR probes

qPCR probes (ZEN™ Double-Quenched, IDT) used for the detection of THB1 cDNA and the reference CBLP cDNA. The 5' end of each probe is labeled with 6-FAM™ and the 3' end with Iowa Black®FQ.

		Sequence (5'-3')
THB1		
	Forward	CGCCTTTATGACTTACGTGTTC
	Probe	/56-FAM/TGATCCGCG/ZEN/AGCAGGGCAT/3IABkFQ/
	Reverse	CTCTTGCAGGGTGGAGTC
CBLP		
	Forward	CGAGTGCAAGTACACCATTG
	Probe	/56-FAM/CTGGGACAA/ZEN/GATGGTCAAGGTCTGG/3IABkFQ/
	Reverse	TCAGCTTGCAGTTGGTCAG
BBS4		
	Forward	GTGATAAACGAAACTACCAACTGC
	Probe	/56-FAM/CGAGACAGG/ZEN/AGTTTGAGGAGTGCTTG/3IABkFQ/
	Reverse	ATGAGCGCCTTGATATAGATGG

Table A2 ^{1}H chemical shifts of the axial lysine (K53) in ferrous Y29F rTHB1[a]

Assignment	δ (ppm)
Hζ	−7.85
Hε,ε'	−3.32, −1.72
Hδ,δ'	−2.99, −1.43
Hγ,γ'	−2.36. −1.60
Hβ,β'	0.99, 0.84
Hα	3.40

[a] Determined in 90% $^{2}H_2O$/10% $^{1}H_2O$ at pH* 9.2, 298 K.

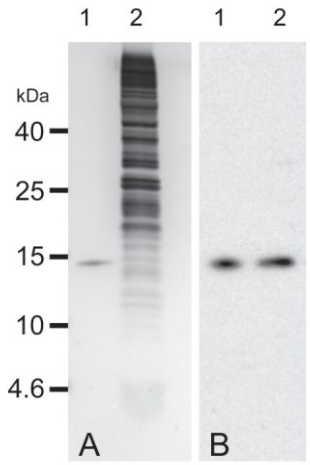

Fig. A17 Comparison of rTHB1 and in-vivo THB1. (A) 1 μg of rTHB1 (lane 1) and 1×10^5 cells of CC-1690 grown in Sager-Granick M medium (lane 2) analyzed on SDS polyacrylamide gel electrophoresis (PAGE) and stained with silver. **(B)** 0.5 ng of rTHB1 (lane 1) and 1×10^5 cells of CC-1690 grown in Sager-Granick M medium separated on SDS-PAGE and transferred to nitrocellulose followed by immunodetection using purified polyclonal rabbit antibodies raised against a portion of the THB1 primary structure.

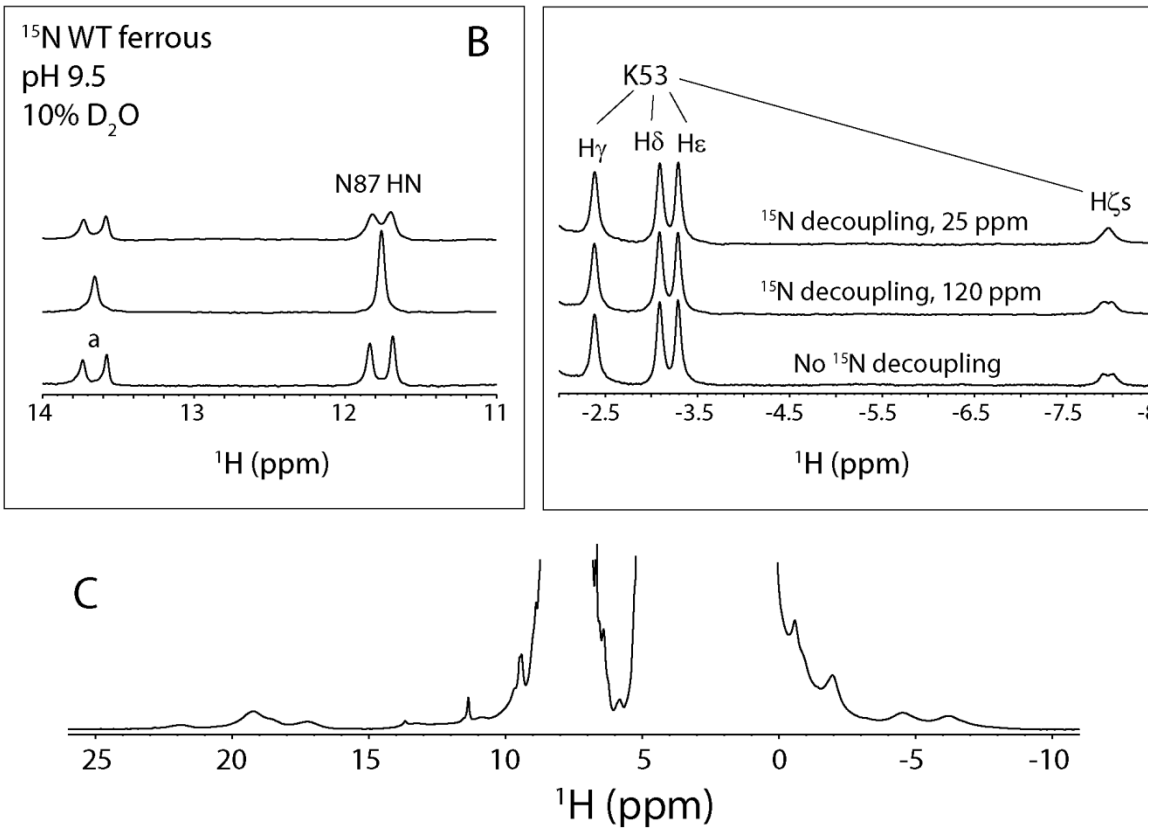

Fig. A18 Assignment of K53 NζH$_2$. **(A)** The highly upfield −8 ppm signal is split into a doublet in ^{15}N labeled ferrous wild-type (WT) rTHB1. ^{15}N decoupling applied in the Lys Nζ region (~25 ppm) caused the doublet to collapse. **(B)** In the downfield region, the amide NH of Asn87 and a histidine NεH signal (marked a) are shown for comparison. Attempts to detect the NζH 2D correlation using HISQC experiments[2] were unsuccessful in large part because of fast ^{1}H transverse relaxation. **(C)** The spectrum of ferrous K53A rTHB1 (10% $^{2}H_2O$/90% $^{1}H_2O$, pH 9.1) demonstrates the absence of the sixth ligand detected in the wild-type protein.

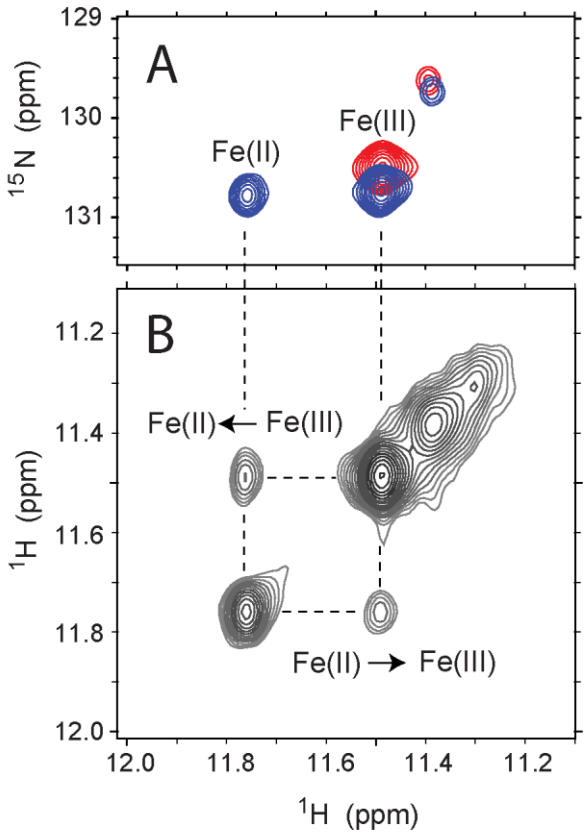

Fig. A19 ESE in wild-type rTHB1. (A) Portion of a ^{1}H-^{15}N HSQC collected on a 3:7 mixture of ferrous:ferric rTHB1 (blue, 1.8 mM rTHB1, pH 9.2, 298 K) superimposed over that of a sample of pure ferric rTHB1 (red, pH 7.5, 298 K). The cross peaks are from Asn87 NH. **(B)** Matching region of a ^{1}H-(^{15}N$_Z$)-^{1}H ZZ exchange NMR spectrum (τ_{mix} = 700 ms) recorded on the ferrous:ferric mixture. The square pattern is caused by redox interconversion.

Chapter 4 Supplementary Table

Table A3 Superposition of TrHb1 structures

	Structures	r.m.s.d. (Å)	# of Cα pairs	% identity	Fig. 4.2
With THB1					
Synechococcus GlbN His–His	4XDI.B / 4MAX.C	1.09	69	46	*a*
Synechococcus GlbN His–CN	4XDI.B / 4L2M.B	0.97	82	46	*b*
Synechocystis GlbN His–His	4XDI.B / 1RTX	1.06	78	47	*c*
Synechocystis GlbN His–CN	4XDI.B / 1S69	0.97	82	47	*d*
C. eugametos CtrHb His–CN	4XDI.B / 1DLY	0.91	82	48	*e*
M. tuberculosis HbN His–O_2	4XDI.B / 1IDR.A	1.02	78	39	*f*
Other pairs					
Synechococcus GlbN His–His / His–CN	4MAX.B / 4L2M.A	0.96	79	100	*c*
Synechococcus GlbN His–CN *Synechocystis* GlbN His-CN	4L2M.A / 1S69	0.67	118	60	
Synechococcus GlbN His–CN *C. eugametos* CtrHb His–CN	4L2M.A / 1DLY	0.73	111	47	
Synechococcus GlbN His–CN *M. tuberculosis* HbN His–O_2	4L2M.A / 1IDR.B	0.78	99	35	
Synechococcus GlbN His–CN *P. caudatum* HbN His–H_2O	4L2M.A / 1DLW	0.97	99	31	

Curriculum Vitae

Selena Loring Rice, Ph.D.

2934 Keswick Road, Baltimore, MD 21211
Phone: (443) 386.1234; Email: selena.l.rice@gmail.com

EDUCATION:

Johns Hopkins University, Baltimore, MD, 2010 - 2015
Cellular, Molecular, and Developmental Biology and Biophysics
Doctorate of Philosophy Thesis Defense: April 2015 Major: Biology

Northeastern University, Boston, MA, 2005 - 2010
Major: Biology Minor: Geology GPA: 3.86
Bachelor of Science *Summa Cum Laude*
American University in Cairo, Cairo, Egypt, Fall 2007
Study Abroad Classes: Biochemistry, Egyptology

WORK EXPERIENCE:

Graduate Student Researcher, **Johns Hopkins University**, Department of Biology, Baltimore, MD, Aug 2010 – Present

- Design, select methods, and execute research plans for individual research into the chemistry and structure of truncated hemoglobins
- Perform protein over-expression and purification and investigate proteins using optical, nuclear magnetic resonance, and crystallographic techniques
- Calibrate, utilize, and maintain specialized equipment such as spectrophotometers, weigh balances, thermocyclers, centrifuges, electrophoresis apparatus, microscopes, and incubators.
- Supervise a first year graduate student and train him in laboratory procedures
- Manage undergraduate lab courses and instruct undergraduate students in biochemistry, cell biology, and protein engineering concepts and laboratory techniques
- Collaborate with other lab members to complete research projects and write papers
- Orally present scientific findings to my advisor, thesis committee members, and department
- Write and provide recommendations on improving scientific reports to my advisor for submission to peer reviewed journals using Microsoft Word
- Design posters and present research at national and international meetings
- Organize order forms and maintain laboratory supplies

Research Assistant, **Harvard School of Public Health**, Department of Environmental Health, Boston, MA, Jan 2009 – Jan 2010

- Assisted in researching the prevention of aerosol transmission of microorganisms to

enhance airline safety. The research is supported by funding from the Federal Aviation Administration sponsored Airliner Cabin Environment Research Center of Excellence

- Performed assays to determine the infectivity and recovery of Influenza A virus from surfaces and airborne particles using aseptic procedures
- Optimized plaque assays to study aerosolized influenza virus recovery
- Responsible for establishing and maintaining cell cultures (MDCK cells, sialic acid modified MDCK cells, and Vero green monkey cells) using aseptic procedures
- Perform general lab maintenance

Integrative Graduate Education Research Traineeship (IGERT) Undergraduate Research Associate, **Northeastern University**, IGERT Nanomedicine, Boston, MA, Sept 2008 – Dec 2008

- Assisted in developing a gold nanowire neural chip
- Cultured rat hippocampal cells on different substrates to determine the optimal base on which the cells would grow in order to choose the most effective base for the chip using aseptic procedures
- Fabricated template chip bases by coating silicon wafers with aluminum using thermal evaporation
- Used anodization and electrodeposition to form a pore matrix in the aluminum oxide substrate and the gold nanowire array

Laboratory Assistant, Molecular Diagnostics Lab, **US Department of Agriculture**-Animal and Plant Health Inspection Service (APHIS, Beltsville, MD, May 2008 – Aug 2008

- Assisted in screening plant samples for specific pathogens using conventional and real-time PCR in conjunction with gene sequencing analysis
- Assisted in preparing the USDA-APHIS-PPQ Molecular Diagnostic Laboratory poster for the 9th International Congress of Plant Pathology, Turin, Italy August 24-29, 2008
- Performed general lab maintenance

Laboratory Assistant, **Dyax**, Cell Biology Department, Cambridge, MA, Jan 2007 – Jun 2007

- Assisted determining the expression of binding proteins for an experimental cancer drug
- Assisted in studying the experimental cancer drugs' effect on angiogenesis in vitro using 2-D co-culture tube formation assays
- Harvested and maintained several mammalian cell lines using aseptic procedures

VOLUNTEER EXPERIENCE:

Volunteer, **Smithsonian National Museum of Natural History**, Q?rius Exhibit, Washington D.C., 2014 – Present

- Ensure the safety of the specimens in the collections
- Set up and take down program materials
- Interact with visitors to engage their scientific curiosity and educate them about the research areas of the museum, i.e. anthropology, geology, botany, zoology
- Encourage visitors to participate in object-based, experimental activities using different media

- Assist visitors as they navigate through the exhibit
- Work with other volunteers to support educational programs within the exhibit
- Work with the volunteer coordinator to develop and improve interactive activities for the public
- Instruct other volunteers of procedures for activity set up
- Inform other volunteers of best practices for public interaction in different parts of the exhibit

Booth Volunteer, **USA Science and Engineering Festival**, Washington D.C., April 2014

- Designed an activity with other graduate students to teach visitors the basics of enzyme kinetics
- Instructed visitors in elementary concepts in biophysics
- Assisted in setting up the booth at the festival

Meyerhoff Summer Bridge Program Volunteer, **Johns Hopkins University**, Baltimore, MD, Summers 2012-2014

- Gave incoming UMBC Meyerhoff Scholars tours of Johns Hopkins University labs
- Answered questions about graduate school life
- Provided guidance on choosing graduate school programs

English Teacher, **Better World NGO**, Cairo Egypt, Fall 2007

- Prepared lesson plans
- Taught middle class Egyptian students in English

Instructor, **Tien Shan Kung Fu**, Columbia MD, 2000 – 2005

- Managed classes of ~20 students from ages 5-50 and instructed them in Tien Shan Pai Kung Fu

PUBLICATIONS:

Rice SL, Boucher LE, Schlessman JL, Preimesberger MR, Bosch J, Lecomte JT. Structure of *Chlamydomonas reinhardtii* THB1, a group 1 truncated hemoglobin with a rare histidine-lysine heme ligation. *Acta Crystallographica Section F*. 2015 Jun; 71(Pt 6): 718-25.

Rice SL, Preimesberger MR, Johnson EA, Lecomte JT. Introduction of a covalent histidine-heme linkage in a hemoglobin: A promising tool for heme protein engineering. *Journal of Inorganic Biochemistry*. 2014 Sep 28. pii: S0162-0134(14): 00251-7.

Johnson EA, **Rice SL**, Preimesberger MR, Nye DB, Gilevicius L, Wenke BB, Brown JM, Witman GB, Lecomte JT. Characterization of THB1, a *Chlamydomonas reinhardtii* truncated hemoglobin: linkage to nitrogen metabolism and identification of lysine as the distal heme ligand. *Biochemistry*. 2014 Jul 22; 53(28): 4573-89.

Pond MP, Wenke BB, Preimesberger MR, **Rice SL**, Lecomte JT. 3-Fluorotyrosine as a complementary probe of hemoglobin structure and dynamics: a (19)F-NMR study of *Synechococcus* sp. PCC 7002 GlbN. *Chemistry & Biodiversity*. 2012 Sep; 9(9): 1703-17.

HONORS and AWARDS:

2010-2012	The Owen Fellowship, Johns Hopkins University
2010	Department of Biology Certificate of Achievement, Northeastern

University

2008	Certificate of Appreciation from USDA-APHIS-PPQ (cash award)
2005 - 2010	Dean's List
2005 - 2010	Dean's Merit Scholarship
2004	The College Board- AP Scholar Award

SKILLS and CERTIFICATIONS:

2004	Black Sash Certification - Tien Shan Pai Kung Fu
	Three-time Grand Champion [2002 and 2005]
2002	Advanced Open Water S.C.U.B.A Certification (PADI)
2002	American Sailing Association Basic Keelboat Sailing Certification